Feedback strategies for enhancing Human Movement Augmentation

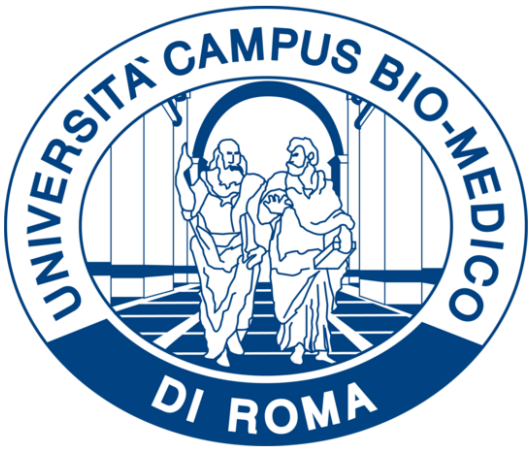

Davide Deiana

Department of Engineering
Università Campus Bio-Medico di Roma

This dissertation is submitted for the degree of
Dottorato di ricerca in scienze e ingegneria per l'uomo e l'ambiente
XXXVII ciclo a.a. 2021-2022

Supervisor:
Prof. Giovanni Di Pino
Co-supervisor:
Prof. Domenico Formica
Coordinator:
Prof. Giulio Iannello

September 2025

A chi ha fatto parte di questo percorso ...

Abstract

Human Movement Augmentation (HMA) aims to further enhance human abilities to move and interact with the environment. HMA is achieved through the use of an augmented device that can be tailored to the specific application and task. In this thesis, we will mainly focus on Supernumerary Robotic Limbs (SRLs): robotic manipulators used in close proximity to the user or worn to increase the user's available degrees of freedom. The success of HMA relies on the design of both a control interface to send commands to the SRL, and a feedback system to provide the user with supplementary sensory information. While one might argue that vision alone provides a sufficiently rich sensory modality to close the sensorimotor loop, we believe that supplementary feedback can offer important benefits. Vision can be occluded, and in some cases (e.g., estimating interaction forces) may not offer reliable cues.

According to motor control theory, every movement emerges from the continuous interaction between motor commands and sensory information: the sensorimotor loop. In the context of HMA, this loop also includes supplementary feedback. Afferent and efferent signals are also linked, in the central nervous system (CNS), through dynamic and kinematic representations (i.e., body schema) that summarize beliefs and knowledge about the body, and tools. The concept of body schema, and more broadly, body representation, is fundamental for both motor control and embodiment i.e. the sense of owning (i.e., ownership) and controlling (i.e., agency) a body part. These internal models allow for the planning and execution of movements, while also enabling users to experience tools or external devices as part of their own body.

In the context of HMA, the goal is to control SRLs as if they were natural extensions of the body. Achieving this requires not only accurate motor output but also sensory feedback. Importantly, motor control and embodiment are not independent but they partially overlap, supporting both coordinated action and the subjective experience of embodiment While most of the literature has focused on the design of control interfaces, comparatively little attention has been given to feedback strategies and devices. In particular, the impact of adding supplementary feedback to close the sensorimotor loop, and how this influences user behavior, remains underexplored.

This thesis seeks to address that gap, offering concrete examples of feedback design and evaluating their behavioral effects in augmented tasks. Designing and implementing effective supplementary feedback is inherently complex. It involves identifying which information should be provided, and how it should be delivered. In addition, task constraints may restrict the possible design choices. Factors such as the type of technology used and the location on the body where feedback is delivered further influence the effectiveness of the system and must be considered to optimize the flow of information.

Given the complexity and relevance of designing a proper feedback strategy, a reasonable approach is to first characterize the users ability to discriminate that particular strategy, and then apply it in a closed-loop scenario to assess behavioral outcomes. For this reason, we carried out some psychophysical preliminary studies to characterize the perceptual properties of the feedback. First, we developed a biofeedback method using eccentric rotating mass (ERM) motors to convey motor units activity (i.e., firing rate).

Results showed that motor placement significantly influenced users' discrimination abilities. Specifically, placing motors on different arms, thereby increasing spatial separation, improved discrimination. Nevertheless, the feedback coding strategy proved to be an even more decisive factor.

In particular, the continuous vibration encoding of firing rate outperformed the burst-based (i.e., spike strategy) encoding of individual action potentials. These findings highlight the necessity of thoroughly characterizing feedback modalities prior to implementation.

The importance of properly characterizing the feedback was highlighted also in the second pilot study. When using electrotactile stimulation via a high-density electrode matrix, it is possible to enhance spatial resolution by exploiting the funneling illusion (i.e., when two pads are activated simultaneously, a phantom stimulus is perceived in a location midway between them). However, to produce a smooth transition in perceived intensity between single-pad and dual-pad phantom stimulation, our results showed that the two pads must be activated with a combined intensity higher than that of the single pad. While these initial results address the perceptual efficacy of the feedback strategies, it remains essential to evaluate their impact in functional, closed-loop contexts. To this end, we tested two different scenarios: a force regulation task and a trimanual coordination task. In the force regulation task, users controlled the interaction force of a wearable robot's end-effector with the environment. Even a simple vibrotactile feedback, proportional to the exerted force, significantly improved their ability to apply and control the desired force. In the trimanual task, the effectiveness of the supplementary feedback was influenced by the coordination required to complete the task. The greatest benefit was observed when all effectors were coupled (i.e., tri-couple task) to achieve a common objective.

The results presented so far emphasize the complexity of designing appropriate feedback strategies and highlight their positive influence on motor performance in HMA. Still, these experiments primarily explore the perceptual and behavioral dimension. However, Human-robot interaction occurs within a continuous loop of afferent and efferent signals which, over time, through multisensory integration, may reshape our internal body representations and users may begin to embody the SRL. While previous work has demonstrated embodiment with simple tools like sticks, evidence concerning the embodiment of SRLs is still limited and inconclusive. To address this, we validated a platform where the SRL is user controlled and congruent supplementary feedback is provided to close the sensorimotor loop. Preliminary results suggest the feasibility of integrating the SRL into the user's body representation and embody it.

Table of contents

List of figures

List of tables

Chapter 1

Introduction

1.1 Motivation and Objective

From an evolutionary perspective, one of the most distinctive traits of the human species has been its extraordinary capacity to create and use tools. This ability not only allowed humans to adapt to a wide variety of environments, but also to modify them, and gaining control over their surroundings. Through tools, we have extended the limits of our own bodies, reaching farther, acting more precisely, and achieving tasks that would otherwise be impossible.

This profound integration between body and tool has culminated in the modern pursuit of Human Movement Augmentation (HMA) [34], a multidisciplinary field that aims to expand motor capabilities. Rooted in our innate plasticity [29] and motor redundancy [60], HMA seeks to go beyond compensation and rehabilitation, unlocking new motor functions and with the objective of expanding the boundaries of human action. Humans are able to seamlessly perform complex movements using a highly redundant system, where even a seemingly simple action, such as reaching for a glass of water, involves the precise coordination of multiple joints, the activation of tens of muscle fibers, and the fine control of numerous motor neurons [82].

These abilities are particularly remarkable when compared to those of robotic systems. Although robots are often equipped with hardware that theoretically outperforms the human body such as high-bandwidth actuators, communication lines capable of transmitting data orders of magnitude faster than neural pathways, and control systems running at KHz frequencies, they still fall short in replicating the flexibility, adaptability, and efficiency of human movement [44]. Nonetheless, humans exhibit smoother movements, interact effectively with the environment, are able to manipulate tools and adapt to the uncertainties of the world. These performance arise from the exceptional capabilities of our "controller"

i.e., the central nervous system (CNS) which is able to compute and send near optimal efferent commands to the muscles.

Most of the empirical data and observations on human motor behavior have led to the formulation of computational models, the most representative being the Optimal Feedback Control (OFC) theory [85, 90]. OFC proposes that movements arise from an optimization process in which every action maximize a reward while minimizing a cost functional. Moreover (as will be discussed in Section 2.2) each human action results from a rich interplay between afferences and efferences. Motor outputs are computed according to our belief about the state of the body and the world, a belief formed by combining two sources of information: the predicted sensory consequences of the previous motor command and incoming afferent signals. In other words, motor commands depend on sensory information, and sensory information is, in turn, influenced by motor commands.

How can we move or control external tools if afferences are not informative enough to provide a proper state estimate?

This question is especially relevant in HMA, where the augmented device (e.g., a robot) usually provides only visual or inherent feedback (e.g., forces exchanged at the connection point). Such information may be insufficient for learning or performing complex interaction and coordination tasks. Supplementary feedback could enrich the flow of information, allowing a better state estimate and the adaptation of body representations.

Body representations are a broad concept whose development and adaptation falls outside OFC's scope and relates more to motor learning [59, 98, 57]. Motor learning is a complex phenomenon, ranging from high level strategy (i.e., learning a completely new task) to low level adaptation. Learning a new task or manipulating an object requires understanding its properties (e.g., mass, length) and dynamic behavior. These properties are summarized into the CNS with in body/tool representations. These models allow prediction of sensory consequences (i.e., forward model in motor control) that are used by the CNS to overcame the delays that characterize the sensory systems [83], and to compute the motor commands necessary to reach a desired state (i.e., inverse model).

The CNS continuously updates these models through afferent input: sensory predictions of the forward model are compared with actual feedback. Discrepancies (prediction errors) lead the CNS to update our beliefs about body and tool kinematic and dynamics [59]. As discussed, internal models can also include external tools. For example, the exceptional skill of a tennis player relies on the CNS's ability to represent the racket as part of the body [98]. These considerations lead to the idea that the human ability to manipulate and execute complex movements relies on the body representations. As stated above, body representations are necessary not only to compute accurate motor commands but also to

generate predictions of the sensory consequences of those commands, thereby compensating for delays in the sensory system. These aspects are also crucial in the context of HMA, where the goal is to control the augmented device as naturally as the user controls their own body. Such results can be achieved if the augmented device is successfully integrated into the body representation.

What discussed so far is also related to the concept of embodiment. Embodiment is a core concept in neuroscience, referring to the sense that our body belongs to us and that we are in control of it. This feeling is not exclusive to our biological limbs: it can extend to external tools. We can define embodiment operationally as the condition in which something (e.g., a stick) is processed, at least partially, as part of one's own body [26]. This phenomenon is made possible by the brain's ability to integrate congruent multisensory afferent signals that shape our body schema (i.e., action oriented representation) and body image (i.e., perceptual representation) [25]. When an external device is integrated into our body representation, it may become embodied [19].

Beyond its conceptual value, embodiment has practical implications. Studies have shown that tools are more effectively controlled when they are embodied [52, 95]. Moreover, several brain regions involved in motor control are also involved in the process of embodiment, suggesting a shared neural basis [91].

In this thesis we will consider as augmented device a supernumerary robotic limb (SRL). A SRL is typically a robotic device that provides additional degrees of freedom and is intended to be used by the user alongside humans' natural arms to perform trimanual tasks i.e., tasks that require the coordinated and simultaneous control of three effectors in order to be successfully completed. SRLs usually operate in close proximity to the user and often share, at least in part, the same workspace. Depending on the application and the specific robotic platform, they can be either worn or positioned near the user. One limitation of SRL is their inability to naturally provide proprioceptive feedback, making their control largely dependent on vision (or on inherent feedback when worn) to close the sensorimotor loop. Nevertheless, during manipulation, the vision is typically focused on the task itself, rather than the arms' movements and postures, and the need of visual feedback from the SRL might instead constitute an additional cognitive load, as reported by patients with proprioceptive impairment [21, 68]. Moreover, vision could be very easily occluded in a real-life applicative scenario because of moving objects; in most cases, it provides poor information, if any, on the interaction forces; and it has proven to be almost discarded in favor of proprioception in some direction of the space [93]. Similarly, auditory feedback, while an interesting option for alarms or for signalling meaningful events, would be a cognitive cumbersome cue if used continuously. Auditory feedback would also present other drawbacks, similar to visual

feedback: for example, in a real-life applicative scenario, it could interfere with sounds coming from the environment, which could be potentially dangerous for the user. Thus, the limited feedback naturally provided by SRLs may hinder their integration into body representations and impair motor learning and performance.

Moreover, the embodiment of SRLs remains largely unexplored. Given the multisensory nature of embodiment [66], we propose that congruent supplementary feedback could play a critical role in fostering this process for SRLs.

To summarize, afferent signals, and by extension supplementary feedback, are vital to motor control at every stage, from learning, adaptation to on-line motion. Embodiment, enabled by multisensory integration and closed-loop interaction with the SRL, may not only enhance performance but also shift the way users perceive the robotic limb from tool to part of the self.

Given this context, the thesis presents studies evaluating the relevance of supplementary feedback in augmented tasks.

1.2 Thesis Outline

Chapter 2 explores all the fundamental theoretical aspects that underlie the entire thesis. In the first part, Human Movement Augmentation and its taxonomy are presented. The following sections illustrate motor control and embodiment. Particular emphasis is given to the role of supplementary feedback and, more generally, afferent signals in the context of HMA.

Chapter 3. Given the importance of afferent signals, and thus of supplementary feedback, assessing the user's perceptual discrimination abilities through pilot experiments constitutes a pivotal step. To this end, this chapter presents two pilot experiments focused on the design of supplementary feedback. The first pilot evaluates the impact of body location and vibrotactile feedback strategies to convey information about the activation states of two motor units' firing rates. In the second pilot, the amplitude perception of the funneling illusion with electrotactile stimulation is characterized.

Chapter 4. The feedback should then be tested in a closed-loop scenario to examine how it influences the user's behavioural responses. In particular, this chapter compares the user's ability to modulate end-effector forces when using a wearable robot, either relying solely on inherent feedback or combining it with supplementary vibrotactile feedback that conveys interaction force information.

Chapter 5 evaluates another crucial behavioural aspect of human motion: the coordination of multiple effectors. After analysing the influence of feedback in a force regulation task,

this chapter examines its role in a coordination task. In particular, it investigates the impact of supplementary feedback in three different types of virtual trimanual tasks. Depending on the condition, the coupling between effectors is mediated by a virtual elastic band. The feedback consists of continuous vibrotactile stimulation, with intensity proportional to the force applied to the virtual spring.

Chapter 6. While the other chapters focus on the impact of supplementary feedback in behavioural tasks, this one evaluates its feasibility and, specifically, the role of feedback in inducing a sense of embodiment toward a supernumerary robotic limb. In particular, this chapter presents a platform designed to elicit embodiment of a supernumerary robotic limb through a trimanual task performed in augmented reality. The user controls the robot via foot movements, and vibrotactile feedback is provided to emulate the sensation of touching virtual buttons through congruent multisensory stimulation. A multisensory reaction time task is also used to assess the boundary of the user's peripersonal space (PPS). An increase in PPS toward the robot is interpreted as a proxy for embodiment.

Chapter 7, finally, summarizes the main theoretical aspects, presents the key results of the thesis, and discusses future steps.

Chapter 2

Background

In this chapter, the theoretical concepts that provide the foundation for the thesis are presented to the reader.

The first section outlines the main theoretical framework of the thesis: Human Movement Augmentation (HMA). A complete taxonomy of augmentation approaches is presented, highlighting both their advantages and limitations, as well as the central role of feedback in ensuring a successful augmentation.

The second section discusses the fundamental principles of motor control. Understanding how humans perform voluntary movements, both in free conditions and when using a tools, is essential in the context of HMA. Although often left implicit, much of the research in this field is grounded in these theoretical ideas and processes. As part of this discussion, a computational model is introduced: the Optimal Feedback Control. Such model provide a concise framework to summarize experimental evidence and, despite same limitations, help explain how movements emerge from the rich interplay between afferent and efferent signals.

In the third section the concept of embodiment is introduced. Embodiment refers to the feeling of owning and controlling one's body, a sensation that can also extend to external tools. Here, the relevance of embodying supernumerary tools is addressed, with particular attention to its practical implications and multisensory nature.

Finally, in the last section, some basic notions of tactile perception are discussed. The focus is placed on tactile perception since, throughout the thesis, this sensory modality has been explored to deliver supplementary feedback.

2.1 Human Movement Augmentation*

*Section based on [34]

Human Movement Augmentation (HMA) aims to extend the motor capabilities of able-bodied users. Depending on the specific aspect of motor function being enhanced, HMA can be classified into the following categories:

- **Power Augmentation:** when the user's speed or strength is increased. Examples include exoskeletons that enhance physical strength and endurance, or vehicles that extend velocity.
- **Workspace Augmentation:** when the user's range of action is extended to operate in areas that are normally unreachable. This can be achieved using tools such as rakes, endoscopes, or teleoperation systems.
- **Command Augmentation:** when the user's motions are processed to compensate for certain human limitations. An example is tremor attenuation in robotic microsurgery.
- **Degrees of Freedom (DoF) Augmentation:** refers to the process of increasing the task-relevant DoFs during interaction with the environment, enabling to complete tasks normally performed by two people.

2.1.1 Technological challenges

A successful implementation of augmentation, with a particular focus on Degrees of Freedom (DoF) augmentation, depends on the design of three components: the command interface, the supernumerary effector, and the feedback device. Together, these elements enable the capture of user intent, the execution of the desired movement, and the closure of the sensorimotor loop through an appropriate feedback strategy.

The correct design of these elements strongly impacts motor performance and the user's ability to effectively embody the augmentation device. Embodiment is a broad concept that refers to the sense of ownership over a body part and the feeling of agency in its control [26] (for a more detailed discussion, see Section 2.3).

These technological challenges are similar to those encountered in other scientific domains such as rehabilitation or prosthetics, but without the constraints of restoring lost functions or preserving a natural appearance. Each component can be customized to better fit the needs of the user and the specific application.

In general, the command interface can be based on the body, muscles, or neural activity:

- Body interfaces are non-invasive systems that capture body movements or applied forces.

- Muscle interfaces detect muscle activation, and can be invasive or non-invasive. Common examples include surface EMG and intramuscular EMG.
- Neural interfaces measure signals from the nervous system using techniques such as EEG, MEG, fMRI, or extracting the motor unit spiking activity from High-density electromyography (HD-EMG).

The term supernumerary effector refers to any tool that provides additional DoFs. It can range from a robotic manipulator to an extra finger or limb.

The feedback interface is necessary to inform the user about the state of the supernumerary effector. Closing the sensorimotor loop is essential for precise control, to induce the sense of embodiment, and improving system acceptability. Feedback can also drive the incorporation of the tool into the body representation [75].

Despite the critical role of afferent signals and sensory feedback, many questions remain open. For instance, what kind of information about the supernumerary effector should be delivered to the user? How should that information be conveyed to maximize understanding while minimizing cognitive load?

Special care must be taken when designing the feedback interface, ensuring it is tailored to the specific context and application.

2.1.2 HMA taxonomy

The different types of augmentation can be clustered into two main groups. The first group (i.e., power, workspace, and command augmentation) enhances the DoFs and capabilities that humans already possess. In contrast, the second group (i.e., DoFs augmentation), aims to endow users with additional DoFs that can be controlled concurrently with their natural ones.

DoF augmentation can be considered the ultimate goal of HMA, as the ability to control additional DoFs has the potential to fundamentally revolutionize human interaction, significantly expanding the range of actions that we can perform. Ideally, this could enable a single individual to perform tasks that would traditionally require the cooperation of two people.

However, DoFs augmentation is a broad concept and can be implemented through various strategies:

- **Autonomous DoF Augmentation** can be considered a form of human-robot collaboration. The additional DoFs are not directly controlled by the user but are automatically managed by an external tool (e.g., a robot). This type of augmentation is the easiest to implement but presents some limitations. Specifically, only structured tasks and environments benefit from this approach. Achieving complex behaviors is possible

by predicting the user's intent or physiological state, or by adopting flexible control-sharing strategies in which the user assumes command in critical situations while routine actions are handled autonomously.

- **Augmentation by Transfer** differentiates between task-relevant and task-irrelevant DoFs. For example, during tasks where only certain body parts are actively engaged (i.e., task relevant DoF) such us seated manual operations, unused body DoFs like those of the legs (i.e., task-irrelevant DoF), can be used to control supernumerary robotic limbs. By mapping task-irrelevant movements to meaningful control inputs, empowers the users to directly control the SRL. Simple examples include using foot motion or pressure sensors as input channels.

- **Augmentation by Extension** introduces new degrees of freedom to the body independently of existing ones preserving the natural movement repertoire. This approach represents the conceptual ideal of augmentation, as it provides additional DoFs without sacrificing or remapping any of the user's original ones.

All of these approaches have the potential to significantly reshape how a task is performed. However, their effectiveness depends on the context of application, the nature of the task, and the specific user capabilities they are intended to support.

Autonomous augmentation offers the advantage of reducing the user's workload and is often simpler to implement. However, its effectiveness depends critically on the predictability of both the task and the system's behavior, as well as the user's ability to anticipate and adapt to it.

With augmentation by transfer, the user gains direct control of the tool, enabling a broader range of operations. Moreover, leveraging already existing DoFs may reduce the learning curve, as the user is already capable of performing those movements and only needs to learn, for example, the robot-leg mapping. However, questions remain about the overall feasibility of this type of augmentation. Effectively and simultaneously controlling three effectors to accomplish a task may increase the user's mental workload, which could limit its potential benefits in a real scenario.

Augmentation by extension, in principle, allows users to expand their control repertoire without interfering with natural movements. However, this approach poses significant challenges in terms of cognitive load and neural resource allocation [33]. This raises a fundamental question: which signals can be harnessed to reliably and intuitively manage the added degrees of freedom?

This challenge finds a possible solution in human anatomy: the body is highly redundant, with many more muscles than mechanical degrees of freedom, and a greater number of

motor-neurons than the number of muscles themselves [82]. These anatomical features suggest the potential to exploit certain physiological signals without interfering with ongoing movements.

For this reason, the concept of null space has been proposed, analogous to that in linear algebra, which refers to a set of physiological signals that are not directly correlated with movement. These signals could be the key to achieve a real DoFs augmentation. An example could be the EMG beta band (13–30 Hz) that has been shown to be partially modulated independently of the muscle force, making it a promising candidate.

2.2 Human Motor Control

Motor control is a vast and multifaceted field that spans from studying the mechanisms of motor learning (such as learning a new task [98, 57], adapting to changes [37, 17] and generalization of that knowledge [86, 65]) to uncovering the underlying principles that govern how and why we move. In this section, we will focus on the latter aspect, introducing the Optimal Feedback Control (OFC) framework. OFC is crucial for understanding how afferent signals contribute to the planning and execution of movement. Investigating HMA within the framework of motor control is an essential step toward building a solid theoretical foundation. Furthermore, adapting and applying existing knowledge from this field can help guide the design of effective solutions and experimental protocols.

Humans exhibit excellent motor abilities and are capable of performing complex tasks seamlessly. These abilities are even more remarkable considering the limitations of the human neuromuscular "hardware" [44].

The ability to perform such motor tasks arises from the coordinated activity of a complex and distributed network within the central nervous system (CNS). The spinal cord, brainstem, and cortex each play distinct roles in producing motor output, operating within a hierarchical architecture. Lower structures manage basic and automatic motor patterns, such as reflexes and locomotion, while higher structures contribute to the generation of more flexible and goal-directed movements [82, 38].

Humans' movements are, in most situations, stereotypical (e.g., straight trajectories when performing pointing or grasping tasks), but they are also characterized by intrinsic variability [90]. Trial-to-trial variability is an inherent property of human behavior and can be observed in everyday life. When hitting a ball with a racket or attempting a basketball shot, each movement and outcome varies over time. This outcome variability can only be minimized through prolonged training, but never completely eliminated.

This variability could arise from the interplay between the physical properties of the body and the optimization strategies adopted by the motor control system. Sensory modalities and motor commands are subject to noise and delays. All these considerations and behavioral characteristics of human movement are addressed and emerge from the seminal work of Todorov[90], who proposed a version of the OFC theory based on the *minimum intervention principle*.

The main idea of this work is that the sensorimotor system is inherently noisy at every stage of movement execution. Consequently, the optimal strategy is to correct deviations only in task-relevant dimensions, while allowing variability to accumulate in task-irrelevant dimensions. This principle is supported by two key arguments: on the one hand, minimizing variability in task-irrelevant dimensions requires increased muscle activation, leading to higher energy consumption. On the other hand, efferent noise is proportional to the mean level of muscular activity, which in turn increases output variance [85]. In other words, attempting to reduce variability in task-irrelevant dimensions leads to greater energy expenditure and also increases the standard deviation along task-relevant dimensions, resulting in a suboptimal performance.

The details described above refer to a specific application of OFC, which is a more general computational model that integrates several known features of motor behavior. The model is grounded in three main principles:

- Humans need to predict the sensory consequences of their motor commands.
- These predictions should be combined with information from afferent signals to obtain an estimation of the system's state.
- This estimation is then used to compute the motor commands for the next state. These commands aim to maximize some form of reward while minimizing a cost function.

These conceptual points can be formalized within different mathematical frameworks. In this section, the formulation proposed by Shadmehr [85] will be presented. This model was chosen as it represents a good compromise between mathematical complexity and explanatory power. On one hand, the equations remain relatively accessible, while on the other hand, the formulation is sufficiently rich to highlight the functional meaning of each block within the Optimal Feedback Control (OFC) framework. Indeed, a broad range of experimental and behavioral findings can still be understood and predicted through these equations.

The model is based on the idea that each action we perform aims to achieve a reward while minimizing the cost of the process. Mathematically, this is expressed using two terms, one that compute how much we want to reach the desired state (Eq. 2.1), and one the tries

to minimize the relative movement cost (Eq. 2.2). The desired state is expressed by the following equation:

$$\sum_{t=1}^{N} \left(\mathbf{y}_v^{(t)} - \mathbf{r}\right)^{\top} \mathbf{Q}^{(t)} \left(\mathbf{y}_v^{(t)} - \mathbf{r}\right) \tag{2.1}$$

In this case, $\mathbf{r}$ represents the target position, defined through vision, while $\mathbf{y}_v^{(t)}$ is the sensed position. $\mathbf{Q}$ is a matrix that defines how strongly we want to minimize the distance from the desired state. In this specific case, all measurements are defined in visual space, but these elements can be generalized to account for different sensory modalities, such as proprioception.

On the other hand, humans must carefully manage their energy resources. Consequently, the cost associated with motor commands (i.e., $\mathbf{u}$ in Eq. 2.2) is typically modeled as a quadratic function:

$$\mathbf{u}^{(t)\top} \mathbf{L} \mathbf{u}^{(t)} \tag{2.2}$$

The quadratic form was chosen because it not only minimizes energy expenditure, but also helps reduce the total noise in the system. Since motor noise scales with mean muscular activity, minimizing a quadratic cost effectively lowers both effort and variability. In this context, $\mathbf{L}$ is a matrix that weights the expected cost.

The global functional is defined as follow:

$$J = \sum_{t=1}^{N} \left(\mathbf{y}_v^{(t)} - \mathbf{r}\right)^{\top} \mathbf{Q}^{(t)} \left(\mathbf{y}_v^{(t)} - \mathbf{r}\right) + \mathbf{u}^{(t)\top} \mathbf{L} \mathbf{u}^{(t)} \tag{2.3}$$

An important consideration is that all the variables in Equation 2.3 are affected by noise. Noise is pervasive at every stage of the process, making the cost functional J a stochastic variable. The theory states that the CNS attempts to minimize the expected value of this functional.

Moreover, mathematically, this process is computed starting from time N in the equation (i.e., the moment the movement is expected to be completed) and than moving backward to the present time. The result of this minimization is referred to as the *cost-to-go*, which represents the remaining cost within a trial.

This process of computing the cost-to-go requires that humans are able to estimate the required movement and the relationship between motor commands and their sensory consequences. This ability is crucial not only for computing the cost-to-go but also for executing movements in real time. Since sensory signals are slow and noisy, humans compensate for these limitations by relying on predictions of the sensory consequences of

motor commands through *internal models* [54]. These models can be mathematically defined with a simplified linear model as follows:

$$\begin{aligned} \hat{\mathbf{x}}^{(t+1|t)} &= \hat{A}\hat{\mathbf{x}}^{(t|t)} + B\mathbf{u}^{(t)} \\ \hat{\mathbf{y}}^{(t)} &= \hat{H}\hat{\mathbf{x}}^{(t)} \end{aligned} \tag{2.4}$$

Where $\hat{\mathbf{x}}^{(t|t)}$ represents the estimated state of the body at time t, incorporating all available sensory feedback up to that moment. This state encompasses both the body and the environment. The variable $\mathbf{y}$ denotes the expected sensory feedback, obtained through the observation matrix $\hat{\mathbf{H}}$, which transforms the internal state into the corresponding sensory signals.

The term $\hat{\mathbf{x}}^{(t|t)}$ represents the prediction of the future state, based on the current state and the motor command sent to the muscles.

These models enable compensation for sensory delays. Nevertheless, during movement, the nervous system receives a continuous stream of afferent signals. These are combined with the internal predictions to form a belief about the current state. One common approach to model this phenomenon is through the statistical framework of the Kalman filter, as expressed in the following equation:

$$\hat{\mathbf{x}}^{(t+1|t+1)} = \hat{\mathbf{x}}^{(t+1|t)} + \mathbf{K}^{(t+1)}\left(\mathbf{y}^{(t+1)} - \hat{\mathbf{y}}^{(t+1)}\right) \tag{2.5}$$

Equation 2.5 describes how prediction and sensory information are combined. This technique allows for the optimization of state estimation through the use of the Kalman gain. Specifically, $\mathbf{X}(t+1|t+1)$ represents the corrected estimate, where the parameter $\mathbf{K}$ enables the system to weigh prediction and sensory modalities differently, based on signal noise and confidence in the available information.

The final stage of computation involves the calculation of the motor commands, as shown in the following equation.

$$\mathbf{u}^{(t)} = -\mathbf{G}^{(t)}\hat{\mathbf{x}}^{(t|t-1)} \tag{2.6}$$

The motor output is obtained by multiplying the estimated state by a gain matrix $\mathbf{G}$, which is computed at each time step. This matrix generates the motor commands that minimize the cost function (see Equation 2.3), based on the current state. This final step in motor control is known as the *control policy*.

This computational model results from the integration of various behavioral and neuroscientific findings. Moreover, all equations and functionals presented in the previous

sections represent a specific mathematical resolution of the problem and serve as a schematic representation of several known human motor behaviors. Nonetheless, one of the main limitations of the OFC framework lies in its broad generality: by adjusting a few parameters, the model can be made to fit almost any dataset, making it difficult to falsify [3].

This complete treatment of OFC, despite the limitations, serves as the foundational theoretical framework for the following chapters, highlighting the pivotal role of afferent signals (and thus supplementary feedback) in the sensorimotor loop. Every motor command, and therefore every movement, explicitly depends on the state of the system. The control policy (Eq 2.6) computes the motor output by multiplying a variable gain with the optimal estimation of the system. This estimate combines the predicted sensory consequences of the current motor command (Eq 2.4) with the sensory information available at that moment (Eq 2.5). Moreover it allows to compute task-optimal corrective response to perturbations [67]. Although the cost function in Eq 2.3 is defined in visual space, it can be extended to include other sensory modalities, such as proprioception. However, in the contest of HMA, also the supplementary feedback could be used as a variable to compute the cost. Finally, the predicted sensory consequences of an action depend on internal models built over a lifetime. Even though OFC does not state this explicitly, sensory afferences drive the creation and refinement of these models. Supplementary feedback may therefore help fostering the inclusion of the robot's dynamics into the body representations, and reduce training time.

Taken together, these considerations show that movement emerges from a complex interplay between motor commands and sensory consequences. Given this context, the supplementary feedback could be both a theoretical and practical necessity for the success of HMA.

2.3 Embodiment

In the previous section, the theory of motor control was briefly illustrated, and an example of a computational model (i.e., the Optimal Feedback Control) was also presented. Motor control is an essential step toward characterizing and formalizing the theory behind the HMA scenario. It encompasses all the mechanisms that allow humans to learn and become proficient in executing a broad range of actions. Understanding which types of mechanisms are involved, and the relative contribution of afferences and supplementary feedback to the global process, is essential to achieving high-level performance in the control of SRLs. However, another aspect that has been demonstrated to influence human performance in the control of external tools, and which will be discussed in this section, is the concept of embodiment [52, 95].

Embodiment refers to the feeling of perceiving a body part as one's own. This experience may involve one's real limbs or extend to tools [19] and external devices.

Moreover, embodiment and motor control are not two separate and distant concepts, as they might seem; rather, they could potentially overlap and share, at least partially, the same neural networks [26]. This makes embodiment another crucial element in achieving successful HMA.

In the context of embodiment, the classical example is the rubber hand illusion (RHI) [13]. In this paradigm, the participant's real hand is hidden from view while both the real and a visible fake (rubber) hand are stimulated either synchronously or asynchronously. When the stimulation is synchronous, participants often experience a sense of ownership over the rubber hand. This illusion is also accompanied by changes in the perceived position of their real hand, a phenomenon known as proprioceptive drift [13].

The RHI is a well-known and widely replicated finding that has laid the foundation for much of the theoretical and experimental work in the field of embodiment. However, while the RHI is a powerful demonstration, it captures only a limited aspect of the phenomenon, namely, ownership. It is now broadly accepted that embodiment consists of two main components: ownership (the feeling that a body part belongs to oneself) and agency (the sense of controlling that body part)[9, 10]. Building on the results provided by the RHI, researchers have sought to deepen the understanding of what can be embodied and to uncover the neural mechanisms that support this process. Although some aspects of embodiment remain debated, and there is not yet full consensus within the scientific community, several findings have proven robust over time.

This section will provide an overview of the current state of knowledge on embodiment, with particular attention to its implications for HMA. In addition, we will highlight the theoretical relevance of supplementary feedback in facilitating embodiment and improving the integration of external devices into the body representations.

An interesting definition of embodiment has been given by De Vignemont [26], where he states: "*E is embodied if some properties of E are processed in the same way as the properties of one's body.*" Some considerations can be made based on this. In particular, within this framework, the concept of embodiment does not require that the embodied object be fully recognized as one's own, but rather that even a single shared property may suffice. This can be observed in the case of the RHI: in this experiment, the artificial hand is perceived as part of the participant's body (i.e., ownership), although no sense of agency is reported.

Humans are capable of embodying external tools, such as a stick, through repeated use. This process leads to plastic changes in the peripersonal space (PPS), the area around the body where interactions with the environment occur [73], causing it to extend and incorporate

the tool. Typically, this form of embodiment is linked to a sense of agency over the tool's actions, but not to a sense of ownership of the tool itself [26].

This could lead to the hypothesis that only our biological body can be fully embodied (i.e., with all of its properties processed as one's own), whereas for external objects, the specific type of embodiment depends on the body representation involved in that particular process.

Body representations constitute a broad field of research. These representations refer to the collection of knowledge that humans possess about their own body. They encompass a wide range of properties, from those essential for movement to perceptual, conceptual, and emotional. In the literature, various classifications of body representations have been proposed, based on different criteria such as level of awareness (conscious vs. unconscious), temporal characteristics (short-term vs. long-term), and functional role (action vs. perception). From this perspective, the complexity of defining a precise taxonomy becomes evident. Given this complexity, usually a dyadic taxonomy is adopted, where body representations are divided into two major clusters: body schema and body image [25].

The body schema is a representation involved in action planning and control, where pivotal information and knowledge of the body (i.e., kinematic and dynamic) are stored. Given this central role in the context of action, the body schema could potentially be correlated with the body representations usually described in the motor control literature. This perspective could lead to the idea that two concepts which may seem distant, such as embodiment and motor control, are actually closer than initially assumed.

The body image is an even more blurred concept, encompassing everything that remains after accounting for the body schema, and is primarily involved in perceptual tasks [25].

Multisensory integration is a crucial aspect of embodiment [9, 20]. Indeed, studies have shown that congruent visuomotor [42, 81] or visuotactile [6] stimulation can lead to the embodiment of objects external to our body. Body representations appear to be highly malleable, capable of incorporating also tools or objects with not human morphology [63, 61].

It has been proposed that sensory information is integrated in a near-optimal fashion, mathematically defined as Bayesian integration. Sensory inputs are compared with prior predictions, and within this framework, different levels of trust can be assigned to each sensory modality depending on the context. Discrepancies between prior knowledge and sensory input act as driving signals, allowing the system to update and refine its body representation. These updates, combined with ongoing sensory input, result in a more coherent and plausible internal model of the body.

In this way, multisensory integration serves as a driving force that can adapt internal representations to include properties and dynamics of external tools, ultimately leading to their embodiment.

Furthermore, the neural structures involved in embodiment overlap with those involved in motor control (e.g., the parietal and ventral premotor cortices, the temporoparietal junction [TPJ], and the insula),[91]. However, the precise relationship between embodiment and motor control remains an open question for future research. Current evidence does, however, suggest a strong interconnection between the two.

All together, these considerations highlight how multisensory congruent afferent signals are critical in shaping human body representations and, as a result, inducing a sense of embodiment. This concept is especially relevant in the context of HMA. Experiencing embodiment toward a supernumerary effector, and perceiving it as part of one's own body, may enhance task performance. Supplementary feedback may be a critical factor in promoting this integration. Moreover, the close connection between embodiment and motor control could potentially allow users to control the supernumerary effector as if it were a natural extension of their body, in coordination with their biological limbs.

2.4 Somatosensory Basis

In the previous sections, the importance of supplementary feedback has been highlighted. This section introduces the sense of touch, which will serve as the sensory channel used as supplementary feedback in the following chapters. An overview of the main mechanoreceptors will also be presented.

The sense of touch relies primarily on four different types of mechanoreceptors. These classes are mainly distinguished by their response to sustained indentation and by the size of their receptive fields, and are categorized as SAI, SAII, FAI, and FAII [92].

FAI and FAII fibers are characterized by a fast-adapting response. The number, instead, indicates the receptive field size: type I fibers have small and well-defined fields, while type II fibers have larger fields with less precise borders. These receptors are particularly relevant for this thesis, as they are responsible for the perception of vibration. FAI fibers, also known as Meissner corpuscles, are most sensitive in the lower frequency range, with a maximum response around 80 Hz [64]. FAII fibers, corresponding to Pacinian corpuscles, and responde to higher frequencies with peak sensitivity around 200–300 Hz [92].

SAI and SAII fibers, on the other hand, are responsible for the perception of constant pressure and sustained indentation. As with FA fibers, the numbering refers to the receptive field size. SAI fibers correspond to Merkel cells, which respond to pressure and texture,

providing detailed information about shape, edges, and curvature of objects. SAII fibers correspond to Ruffini endings, which respond not only to pressure but also to skin stretch. Importantly, some Ruffini cells are directionally selective, meaning they respond differently to stretch in specific orientations. The spatial properties of the receptive fields depend not only on the intrinsic characteristics of mechanoreceptors but also on their location within the skin. The skin is organized in three main layers: the epidermis, the dermis, and the hypodermis. SAI and FAI receptors are typically located in the more superficial layers of the skin compared to SAII and FAII receptors. Specifically, FAI receptors are found near the skin surface, within the papillary ridges of the dermis, whereas Merkel cells of the SAI units are positioned at the tips of the intermediate epidermal ridges. Pacinian corpuscles (FAII) are located in the subcutaneous tissue, while Ruffini endings (SAII) are embedded deeper within the dermis [92].

The description above mainly refers to glabrous (hairless) skin. In hairy skin, low-frequency vibration is not detected by Meissner corpuscles but instead by hair follicle afferents (HFA). Another important difference is the depth of FAII corpuscles: in hairy skin, these mechanoreceptors are situated deeper, within the underlying tissues surrounding joints and bones [64].

This aspect is particularly relevant in the context of the present thesis, since supplementary feedback was delivered through vibrotactile stimulation applied to the hairy skin of the participants. Although glabrous skin exhibits comparable performance in terms of vibrotactile discrimination, the main difference lies in the detection threshold. This difference is partly explained by the greater depth at which FAII fibers are located in hairy skin.

Moreover, the location of mechanoreceptors within the skin is of paramount importance also in the context of electrotactile stimulation. In this type of stimulation, pairs of electrodes are placed on the skin surface to deliver electrical currents or voltage pulses, thereby directly activating the nerve fibers within the skin. By adjusting stimulation parameters (e.g., current frequency), it is possible to evoke different types of sensations, ranging from pressure to vibration. These parameters (e.g., voltage intensity) strongly influence how the electric field spreads through the skin, depending on the depth and size of the stimulated area. In addition, the impedance between the skin and the electrodes, which changes over time, represents another critical factor in shaping the field inside the skin [100].

Chapter 3

Designing feedback strategies for enhancing SRL control and embodiment

3.1 Introduction

In the background, the critical role of afferent signals in motor control framework has been emphasized, both for the execution of movement and in enabling the embodiment of external tools. Nevertheless, the literature in the field of human movement augmentation has primarily focused on the generation of motor commands for the augmented device. In most cases, the only afferent information available to the user is visual or incidental auditory feedback produced by the device itself.

Although vision is a highly informative sensory modality, it requires continuous monitoring of the augmented limb, which can impose a significant cognitive load. Moreover, it lacks the ability to provide essential information about forces and interactions with the environment [16]. In contrast, somatosensory feedback may offer substantial advantages by reducing reliance on visual input and delivering information through faster sensory processing pathways [22].

Despite the potential benefits of supplementary feedback, several key issues remain to be addressed. On one hand, what type of information should be provided to the user? In the context of Human Movement Augmentation (HMA), possible feedback could include the position of the end-effector, joint variables, or interaction forces with the environment. Furthermore, how should this information be conveyed (e.g., auditory or vibrotactile feedback). Should the feedback use the same sensory modality (e.g., pressure to convey force), or are cross-modal stimulations viable alternatives [75]

The body location where feedback is applied is also crucial. Feedback should be delivered in a way that minimizes interference with motor tasks while still targeting body areas with sufficient sensory sensitivity.

At first glance, the number of open questions reveals the challenge of finding a balance between providing rich feedback, minimizing the cognitive load required to interpret it, and avoiding interference with natural movements.

Another limitation is the generalizability of the existing literature. Different tasks and applications may require tailored feedback strategies that, if applied to another experimental paradigm, might result in reduced performance. Therefore, designing customized solutions for each condition could be a crucial step toward achieving optimal feedback strategies.

In light of this, this chapter presents two pilot experiments in which two feedback strategies ([28, 27]) are designed and optimized with a limited number of participants, prior to the proper experiment. These two case studies differ substantially in their technological setup (i.e., vibrotactile and electrotactile stimulation) and in their intended application scenarios.

They are meant to highlight the design and characterization processes required when dealing with either highly complex strategies (e.g., the spike strategy in Section 3.2.3) or novel technologies (e.g., electrotactile stimulation), which demand precise calibration to fully exploit their potential. Despite these differences, they are presented together in this chapter as complementary examples of how feedback strategies can be systematically designed and characterized, especially given the central role of feedback in this thesis. It is worth noting, however, that the specific feedback techniques investigated here are not employed in the subsequent chapters.

- The first study aimed to validate a biofeedback that encodes the activity of two motor units. Indeed to achieve real degree of freedom augmentation, participants should be able to voluntarily manipulate the same physiological parameters without interfering with natural motion, thereby exploring the concept of *null space*. A change in a physiological signal from the null space does not produce a movement in the body, or if it does, it does not affect the status of the end-effector [34].

  The null space of motor units (MUs) has been investigated through real-time algorithms that extract MU activity using high-density surface electromyography (HD-sEMG) recordings. With this non-invasive methodology, the authors of [14] examined whether participants could learn to flexibly and independently recruit different MUs to control a cursor on a screen and only visual feedback has been provided to participants for learning motor unit control.

For this reason, in Section 3.2, a two-alternative forced-choice task was carried out to assess participants' ability to discriminate between pairs of simultaneous vibrations delivered by two stimulators. The Esteem Accuracy (EA) (i.e., a measure of the steepness of the psychophysical curve, where smaller values indicate easier discrimination between frequencies) was calculated across different feedback strategies and body locations, with the aim of identifying the most effective strategy (i.e., the one associated with the smallest EA). The study was structured into two sub-experiments, each focusing on different combinations of strategies and body locations.

- The second study presents a calibration procedure that exploits the *funneling illusion* (i.e., a phantom sensation perceived midway between two physical stimuli on the skin [8]) in the context of electrotactile stimulation. The objective was to increase the spatial resolution of an electrode matrix designed by Tecnalia, ultimately intended to provide feedback regarding the state (e.g., end-effector position) of a supernumerary robotic limb.

  The leg was chosen as the stimulation site because of its large surface area and with the idea that, in future applications, it could be used in parallel with vibrotactile feedback delivered to the upper limbs.

  By leveraging the funneling illusion, it is possible to enhance the spatial resolution of electrotactile feedback. Adjusting the intensity ratio between two stimulators allows the perceived phantom sensation to shift toward the electrode delivering the stronger stimulus. Thus, a crucial step in harnessing this illusion effectively is to understand how the physical parameters of stimulation map onto perceived sensations. Indeed, preliminary tests suggest that perceived intensity may vary with the number of activated electrodes and may not linearly correspond to the total current delivered. These discrepancies could affect the consistency of the funneling illusion and lead to unintended variations in the perceptual outcome.

  Therefore, a two-alternative forced-choice task was performed to determine the point of subjective equality (PSE) in perceived intensity when transitioning from a single active pad to a two-pad configuration (i.e., the funneling illusion). The PSE was evaluated as a function of the phantom perceived location, which was manipulated by varying the activation ratio between the two pads.

3.2 Validation of vibrotactile feedback to improve selective motor units recruitment*

3.2.1 Participants

In each experiment, five participants were enrolled (3 females). The average age of participants was 25.2 ±3.3 years in Experiment 1 and 23.8 ±0.5 years in Experiment 2. All participants were healthy and provided written informed consent in accordance with the declaration of Helsinki and following amendments and with the Ethical Committee of Università Campus Bio-Medico.

3.2.2 Experimental Setup

Participants comfortably sat on a chair with their arms laid back on the armrests and their hands' palms down. The subject was then required to wear headphones delivering white noise to avoid any auditory cues from the motors. Vibration feedback was provided through a vibrotactile stimulation interface previously developed and here further optimized, [72].

The wearable interface was composed of two Eccentric Rotating Mass (ERM) motors (Model: 307-103 by Precision Microdrives Inc.) and a custom Printed Circuit Board (PCB). The PCB consisted of a compact (6x6 cm^2) wearable device that enables independent control of up to 6 motors. The Board incorporated h-bridge drivers (L2293Q, STMicroelectronics Inc) and a microcontroller (μC) (STM32F446RET6, STMicroelectronics Inc).

In the present study, only two vibrator motors were employed and fixed on the participants' arms using medical tape.

To let the experimenter set the type of feedback modality, frequency, and activation timing of the stimulators, we implemented a graphical user interface (GUI) using the C++ language in Qt Creator 8.0.1 environment. The μC, based on information coming from the control GUI through serial communication, modulated the vibration intensity by generating a Pulse Width Modulation (PWM) signal. The input voltage applied to the motors was proportional to the duty cycle of the signal as defined by the following equation:

$$V_s(t) = \delta(t)V_m, \tag{3.1}$$

*This section is based on the accepted article [28]

where V_s is the supply voltage of the stimulator, $\delta(t)$ is the duty cycle of the PWM, and V_m is the supply voltage of the motor drivers. By varying the duty cycle value from 0 to 1, according to the feedback strategy, we vary the vibration intensity[1].

3.2.3 Experiment 1

In Experiment 1, we tested a “spike strategy", designed to be time-locked with the activity of selected MUs (i.e., mimicking the MU’s frequency). Considering the experiment conducted by Bracklein et al. [14] as a practical implementation of this feedback, whenever the decomposition algorithm of high-density surface electromyography (HD-sEMG) would detect an action potential from the selected motor neuron, the stimulator is activated for 15 milliseconds by delivering a power supply of 3 V (V_m in equation 3.1) and then deactivated (see Figure 3.1 for more details).

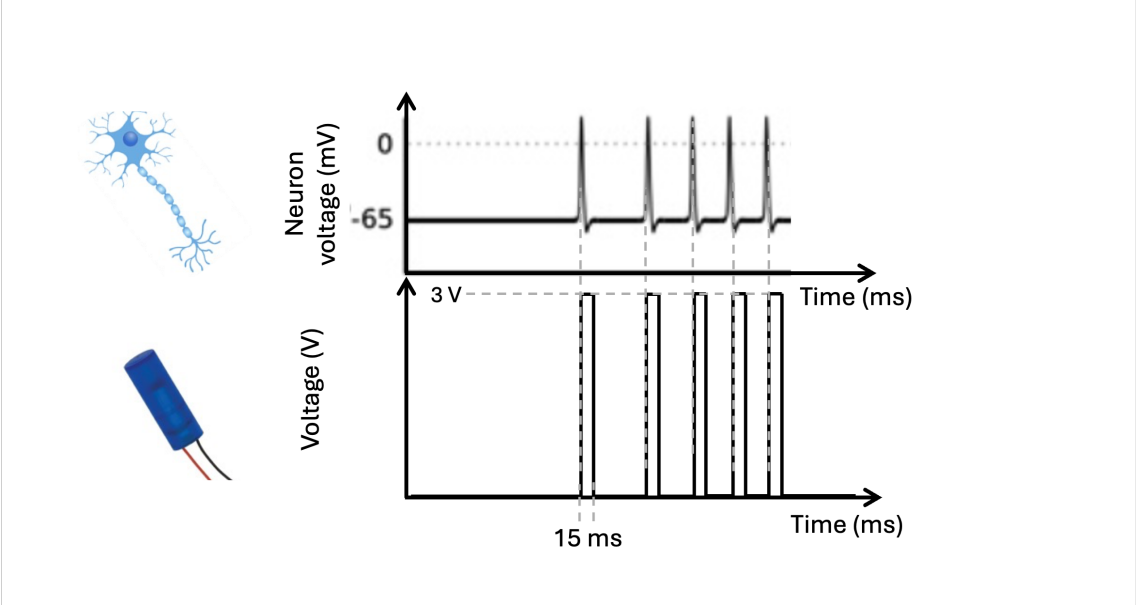

Fig. 3.1 The figure illustrates the spike strategy, in which each detected motor unit (MU) action potential [14] triggers the activation of an eccentric rotating mass motor for 15 ms. This vibration pattern is designed to closely approximate MU activation (i.e., frequency). However, in the proposed experiment, the motor neuron activation pattern was not decomposed from EMG but simulated.

In the present work, we simulated the activity of two different MUs by activating stimulators in a physiological fashion. For this purpose, we limited the frequency range at which

[1]Vibration frequency and amplitude are not independent in ERM vibrating motors, so increasing the supply voltage of the motor increases both vibration frequency and amplitude.

bursts could be delivered to 4-18 Hz. Additionally, we set the difference in burst activity between the two stimulators, computed as right stimulator (RS) frequency minus left stimulator (LS) frequency, in the range $[-3, +3]$ Hz, with 1 Hz steps, resulting in 7 comparisons.

To assess the participants' ability to perceive these differences, we used a two-alternative forced-choice task, in which the two stimulators were activated simultaneously for 3 seconds. We selected a duration long enough to well perceive the lowest frequencies. Participants had to verbally report which of the two stimulators they perceived as activated at the higher frequency. The sequence of stimulation and subjects' response corresponded to one trial, and was repeated 280 times per condition (40 trials per each comparison), resulting in a total of 560 trials, with an inter-trial pause of 2 seconds (Fig. 3.2, Top).

To investigate the efficacy of the feedback delivered in different body location, Experiment 1 was performed in two different conditions: 1) with both stimulators on the same arm; 2) with one stimulator per arm.

In the first case, stimulators were placed on the lateral and medial aspect of the right forearm, corresponding to C7 dermatome (see Fig.3.2 Bottom, A); whereas in the latter condition, vibrators were placed one per arm, on the lateral aspect of the forearm (see Fig.3.2 Bottom, B). We selected to stimulate participants on the C7 dermatome as it has been shown to be the location on the arm with the highest spatial and temporal discrimination for vibrotactile stimuli [88]. When stimulators were placed on the same arm, we ensured that they were at least 8 cm apart to minimize the impact of one stimulator's vibration on the perception of the other [58]. The two conditions were evaluated in two different sessions, in a pseudorandomized order.

3.2.4 Experiment 2

In Experiment 2 we tested a "continuous strategy" in which stimulators were activated continuously for 1.5 seconds for each trial with a vibration frequency modulated to cover the entire operating range of the motors (40 Hz - 230 Hz). Being the vibration continuous and the frequency higher, we decreased its duration with respect to Experiment 1 to avoid habituation or annoyance. To map the activity of motor units on the stimulators' operating range, we used two different approaches:

1 *Flat approach*: we divided the motor's bandwidth into 15 evenly spaced intervals, so that each interval corresponded to a single step on the range of MU activity (4-18 Hz with 1 Hz step) maintaining a constant, flat difference between each interval (i.e., 13.6Hz).

2 *Percentage approach*: similar to the *Flat approach* but instead of a fixed increase between each interval, we used a percentage increase of 13.3%, so that every step is increased by the 13.3% of the previous one. The specific percentage value to cover the entire range of MU activity was selected using the following equation:

$$f(i) = f_0(1+p)^i, \qquad i \in [0 \div 14] \tag{3.2}$$

Where f_0 is the lowest value of the motor's frequency (corresponding to the lowest value of MU's frequency, i.e. 4Hz), $f(i)$ is the frequency associated with the $(i+1)^{th}$ MU's value, and p=0.133 is the constant percentage increment.

We report in Figure 3.3 all the vibration frequencies and duty cycle values associated to the MU discharge rate, for both *flat* and *percentage* approach. To assess the efficacy of this feedback strategy we adopted the same task as in Experiment 1, considering Flat and Percentage approaches as conditions instead of stimulator configuration. Based on the results from Experiment 1, in this case we considered only one configuration, i.e. one stimulator on each arm.

3.2.5 Data Analysis

Responses from all participants were merged for each condition of the two experiments and fit with a psychophysics sigmoid function [96] using a least-squares-based algorithm (Matlab R2022b, The MathWorks, Inc., Natick, Massachusetts, United States). 95% confidence intervals (CI) for the estimated parameters were also calculated.
The psychometric function P (where P is the probability of "right" as answer) was defined as follows:

$$P(MUd, PSE, EA) = \frac{1}{1+exp(-\frac{MUd-PSE}{0.5EA})}, \tag{3.3}$$

denoting MUd the Motor Unit Difference (independent variable), PSE the Point of Subjective Equality and EA the Esteem Accuracy. PSE refers to the frequency difference between the two stimulators in order to be perceived as having the same frequency (i.e. 50% of chance to say "right"). EA is the inverse of the slope of the curve (with a multiplication factor of 0.5), calculate at MUd=PSE, and is a measure of how steep the curve is. The smaller the value of EA, the more the esteem is accurate.

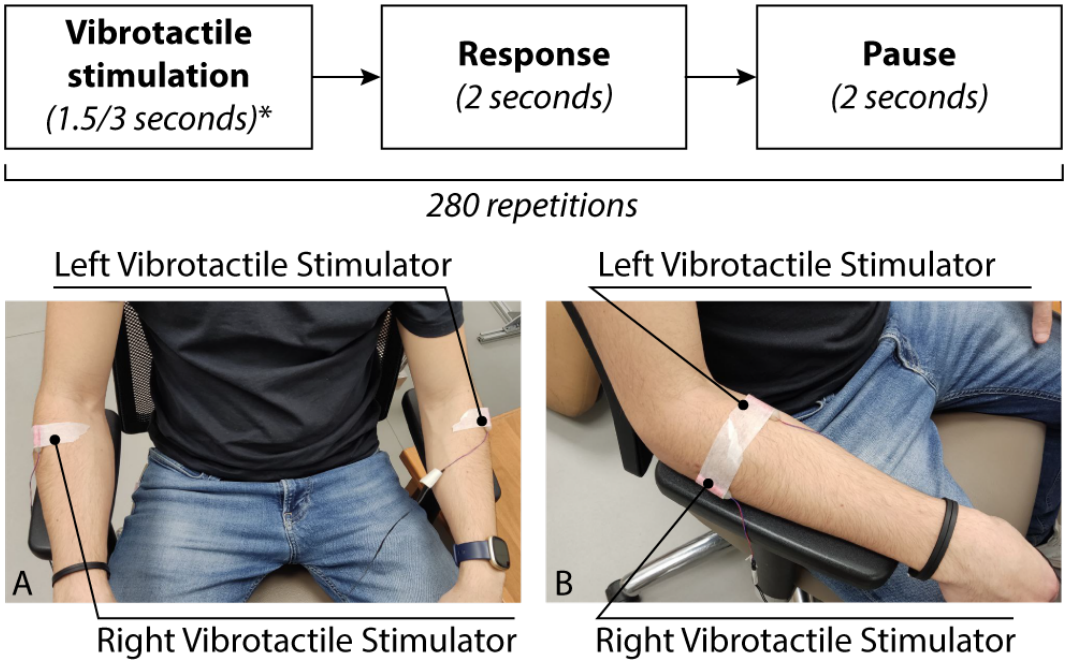

Fig. 3.2 Top: Experimental protocol. The two motors were activated for a brief amount of time (3 seconds in Experiment 1, and 1.5 seconds in Experiment 2). Participants were asked to indicate which stimulator they perceived to be vibrating at a higher frequency (right or left), typically within 1-2 seconds, followed by a brief pause. This sequence was repeated 280 times for each conditions, for a total of 560 trials in each experiment. Bottom: Stimulator's placement on two different arm for Experiment 1 and 2 (A), or on the same arm for Experiment 1 (B).

MU freq (Hz)	Flat approach		Percentage approach	
	Freq (Hz)	Duty cycle	Freq (Hz)	Duty cycle
4	40	0.1325	40	0.1325
5	53.6	0.1946	45.4	0.1572
6	67.2	0.2567	51.4	0.1846
7	80.6	0.3161	58.2	0.2156
8	94.2	0.38	66	0.2512
9	107.8	0.4421	74.8	0.2914
10	121.4	0.5042	84.6	0.3361
11	135	0.5663	96	0.3882
12	148.6	0.6284	108.6	0.4457
13	162.2	0.69	123.2	0.5124
14	175.8	0.7525	139.6	0.5873
15	189.4	0.8137	158	0.6713
16	203	0.8758	179.2	0.7681
17	216.6	0.9379	203	0.8767
18	230	1	230	1

Fig. 3.3 In the table is shown the relation between MU's frequency and the continuous vibration of Experiment 2. More in detail, column 1 is the MU's frequency, column 2 and 3 are respectively the stimulator's frequency and the duty cycle (see equation 3.1) of the PWM control signal for the flat approach. Column 4 and 5 are the same as 2-3 but for the percentage approach.

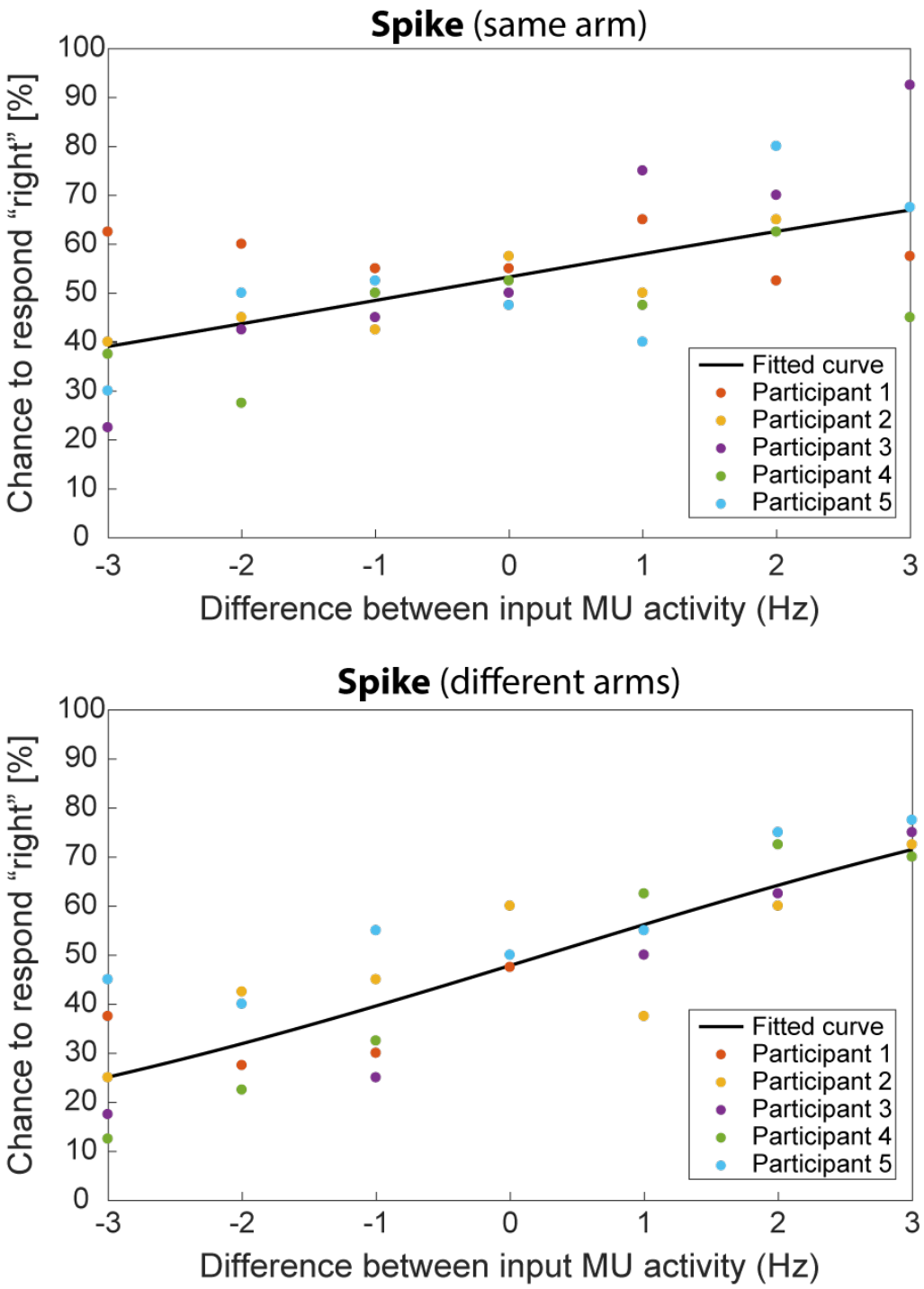

Fig. 3.4 Results of Experiment 1, representing the psychometric curve for the "spike strategy" with stimulators on the same arm (top) or on different arms (bottom). The continuous line represents the fitted equation (as described in Equation 3.3), and the dots represent the mean performance of the subjects for the relative difference of MU activity. X-axis is the difference in the activation of the stimulators, computed as RS - LS, and expressed in Hz. Y-axis is the chance that participants report the RS as the one with the higher vibration intensity.

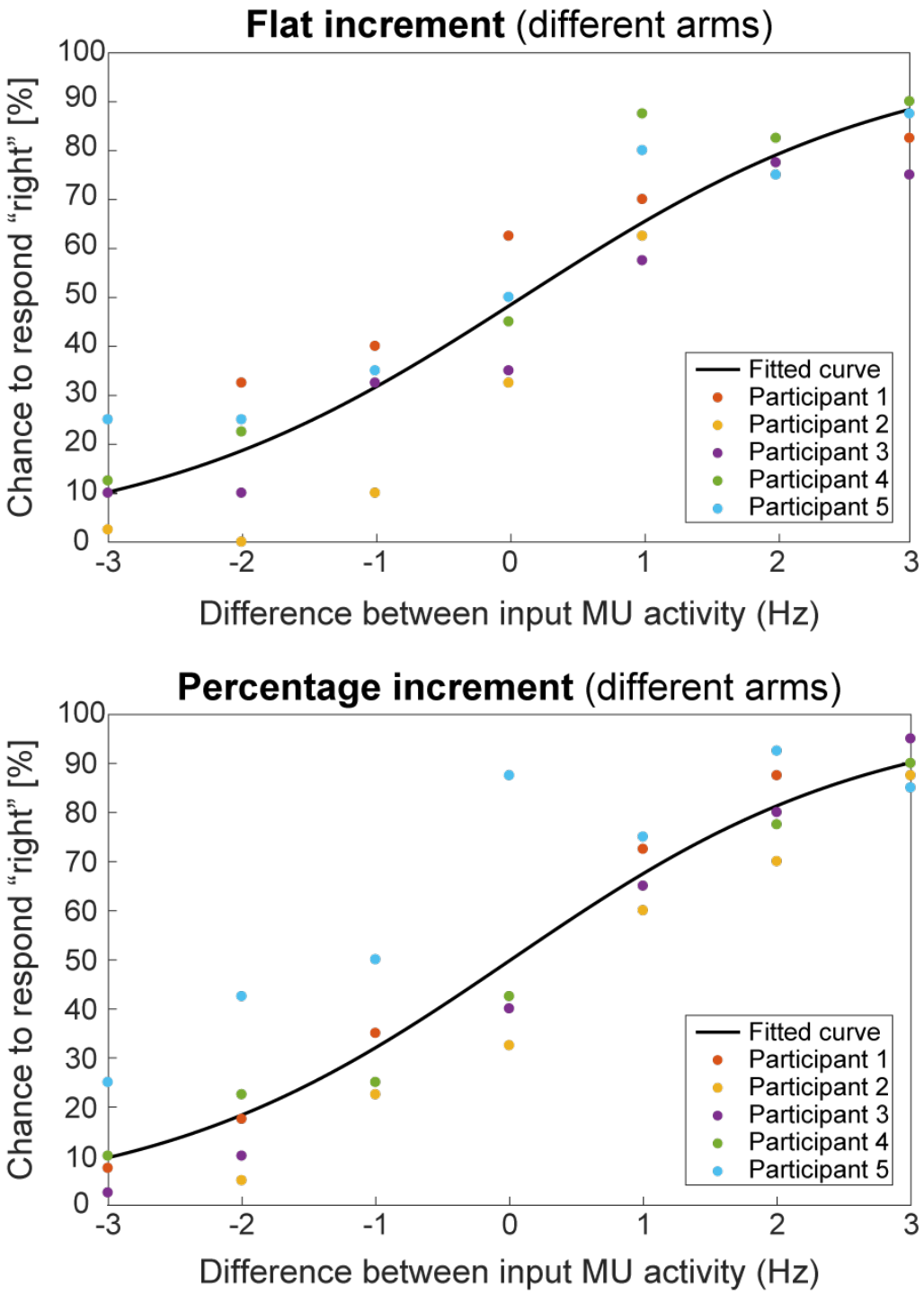

Fig. 3.5 Results of Experiment 2, representing the psychometric curve for the "continuous strategy" with using a Flat increment approach (top) or a Percentage increment approach (bottom). The continuous line represents the fitted equation (as described in Equation 3.2), and the dots represent the mean performance of the subjects for the relative difference of MU activity. X-axis is the difference in the activation of the stimulators, computed as RS - LS, and expressed in Hz for the Flat approach (top) or as percentage increment for the Percentage approach (bottom). Y-axis is the chance that participants report the RS as the one with the higher burst activity frequency.

3.2.6 Results

Experiment 1

The results of Experiment 1 are shown in Fig. 3.4. It is visible how participants' responses were quite spread, especially in the case of *same arm* condition. The fit with the sigma-shaped psychometric curve was poor, as indicated by the AE values obtained. Specifically, AE values were 5.96 Hz (CI 4.56–7.36 Hz) and 10.43 Hz (CI 8.10–12.77 Hz) for the *different arms* and *same forearm* configurations, respectively. This is also supported by visual inspection of the figure, where the characteristic S-shape of the sigmoid curve is not apparent. Moreover, even though one participant (participant 3, Fig. 3.4) reached values of 20% and 90% for the biggest frequency differences, in the *same arm* condition, the overall fitting ranged between 40% and 60%, thus very close to the situation in which subjects reply randomly. In the case of *different arms*, data were slightly less scattered and the fitting range widened to 25-70%.

Experiment 2

The results of Experiment 2 are shown in Fig. 3.5. The performances of the two conditions are close, both ranging between 10% and 90%. A small difference emerges from the slope analysis: the curve related to the *percentage approach* (Fig. 3.5, Bottom) is slightly steeper than the one related to the *flat approach* (Fig. 3.5, Top). This is also evident from the EA values of the *percentage approach* (2.70 Hz), (CI 2.51-2.8868 Hz) which is smaller than the one of the *flat approach* (2.85 Hz), (CI 2.26-3.43 Hz) (see Eq. 3.3).

3.3 Characterization of electrotactile stimulation intensity to exploit the funneling illusion*

3.3.1 Participants

Six healthy volunteers (3 females, 29 $\pm$ 3.7 years old) participated in the experiment, after having provided written informed consent. The experimental protocol was approved by the Ethics Committee of Newcastle University (23-041-NOC) and conducted according to the ethical standards of the Declaration of Helsinki.

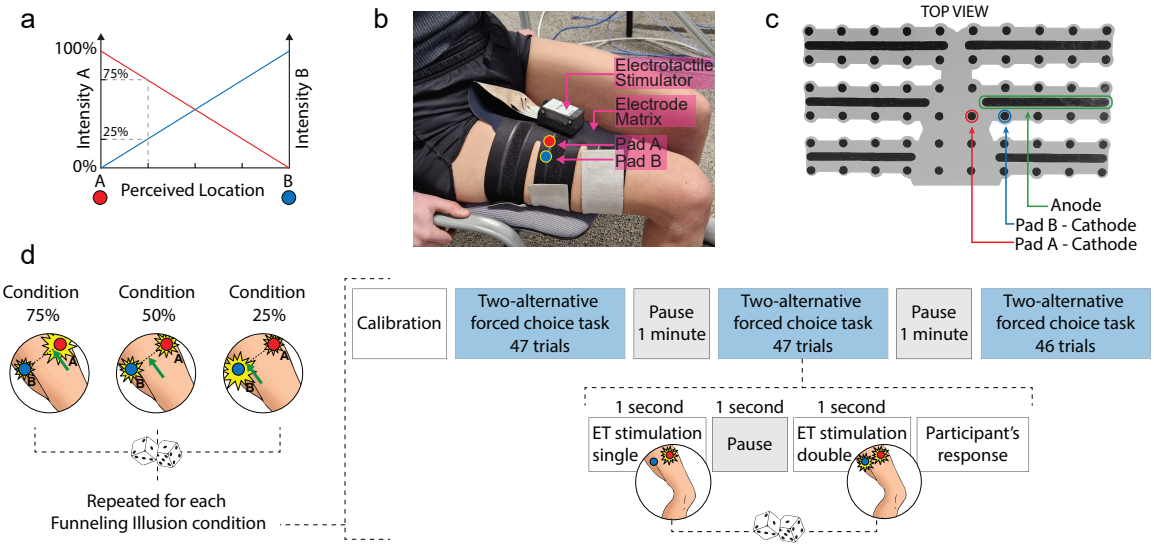

Fig. 3.6 a) Scheme of the funneling illusion phenomenon. The perceived location should move linearly from A to B by linearly varying the intensity of stimulus A and stimulus B from 100% to 0% and vice-versa. b) Photograph of the Experimental Setup. The participant sat on a chair wearing the electrode matrix on the right thigh. The matrix was connected to the electrotactile stimulator. In red and blue, respectively, are highlighted the position of the two pads (A and B) employed for the experiment. c) Detail of the electrode matrix with the anode and cathode pads highlighted. d) Experimental protocol. The experiment consists of three sessions in random order, one for each Funneling Illusion condition (75%, 50%, 25%), illustrated in the upper part. The red and blue dots indicated with A and B respectively represent active stimulation pads and the green arrow indicates the perceived position of the stimulation as a result of the illusion. The percentage shows the distribution of the stimulation intensity between the two pads. Each session is preceded by a calibration to set sensitivity and discomfort thresholds. Within each experimental session, the Two-alternative forced choice tasks are organized in three blocks (47 or 46 trials each), intermingled with a 1-minute pause, for a total of 140 trials. During each block, a 1-second stimulation is delivered with a single pad (reference) and after a 1-second pause, another stimulation is delivered through both pads. The order of single and double pad stimulation is randomized. The participant's response is collected immediately after the single-double stimulation dyad.

3.3.2 Experimental Setup

As depicted in Figure 3.6b, participants were seated comfortably in a chair while wearing an electrode suit fixed on their right thigh and connected to an electrical stimulator (Tecnalia Serbia Ltd, [12]). The suit consisted of 60 electrodes, each 1 cm in diameter, arranged in six rows of 10 electrodes with an inter-electrode distance of 4 cm.

The stimulator generates a biphasic current whose frequency, pulse width and amplitude could be independently modulated. Stimulation frequency and pulse width were kept constant for the all experiment and set to 30 Hz and 300 μs, respectively [11]. The amplitude, hereafter refer to as intensity, varied with the experimental conditions, as described in the following sections. To minimize skin-electrode impedance, the skin was cleaned and moistened with water before the electrode matrix was applied.

The stimulation parameters and experimental protocol were controlled via a custom graphical user interface (GUI) developed in C++ using Qt libraries and run on a Windows computer. The connection between the PC and the stimulator was established via Bluetooth.

3.3.3 Experimental Protocol

The experimental protocol consisted of three blocks, each one related to a different funneling illusion condition: closer to stimulus A (condition 75%), halfway (condition 50%) and closer to stimulus B (condition 25%) based on the proportion of activation between the two pads. The different phantom position were performed in counterbalanced order among participants. Each block started with a calibration phase followed by a two-alternative forced choice task (see fig. 3.6c).

Calibration

During the calibration phase, we identified for each electrode the intensity I_s corresponding to the sensation threshold (defined as the minimum current at which the participant reported feeling a sensation), and the discomfort threshold I_d (defined as the minimum current at which the sensation became unpleasant or annoying). During the experiment, the stimulation intensity was defined as a percentage considering the 0% corresponding to I_s and the 100% to I_d.

Once the discomfort threshold was identified, the related current was reduced by 0.1 mA. This reduction ensured to avoid actual discomfort throughout the experiment, particularly in the condition where the intensity might exceed the value of 100%. Note that, even if the

*This chapter is based on the article [27] (Accepted)

current was reduced, we will continue to refer to it as “discomfort threshold", for the sake of brevity.

A secondary calibration step was performed to equalize the perceived intensities of the two electrodes for both sensation and discomfort thresholds. To achieve this, the two electrodes A and B were sequentially activated multiple times at the same identified threshold (either I_s or I_d), and the current was fine-tuned until the participant reported equal perceived intensity at both locations. This step was crucial to prioritize the perceived intensity of the stimulation.

Two-alternative forced choice task

The 2AFC task consisted of a total of 140 trials per block, with a 1-minute pause every 47 trials to avoid participants' fatigue and habituation. Each trial involved a pair of 1-second stimulations separated by a 1-second pause (see Figure 3.6c). The participants were asked to verbally refer which of the two stimulations was perceived as more intense.

We asked participants to focus exclusively on the perceived intensity, regardless of the perceived location. However, we verified before and throughout the task, the occurrence of the funneling illusion, i.e., that participants actually perceived a single-point stimulation rather than two concurrent but distinct stimuli. No participants reported perceiving double stimulation (i.e., failing to experience the funneling illusion) during the experimental procedure.

Within each trial, the stimuli pair was composed of a reference stimulation (i.e., single electrode, A or B, activated at intensity 100%) and a two-pad stimulation. The two-pad stimulation was achieved by activating both pads simultaneously to create a phantom sensation, according to the funneling illusion. The intensity I of the the individual electrodes was defined according to:

$$I = \left(\frac{\text{Percentage Value}}{100}\right)(I_d - I_s) + I_s \tag{3.4}$$

The *Percentage Value* varied with the experimental conditions as described below:

$$\begin{aligned} \text{Percentage Value A} &= K_s \times \text{Level}\,; \\ \text{Percentage Value B} &= (1 - K_s) \times \text{Level}\,. \end{aligned} \tag{3.5}$$

Level varied in the range {50, 75, 100, 125, 150, 175, 200} and represents the overall two-pad intensity, that is the sum of the individual intensities I_A and I_B obtained in each condition.

K_s represents the distribution of the overall intensity between the two stimuli and was kept constant within each experimental condition (i.e., block). Three conditions were evaluated, corresponding to three distinct phantom positions:

- **Condition 75%:** Phantom sensation closer to pad A. $K_s = 0.75$
- **Condition 50%:** Phantom sensation located halfway between pad A and pad B. $K_s = 0.5$
- **Condition 25%:** Phantom sensation closer to pad B. $K_s = 0.25$

For example, in Condition 50%, the two pads were activated with the same intensity (always evaluated as percentage of the sensation and discomfort threshold range), while in Conditions 75% and 25%, the percentage of activation was divided asymmetrically between the two pads.

The output current for each trial was uniquely determined based on the experimental condition and the specified current level according to with eq. 3.5. It is worth noting that the choice of reducing the discomfort value during the calibration phase, aimed at avoiding actual discomfort in Conditions 75% and 25%, where the individual electrodes might exceed the 100% intensity. The reference stimulation was always performed activating a single pad at 100% intensity (i.e., corresponding to I_d).

Each level was tested 20 times per condition, balancing the reference pad across trials: 10 trials employed pad A as the reference and 10 trials pad B. The order of the stimulations was randomized, both in terms of intensity levels over trials and within trial in terms of order between of single (reference) and two-pad stimulation.

3.3.4 Data Analysis

Data analysis was conducted using Matlab 2022b and the three experimental conditions were analyzed separately. For each participant and intensity level, we computed the probability of perceiving the two-pad stimulation as having a higher intensity compared to the reference stimulation (i.e., single pad activated at 100% intensity). This process resulted in 6 data points (i.e., one per participant) for each current level. These data were then used to fit, through a least-squares algorithm, the sigmoid function [28]:

$$P(\text{Level}) = \frac{1}{1 + \exp\left(\frac{\mu - \text{Level}}{0.5 \cdot \sigma}\right)}, \tag{3.6}$$

where $P(\text{Level})$ is the probability that participants report the two-pad stimulation as more intense, based on the level of activation of pad A + pad B.

The parameter σ is the inverse of the slope, scaled by a factor of 0.5. A smaller σ value indicates a steeper curve. In contrast, μ represents the inflection point of the curve. Psychophysically, μ corresponds to the Point of Subjective Equality (PSE, i.e., the point where the probability is 0.5). The PSE represents the overall intensity level (pad A + pad B) at which participants perceive the two-pad stimulation as having the same intensity as the reference electrode. The *R-squared* (R^2) value was also computed to assess the goodness of fit.

3.3.5 Results

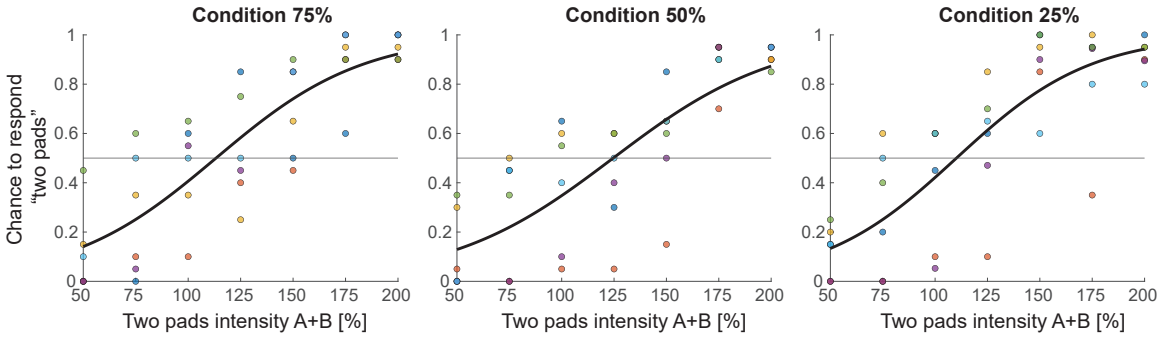

Fig. 3.7 Results for the condition (75%, 50%, 25%). Each dot represents the chance of perceiving the two-pad stimulation with higher intensity compared to the single reference pad, for each variation of the intensity sum of the two pads in the range 50% - 200 %. Different colors represent different participants. The black line represents the fitting curve obtained according to eq. 3.6.

Figure 3.7 illustrates the results of the three experimental conditions (75%, 50%, 25%). The x-axis represents the summed intensity of pad A and pad B in the two-pad stimulation, while the y-axis indicates the probability of perceiving the two-pad stimulation (i.e., phantom sensation) as more intense compared to the reference stimulation (i.e., the single pad, either A or B, activated at the discomfort level, that is intensity 100%). Individual participant data are shown as colored dots, with each color corresponding to a different participant. The black line represents the fitted model obtained according to eq. 3.6.

The intersection between the fitted curve and the horizontal line at 0.5, represents the Point of Subjective Equality (PSE). The x-coordinate of the PSE indicates the percentage level at which the two-pad stimulation was perceived as having intensity comparable to the one of the reference stimulation. PSE corresponds to the μ value and is reported in table 3.1 for the three experimental conditions, together with the parameters σ and R^2.

Conditions 75% and 25% show comparable PSE values (113% and 110%, respectively). Instead, condition 50% required a higher overall activation (124.6%) of the two pads to produce an phantom sensation with intensity comparable to the reference stimulation.

Similarly, the slopes of the curves, mathematically expressed by the σ values, appear to be similar across conditions. Nonetheless, condition 75% and 25% show slightly faster transitions, as confirmed by the a smaller σ value (i.e., the smaller the value, the steeper the function) compared to condition 50%.

In all cases, the mean performance ranged from 0.15 to 0.9, indicating that, in the limit cases, the difference between the reference stimulation and the phantom stimulation was sufficiently distinct to be recognized by participants well above chance level.

The goodness of fit, expressed through R^2 in table 3.1, ranged between 0.67 to 0.72.

Condition	**75**	**50**	**25**
μ	113.27	124.6	110
σ	70	78	64
R^2	0.72	0.67	0.68

Table 3.1 μ (i.e., PSE) and σ values obtained from the fitting of Eq 3.6 in all the experimental conditions.The goodness of fit is also reported as R^2

3.4 Discussion

In this chapter examples and rationals of how to refine and optimize supplementary feedback strategy was propose with psychophysical experiment based on a two-alternative forced-choice task. Moreover, two different examples of application and device were provided. In the first study, feedback strategy to convey the activation state (i.e., frequency) of motor units was provided. Both body location and type of feedback implementation were evaluated. The results of the spike strategy (i.e., when the motor unit activity is translated into the same pattern of burst) in figure 3.4 showed a trend which is far from the classical s-shape of psychophysical curve, with a central part quite flat. In particular, image 3.4 top, which is related to the same arm configuration, shows performances that are always around chance. In the the case two arms (i.e., one motor per arm), the situation seems better (figure 3.4 bottom). In this case is possible to find a clear pattern, both in the fitted curve than in the behavior of each participant. Nevertheless the performances are lower than expected, with an error always higher than 25 %. This difference in performance between the two conditions is also observable analyzing the estimated EA. In the case of same forearm EA is 10.43 (CI 8.10-12.77), while in the two arm condition is way smaller: 5.96 (CI 4.56-7.36). In the

second experiment, the firing rate was conveyed using a continuous vibration where each possible MU's firing rate value was associated with a well-defined continuous frequency value of the stimulator. In the first approach this relation was obtained by dividing all the working range of the motor into 15 equally distributed steps. In the second approach, a percentage value was calculated to pass from the minimum to maximum frequency value of the motor (see eq. 3.2, and table 3.3). In Experiment 2, participants exhibited higher accuracy and a greater percentage of correct responses in the all range.
Between the two mapping strategies (flat and percentage) the difference was small. Still, the percentage approach appears to work slightly better than the flat one as indicated by the accuracy values of 2.698 (CI: 2.509-2.8868) and 2.8547 (CI: 2.2754-3.4339) for the percentage and flat approaches respectively. The most noticeable difference between the two is the width of the CI, which is narrower for the percentage approach.

In the second study the characterization of the amplitude perception with the electractile feedback was performed to ensure a smooth transition between the single pad activation and the phantom one, ensuring a continuity in the perceived intensity with the idea of convey information about the state (e.g., end-effector position) of a supernumerary robotic limb. We evaluated the intensity perceived eliciting the funneling illusion at three different phantom locations (i.e., condition 75%, 50% and 25%). Our results suggest that, to match the single pad intensity, the combined activation of the two pads must exceed the total intensity of the single one, i.e., 100%. Specifically, our results show that the closer the phantom sensation is to the real stimulation, the lower the sum of the intensities A + B that matches the reference stimulus. Moreover, the condition 25% and 75% show a similar point of subjective equality (PSE), respectively of 110% and 113.27%. This is coherent with the symmetry in the distance between the phantom location and one reference pad. The point where the results shows an higher PSE in the condition 50% with a value of of 124.6%. These results brought to the idea that as the phantom position gets closer to one pad, the sum of the two activations should asymptotically approach the activation of that electrode. Furthermore, the point where the sum should be highest is the middle, i.e., the point where the minimum phantom-real electrode distance is maximized.

3.5 Conclusions

Although supplementary feedback plays a crucial role in both motor control and embodiment, research in the field of human movement augmentation has largely prioritized command interfaces over feedback systems. This imbalance may be attributed to the immediate and visible impact that command interfaces offer: they enable control, produce movement, and

provide measurable outcomes right away. In contrast, the value of feedback is more subtle, it is harder to quantify and cannot be assessed in isolation without a functioning control interface.

Another challenge is the complexity inherent in designing effective feedback systems. This is a highly multidimensional problem involving numerous factors such as stimulation site, encoding strategy, and the sensory modality employed [75]. Moreover, the final application context introduces additional constraints: different tasks may require distinct body parts for stimulation or demand specific types of sensory information. Thus, developing a universal feedback rule is nearly impossible. However, psychophysical findings from related studies may still offer useful insights, even across different contexts.

This chapter explored the importance of feedback configuration and its interaction with body location. In the first study using vibrotactile feedback with spike strategy, two motors were placed on the same arm. In this condition, participants performed close to chance level, likely due to the proximity of the motors, which made it difficult to differentiate their output 3.4 top. When the motors were placed on different arms, performance slightly improved 3.4 bottom, but without reaching a sufficient performance. Indeed, for a successful application, participants should be able to reliably distinguish even a 1 Hz difference, since MU firing frequencies are usually very similar and large differences are uncommon. However, our results showed performance close to chance with 1 Hz of difference and error rates above 25% even with a 3 Hz difference.

To address this, a second experiment introduced a different encoding method: instead of short bursts, motors were activated with continuous vibration. Each motor's frequency corresponded to a specific motor unit firing rate, tested using two mapping strategies: flat and percentage approach. As illustrated in the results (and Figure 3.5), this method led to higher accuracy, suggesting a more robust and effective feedback encoding approach.

In a separate study, we performed a psychophysical assessment of the funneling illusion for the electrotactile stimulation. The goal was to leverage this illusion to improve spatial resolution without introducing inconsistencies in perceived intensity. Discontinuities in sensation could reduce the clarity of feedback and act as confounding factors. Our results underline the importance of carefully calibrating electrotactile stimulation to ensure perceptual continuity.

While our focus was primarily on intensity perception, it is equally important to characterize how stimulation affects perceived location. This is a crucial step toward real-world applications where precise spatial resolution is necessary.

Finally, it is worth noting that all experiments were conducted in simplified settings where participants were asked to focus solely on the feedback, and without moving. In actual

applications, feedback will be used concurrently with ongoing motor activity in a closed-loop control system. Therefore, even though our psychophysical findings are promising, definitive validation should take place in the final, task-relevant setting under realistic conditions.

Some examples of augmented tasks where supplementary feedback was introduced to close the loop will be presented in the following chapters. It is important to note, however, that the feedback used in those experiments is not one of the techniques evaluated in this chapter. The characterization of participants' perceptual abilities presented here was performed in the context of other studies (e.g., the study [14]) outside this thesis, and was included as an illustration of how complex feedback strategies can be designed and assessed, for instance, when dealing with intricate approaches such as the spike strategy or with demanding technologies like electrotactile stimulation.

Moreover, in Chapters 4, 5, and 6, vibrotactile feedback was selected. This choice reflects the practical advantages of vibrotactile stimulation: it is simple to implement, does not require precise calibration, and is well-suited for tasks where the feedback to be conveyed is relatively low-dimensional. In these experiments, the information was relatively simple, and continuous vibrotactile stimulation was selected. Since human perceptual abilities with continuous vibration are well documented in the literature (e.g., [64]), no additional characterization was deemed necessary prior to these experiments.

Chapter 4

Effect of vibrotactile feedback on the control of the interaction force of a Supernumerary Robotic Arm*

4.1 Introduction

In the previous chapter, we explored the design and characterization of supplementary feedback strategies. While those studies provided valuable insights into the perceptual aspects of the feedback, they did not address how such strategies perform when integrated into a closed sensorimotor loop. Therefore, in this chapter, we assess the behavioral impact of a simple vibrotactile feedback on the user's ability to regulate the interaction force between a wearable Supernumerary Robotic Limb (SRL) and the environment.

The SRLs worn as wearable devices naturally provide visual and haptic feedback on the user's body, which perceives not only the presence of the robot but also part of the interaction forces that arise from the contact of the SRL with the environment through the mechanical coupling to the human body. This type of sensation is called inherent feedback since it provides the individual with intrinsic information naturally available when wearing the device. This type of feedback was recently investigated by Guggenheim and Asada [40], who demonstrated that the inherent feedback provided by the SRA on the users' lower back would be sufficient for a user to control the output force at the SRA end-effector level. Nonetheless, this result was obtained with a simple rigid 1 DoF robotic arm, an optimized fixation to the operator's body and a simplified task with the robot end-effector being attached to the

*This chapter is based on the article [16].

As a co-author, my contribution focused on the development of the experimental setup, particularly the supplementary feedback, the definition of the protocol, the data analysis, and the revision of the manuscript.

environment. Considering more realistic scenarios with heavy multi-DoF reconfigurable robots and intermittent interaction with the environment, the question of providing the operator with additional feedback cues, as well as which type of cues to rely on, remains open.

In these application scenarios, the operator often has no information on the interaction between the SRA and the environment, except through visual feedback. However, visual feedback alone is often insufficient to complete complex tasks, especially when vision is occluded or when the environment is rigid and does not visibly deform under force. In such cases, it becomes impossible to estimate the amount of force applied based on vision alone. Conversely, haptic feedback can provide this missing information by offering a direct perception of contact forces even in the absence of visual cues.

One of our hypotheses was that inherent feedback is sensitive to the variability of several external environment parameters, such as the mechanical characteristics of the interactive environment (i.e. rigid versus soft contact interface) or some characteristics of the SRA such as its geometrical posture or its joint compliance. In this study we therefore tested whether inherent feedback is informative enough to provide a precise perception of the SRA interaction forces or if an additional explicit feedback of the interaction force can help improving the robustness of user's perception. In fact, we believe that relaying simple additional artificial sensory feedback to provide users with the rich sensation of the force exerted by a SRA is essential for bringing human sensorimotor augmentation to the next level, in which humans can effortlessly feel through and control SRAs as part of their own body.

This research aims therefore to assess, in a simplified but realistic scenario, the usefulness of relaying information of the force applied by an SRA when interacting with the environment, through a supplementary vibrotactile feedback providing a simple, yet informative, sense of the level of the force applied by the user on the environment at the SRA end effector level. Vibrotactile feedback was chosen because it is painless and can be easily modulated and delivered, since it does not require a subject-specific calibration (as it happens with electrotactile feedback, see section 3.3). Additionally, vibrotactile feedback has proven to be effective as supplementary feedback to improve motor control and motor learning in both healthy and impaired people [80, 23, 58]. Moreover, while it could provoke adaptation in the long run, our extensive experience with this vibrotactile feedback has proven that it is never the case when continuous stimulation is frequently interrupted, as in experimental protocol when switching between trials [76, 72, 28].

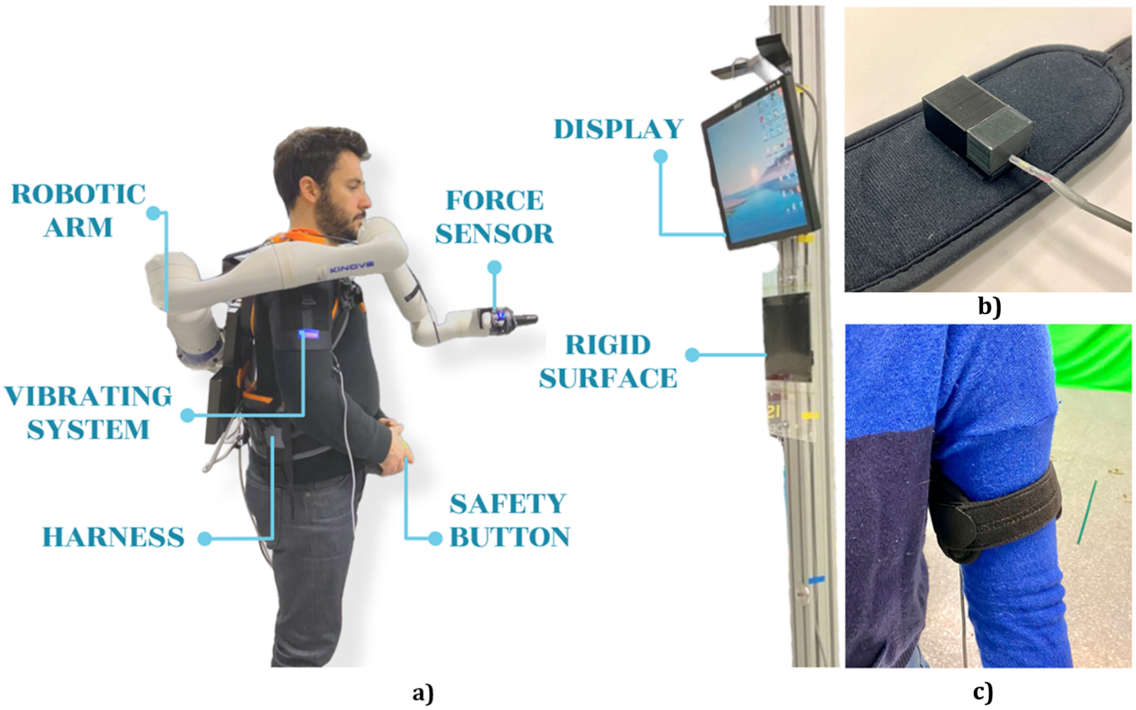

Fig. 4.1 (**a**) Scheme of the experimental setup; (**b**) the vibrotactile feedback system; (**c**) how the vibrotactile system is mounted on the participant arm: the case and the elastic band.

4.2 Methods

4.2.1 Participants

Thirteen participants (eleven males, two females) aged over 18 years (mean age 23.8 $\pm$1.4 years) participated in the experiment, after having provided written informed consent. The experiment was approved by the Sorbonne Université research ethics committee (CER-SU) and conducted according to the Declaration of Helsinki.

4.2.2 Experimental Setup

During the experiment, the participant stood in front of a vertical surface with a display (placed at the head level) while wearing the SRA which remains still in a predefined position (see Fig. 4.1 (**a**)). The participant could control the end-effector position using their body movements in order to apply a force with the SRA end-effector against the vertical surface (whose compliance can be changed from rigid to soft and vice versa). Participants were asked to exert specific amounts of force, as displayed by the graphical user interface (GUI).

The SRA is composed of the 7-DoFs robotic arm Kinova Gen 3 Ultra lightweight attached to a modified Pellenc comfort harness developed by the AGATHE team of ISIR-SU [55]. This robot form factor, lightweight, and default hardware make it safe for cobotic applications (ISO TS 15066) in close interaction with the human body. The robot is turned on during the experiment but it remains still in a given posture (achieved through joint position control), behaving like a rigid tool attached to the body. The SRA end-effector is equipped with a Robotiq FT 300-S 6-axis force sensor, characterized by a sampling rate of 100 Hz and a resolution of 0.0091N, to measure the force applied by the end-effector to the environment.

The vibrotactile feedback system is composed of an electronic board and a vibrating system and has been developed by improving a previous system [78, 76, 72]. The electronic board includes 3 motor drivers (L2293Q by STMicroelectronics) to independently control up to 6 motors, a microcontroller unit (MCU)(STM32F446 by STMicroelectronics), an FTDI module (FT232RL by FTDI Chip), voltage regulators, a battery charger and a module for Bluetooth. The electronic schematic and board were realized on the EAGLE software (by Autodesk, Inc.).

In the present work, only one motor has been employed. The vibration motor (Model: 307-103 by Precision Microdrives Inc.) was placed in a 3D printed case equipped with an elastic band (see Fig. 4.1 (**b**)). The case has a parallelepiped shape to maximize the contact surface with the body, a cylindrical hole that holds tightly the vibrator motor, avoiding any vibration waste inside the case, and a small hole to tighten the cable. The vibrotactile stimulator was placed on the bicep of the preferred arm (see Fig. 4.1 (**c**)), according to [4] which demonstrated a high tactile acuity in this region.

On the display placed in front of the user, a GUI, shown in Fig. 4.2 (**a**)(**b**)(**c**), provides the user with the task instructions (i.e., to exert with the SRA the amount of force highlighted on the monitor), together with a bar displaying the norm of the forces measured at the end-effector through the sensor. In particular, 3 different force levels are highlighted with an arrow-shaped text and a different colour of the bar: Low Force (in green), Medium Force (in yellow) and High Force (in red). Each level is a force interval that consists of a fixed mean threshold (7N, 14N, 21N, represented by a thick dashed line) and a standard deviation of $\pm$2N (represented by two thin dashed lines). Additionally, we considered a Rest Level with a threshold of 0N and a deviation of +2N only in the positive range, to discard the non-contact case.

4.2.3 Vibrotactile feedback and data Processing

The interaction between the SRA end-effector and the vertical surface is measured by the FT sensor. The output is a 6x1 force and torque vector which is serially received by a computer

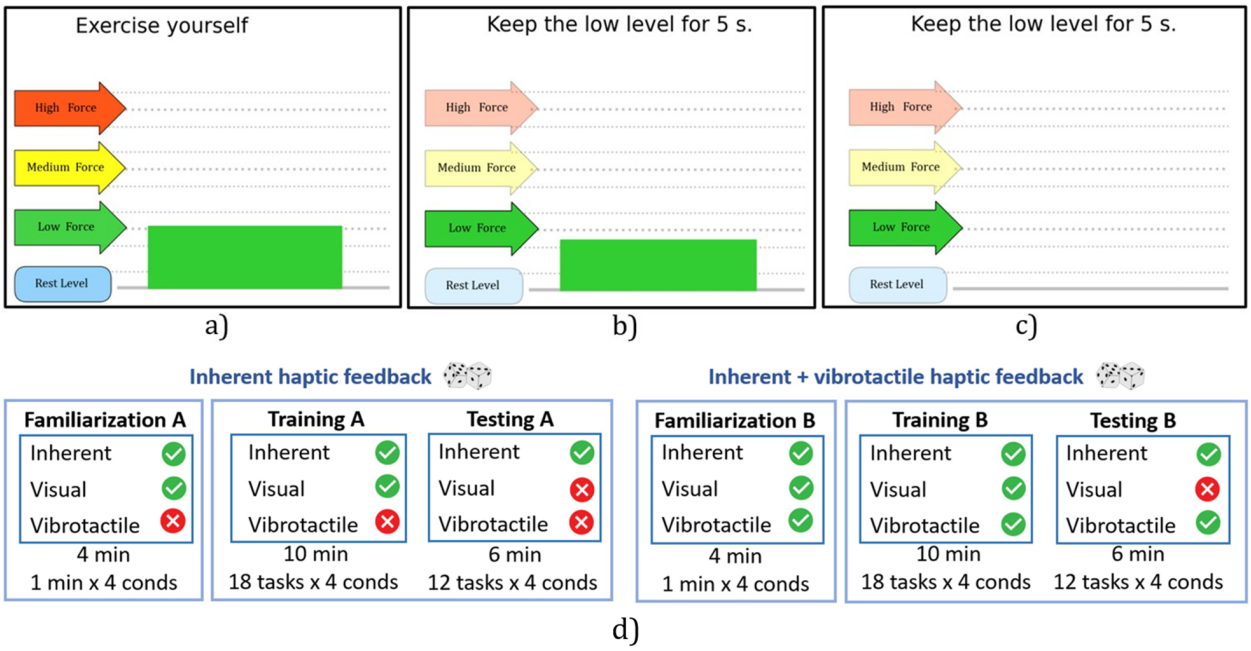

Fig. 4.2 Graphic interface during the familiarization (**a**), training (**b**) and testing (**c**) session. The level to reach is highlighted (training and testing sessions) with a darker colour of the arrow. (**d**) The experimental protocol was divided in two blocks presented in a randomized order: with the inherent haptic feedback alone and with the addition of the vibrotactile haptic feedback. In both blocks the subject faces a familiarization, a training and a testing session.

a) b) c) d)

Fig. 4.3 (**a**) The *centered* and (**b**) the *lateral* kinematic configurations of the SRA from a front view. The vertical surface (**c**) without the foam (*rigid*) and (**d**) with the foam (*compliant*).

and processed by a Python script. Specifically, it computes the norm of the forces, filters (Butterworth low pass filter, 1st order, 20Hz) and both shows it on the display through the coloured bar and drives the vibrotactile system through communication with the MCU.

Using STM32CubeMX and an IDE based on Eclipse called SW4STM32, the MCU on the board was configured to receive the norm of the force value through serial communication. It then delivers to the motor drivers a Pulse Width Modulation (PWM) signal, whose duty cycle, proportional to the force value, accordingly modifies the velocity of the rotating mass and thus the intensity of the vibration. In order to cover the entire span of duty cycle the motors can operate with, the following linear mapping was used:

$$\delta(t) = \delta_{min} + \left| \frac{F(\delta_{max} - \delta_{min}))}{F_{max}} \right| \tag{4.1}$$

Where δ is the duty cycle of the PWM, $\delta_{min} = 0$, $\delta_{max} = 1$, they define the range of possible values of the duty cycle, while F is the force measured, with $F_{max} = 30$ N the maximum value.

4.2.4 Experimental Protocol

The task consisted of reaching, as fast as possible, the force level highlighted in the GUI (Fig. 4.2 (**a**)(**b**)(**c**)) by pushing with the robot end-effector against the vertical surface, and maintaining the required force level until the end of the trial, which lasted 5 seconds. After that, participants had 3 seconds to return to the rest level, in order to start each trial from

the same starting condition. Each level of force (three levels in total) was repeated the same number of times in a random order.

Additionally, to evaluate the participants' ability in controlling the interaction force in different environmental situations, we used foam to change the stiffness of the vertical surface from *rigid* to *compliant* (Fig. 4.3 (**c**)(**d**)) and we modified, through the KINOVA® KORTEX™ Web App, the robot posture from a *centred* (end-effector placed in front of the participant at the sternum level) to a *lateral* (Fig. 4.3 (**a**)(**b**)) configuration.

Those postures were chosen because they would provide different inherent feedback. Additionally, they avoid any unforeseen contact between the SRA segments and the participant's body during the experiment, taking into account different body sizes.

Hence, for each parameter (i.e., *SRA kinematic configuration* and *stiffness of the environment*) we tested two different conditions (i.e., *centred/lateral* and *rigid/compliant*, respectively), resulting in four possible combinations that each participant faced in random order during each experimental session.

The experimental protocol is repeated twice, one for each feedback condition in random order: *with vibrotactile and inherent feedback* and *with inherent feedback only*.

As depicted in Fig. 4.2 (**d**), each experimental block unfolds in the following way:

- Familiarization session.
  Participants experience 1 minute in each of the 4 combinations while controlling the SRA with their body to exert a force against the vertical surface and observe on the graphical interface the amount of force exerted (Fig. 4.2 (**a**)).

- Training session.
  Then, participants are asked to execute the task 18 times, 6 for each force level, for each of the 4 combinations of conditions. Thanks to the visual feedback provided through the GUI (Fig. 4.2 (**b**)) they are able to check the level of force exerted.

- Testing session.
  Finally, participants perform the task 12 times, 4 for each force level, repeated for each of the 4 combinations, without any visual feedback of the level of force exerted (Fig. 4.2 (**c**)).

At the end of the two blocks (with and without the vibration feedback), the participant fills a questionnaire based on a 5-points Likert scale (1 = a very little, 5 = a lot). The four most relevant questions to evaluate participants' perception about the usefulness of the feedback were:

- How much did you find the vibration helpful?

- How much did you find the inherent sensation helpful?
- How much was the vibrotactile feedback useful to adapt to the different conditions?
- How much was the inherent sensation useful to adapt to the different conditions?

4.3 Analysis

The force data collected were analyzed with Python scripts, while the statistical analysis was performed on JASP (Version 0.13.1—Amsterdam—Netherlands). All the force data have been preliminary filtered using a 1st order Butterworth Low Pass filter with a cut frequency equal to $45Hz$.

Four metrics have been extracted from the force data (always considering the norm of the force on the three axes) of the testing sessions:

- The *average error* (e): the difference between the requested and the actual force, computed and averaged for each trial from the moment the participant reaches for the first time the requested force interval to the end of the trial;
- The *normalized error* ($||e||$): the *average error* divided by the requested force level;
- The *maintaining time* (t): the sum of all the time intervals in which the participant maintained the exerted force within a band of ± 2 N around the requested one;
- The *settling time* (ts): the time from the instant in which the participant overcomes 10% of the requested force level until the moment when they maintain the requested level for at least 0.15 s.

The normality of the data distribution was assessed using a Shapiro-Wilk test ($p-value > 0.05$). If the data distribution resulted to be not normal, the log10 transformation was applied. After transformation, the data exhibited a normal distribution. Statistical differences among conditions have been tested using a three-way Repeated measures ANOVA with the feedback (*vibrotactile + inherent* and *inherent*), the environment stiffness (*rigid* and *compliant*) and the robot posture (*centred* and *lateral*) as factors.

4.4 Results

4.4.1 Overview of force profiles

Fig. 4.4 shows the norm of the force collected during the training and testing sessions in both *inherent* and *inherent+vibrotactile* conditions, for one repetition of a representative participant. In the training sessions, in which they are provided together with the visual feedback of the exerted force, (Fig. 4.4 (**a**)(**b**)) the measured forces (blue) seem to follow the requested levels (green) regardless of the conveyed haptic feedback. It is evident how in the testing sessions, where the visual feedback is absent, the removal of the vibrotactile feedback (Fig. 4.4 (**d**)) leads instead to an increase in the error, with the exerted force regularly reaching values over 50N while maximum requested level was 21N $\pm$ 2N (see Fig. 4.4 (**c**)(**d**),).

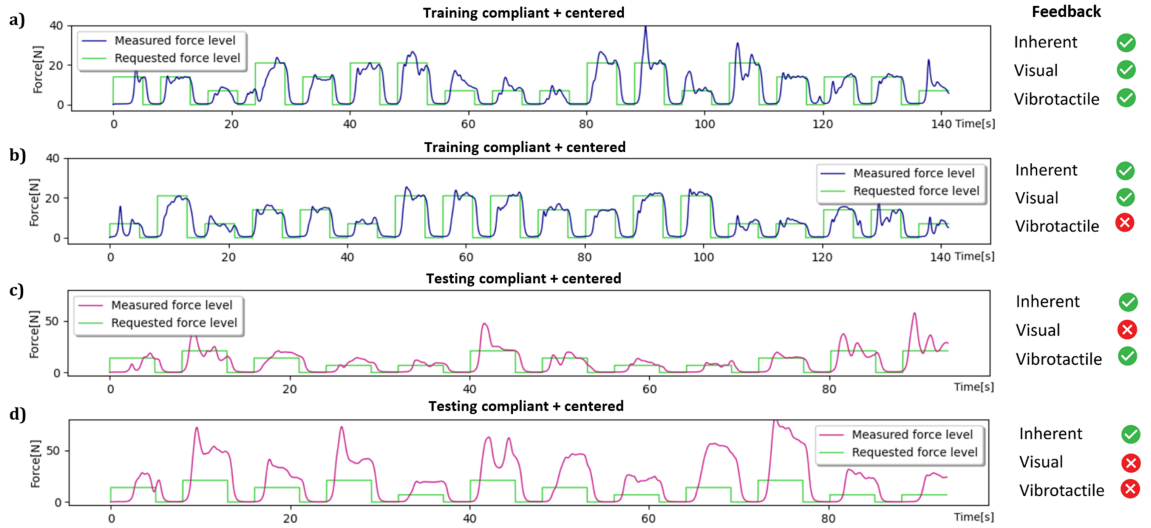

Fig. 4.4 Example of force profiles of one participant during a training session (**a**) (**b**) and a testing session (**c**) (**d**) obtained in the two feedback conditions (*inherent* and *inherent+vibrotactile*), with the same combination of conditions (*compliant* vertical surface and *centered* kinematic posture). On the right is highlighted with the green tick the feedback available while with the red cross the feedback unavailable. The threshold of the requested level of force is represented by the green line and the measured (and filtered) level of force respectively by the blue lines for the training sessions and the pink ones for the testing sessions.

4.4.2 Effect of the variation of environmental parameters

Considering the results averaged over the group of 13 participants, no significant effect of the surface stiffness (*rigid* and *compliant*) or the robot kinematic posture (*centred* and *lateral*) nor the interaction between factors was observed on the overall performance (Fig. 4.5).

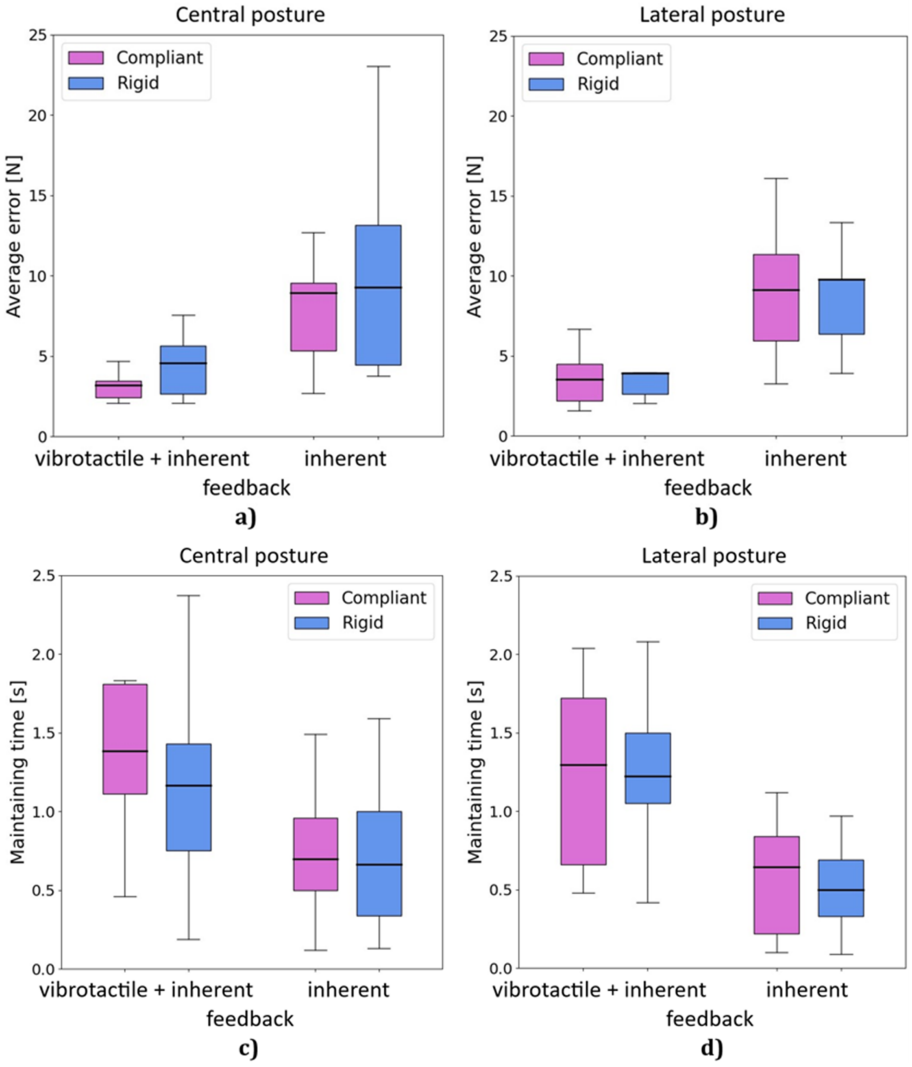

Fig. 4.5 Performance comparison between the two feedback conditions and for different environmental conditions (i.e. stiffness level and SRA posture) in terms of (**a,b**) average error, and (**c,d**) maintaining time. The mean and the standard deviation of the metric over all the trials and participants with the same conditions is shown.

4.4.3 Effect of the feedback

We found an effect of the feedback condition on the performance. Specifically, a statistically significant difference between feedback conditions (*inherent* and *inherent+vibrotactile*) was observed on all metrics as shown in Fig. 4.6. The presence of vibrotactile feedback significantly enhanced performance by reducing both the average and normalized errors. In addition, the feedback increased the maintaining time and reduced the settling time. A summary of these results is provided in Table 4.1.

Table 4.1 Effect of feedback condition on performance metrics (mean values ± statistics).

Metric	**Inherent**	**Inherent+Vibrotactile**	F	p
Average error [N]	9.271	3.81	38	<0.001
Normalized error [$-$]	0.72	0.311	42	<0.001
Maintaining time [s]	0.627	1.227	26	<0.001
Settling time [s]	2.96	2.34	16	0.002

4.4.4 Subjective perception of participants

The answers from the questionnaire are summarized in the pie charts presented in Fig. 4.7. At the question *"How much was the vibration helpful?"* 100% answered either 4/5 or 5/5, while at the same question with "inherent sensation" 77% answered with 3/5 or less. At the question *"How much was the vibrotactile feedback useful to adapt to the different conditions?"* 100% answered 4/5 or 5/5, while at the same question with "inherent sensation" 85% answered 3/5 or less.

4.5 Discussion

In this study, we assessed the impact of a supplementary vibrotactile feedback on the control of a wearable SRA during a force regulation task, compared to the condition in which only the inherent feedback (due to the contact between body and robot) is present.

Examining the force profiles illustrated in Fig. 4.4, it is evident that during the training sessions, with the visual feedback, the user effectively reaches and maintains the desired force levels regardless of the feedback condition. On the contrary, during the testing session without the visual feedback participants performed worse when relying solely on the inherent feedback. In instances with inherent feedback alone, the participants struggled to consistently reach the requested force interval. However, the addition of the vibrotactile feedback mitigates this deficiency enabling them to successfully attain and sustain the desired force levels.

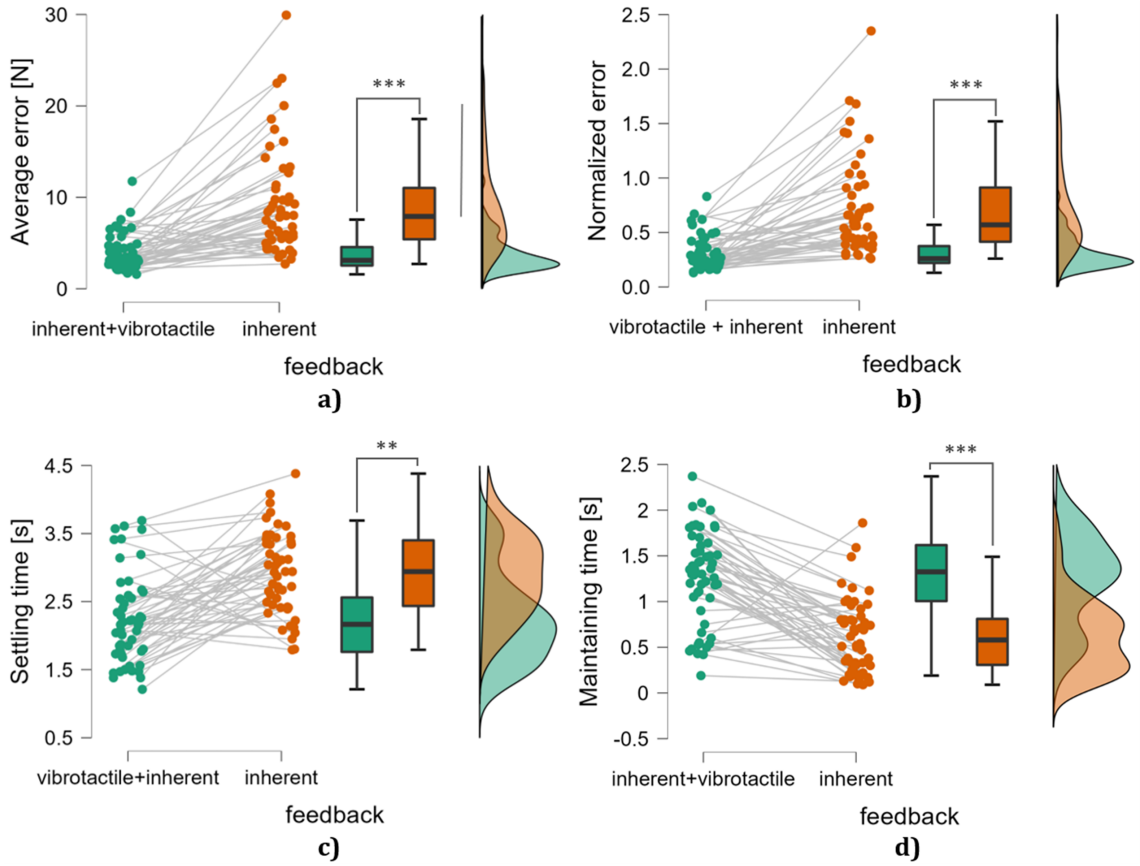

Fig. 4.6 Performance comparison between the two feedback conditions in terms of (**a**) average error, (**b**) normalized error, (**c**) maintaining time and (**d**) settling time. Each dot represents the mean of the metric over the trials with the same combination of conditions of one participant. These results are relative to all the participants, including both the stiffness and posture conditions. The asterisks (*) represent the p-value of the statistical test: * $p \leq 0.05$, ** $p \leq 0.01$, *** $p \leq 0.001$.

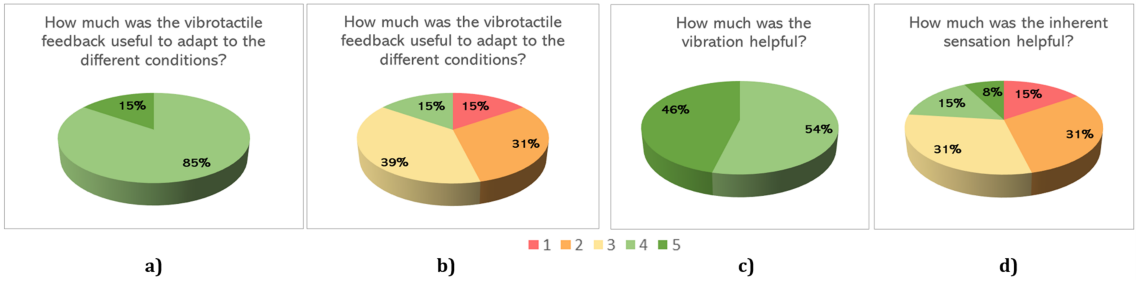

Fig. 4.7 The figure presents pie charts summarizing participants' responses to the questionnaires. Each chart corresponds to a specific question, reported above the pie. Colors indicate the rating scale from 1 to 5, as shown in the legend at the bottom of the figure. The size of each slice is proportional to the percentage of participants selecting that rating. Data are based on the responses of 13 participants.

From the statistical analysis, we obtained for all the analyzed metrics a significant improvement in users' performance due to the addition of the vibrotactile feedback. This result was supported by participants' perception, given that 100% of the users found the vibration useful during the experiment.

As regards the effect of the environmental conditions and their interaction with the feedback, we did not find any significant result as shown in Fig. 4.5. However, this could be due to the small dimension of the population, combined with the high number of conditions. Indeed, when receiving the vibrotactile feedback, participants not only perform better, but they seem to improve their performance even more when dealing with a compliant environment (Fig. 4.5). The questionnaire shows that 100% of the users felt a better ability to adapt to the different surface stiffness and robot postures with the addition of the vibrotactile feedback. One possible explanation is that relying solely on inherent feedback, consistently yields high error rates regardless of the object's properties, such as stiffness. This could have masked the difference between the different types of surface.

4.6 Conclusions

Supernumerary Robotic Limbs (SRLs), prostheses, and other assistive devices can greatly benefit from closing the sensorimotor loop. These types of devices inherently provide visual feedback and could provide intrinsic feedback, i.e., sensations arising at the physical interface between the user and the device. In many application scenarios, visual information or intrinsic feedback alone may be sufficient to achieve basic control of such devices [40].

Despite their utility, especially visual feedback has a significant limitation: it do not effectively convey the interaction forces with the environment. This limitation becomes

particularly critical in scenarios involving interaction with static or rigid environments, where it is difficult to infer contact forces based solely on visual deformation of the environment.

Although specific contexts, such as the one exemplified by Guggenheim et al. [40], may find inherent feedback satisfactory, our investigation shows that vibrotactile feedback allows enhanced performance in tasks involving force regulation.

A particularly relevant aspect of these results lies in the fact that all performance metrics showed improvement despite the simplicity of the implemented vibrotactile feedback system. This suggests that even a minimal and low-bandwidth form of feedback can have a meaningful impact on force regulation tasks. Such an outcome is especially promising for future applications where more complex or informative feedback modalities could be designed.

However, the experiment has been performed on a limited population but as future developments, it could be extended to more participants. Moreover, similar experiments should be conducted testing more variables and parameters: the ability of the users to adapt to the different environmental conditions using the vibrotactile feedback could be deepened, as well as the influence of the environmental stiffness and robot postures on the control of the application force. Also, the ability to perform a force application task actively controlling the SRA movements not only through body action, could be tested.

Another limitation lies in the fact that the arm remained still during the experiment. While this simplification does not fully reflect real-world scenarios, where arm movements could partly interfere with the perception of vibrations and reduce their effectiveness, previous studies (e.g., [Noccaro et al.], discussed in the following chapter) have shown that supplementary vibrotactile feedback can still provide a positive contribution to performance even when the limbs are moving.

These results validate our hypothesis that the inherent feedback might be not robust enough to be used alone and that the vibrotactile feedback (i.e., adding a supplementary feedback) could provide information on the interaction in an intuitive way. We thus believe that these findings provide preliminary evidence that supplementary feedback can have a tangible impact, not only from a theoretical perspective but also in practical, task-oriented applications, particularly in scenarios where users are required to exert or sense force during interaction with the environment.

Chapter 5

Vibrotactile feedback improves performance in 3-coupled trimanual tasks*

5.1 Introduction

Even when we move just one limb, the movement is never entirely isolated from the rest of the body. For example, executing a fast motion while standing still requires the activation of other body segments not directly involved in the task. This kind of coordination becomes even more prominent when multiple body parts must work together toward shared goals. As outlined in the Optimal Feedback Control theory, movements are coordinated because the motor output depends on the estimated state of the whole system (Section 2.2, Eq 2.6). This idea becomes especially important in Human Movement Augmentation, where, in trimanual tasks, the user is asked to concurrently control and coordinate three effectors. Given the complexity of the task, adding supplementary feedback could result in a better estimation of the system state (Section 2.2, Eq 2.5), and consequently in an overall increase in accuracy and dexterity, making the control more feasible, efficient, and potentially less demanding for the user [31]. Yet, assessing the human ability to perform such tasks underlies the whole field of human movement augmentation.

The few studies conducted in this respect fall under the category of augmentation by transfer. While the ultimate goal of HMA is to achieve real degrees of freedom augmentation, augmentation by transfer represents an important intermediate step with strong practical relevance. This approach exploits existing user movements rather than introducing entirely

*This chapter is based on the article [70] [Noccaro et al.] (under review)

new ones, which in many scenarios can still be highly valuable. It also enables research to advance by evaluating users' behavioral abilities within a more controlled and accessible paradigm, such as the one explored in this chapter. In fact, by leveraging movements that humans already perform with great proficiency, this strategy can reduce learning time while still providing meaningful augmentation.

Within this framework, previous studies showed that it is possible for people to simultaneously control three limbs in a virtual environment [1, 47], and even achieve higher performance than with two hands in a demanding catching task, with negligible physical and mental effort [2], especially after prolonged training

While participants were found to generally achieve better performance in trimanual tasks by sharing the control of the three limbs with another individual, this performance gap significantly decreases when the three (virtual) limbs are mechanically coupled together [71]. Furthermore, following appropriate training, participants showed an improvement of their initial augmented skills [5] in trimanual tasks both with and without mechanical coupling among the limbs, achieving performance comparable to the one of two collaborating persons when all the three limbs are coupled together [46].

Although providing a valuable contribution to the knowledge of the human ability to perform augmented tasks, these studies neglect a fundamental aspect of the sensorimotor loop, i.e., the sensory feedback related to the supernumerary limb. Indeed, sensory feedback has proven to be essential in closing the sensorimotor control loop and improving motor performance [77, 53, 79].

Therefore, in this chapter, we aim to address the relevance of supplementary haptic feedback in human augmentation, since haptics exploit a more discreet sensory channel, whose information travels along our nervous fibers faster than other sensory modalities, such as vision [22].

Specifically, we investigated the effect of supplementary vibrotactile feedback (see Chapter 4, Introduction, for the rationale behind its selection) across different experimental conditions. The central scientific question concerns how this feedback influences motor performance in trimanual tasks with different coordination constraints. In addition, we examined whether the impact of supplementary feedback differs when the task is performed individually (solo condition) or collaboratively, with control shared with a partner (dyad condition).

The supplementary feedback was delivered in the form of a vibrotactile stimulation encoding, with different patterns, the force applied to the effectors by the virtual mechanical coupling, the event of the breaking of this link and the collision between effectors. We evaluated the effect of the supplementary feedback on task performance, both in terms of

task-specific indexes (e.g., score) and motion characteristics (e.g., smoothness); moreover, we collected several physiological measures (such as electrocardiography, breathing frequency and electrodermal activity) to monitor the physical and cognitive burden caused by the augmented task, and to compare such measures with the subjective perception of enjoyment, difficulty and workload assessed through questionnaires.

5.2 Methods

5.2.1 Participants

Twenty healthy participants (aged 26.34 ±6.6 years, 14 women, 18 right-handed), randomly organized into dyads, were enrolled in the study after having provided written informed consent. The experimental protocol was conducted according to the Declaration of Helsinki and approved by the Ethical Committee of Università Campus Bio-Medico di Roma (HUROB protocol).

5.2.2 Experimental setup

The participants were comfortably seated on a chair positioned in the centre of a metallic structure equipped with 6 infrared cameras (Prime 13W by OptiTrack) operated with Motive software (NaturalPoint, Corvallis, Oregon, USA). Passive reflective markers were placed on participants' hands and dominant foot (determined according to the ball-kick dominant leg test [94]) so that cameras could track their movements. To avoid foot fatigue, the foot was also fixed to a slippery shoe liner which allows it to easily slide on the floor. The foot was selected as a controller for moving the third effector because lower limb movements are one of the most commonly employed control approaches in human augmentation [1, 47, 49], leading to good performance with a relatively short training time, even in dexterous and complex tasks such as laparoscopy [43]. Indeed, previous work in HMA demonstrated that other, more complex approaches (e.g., based on neural signals), although promising, at present lead to poor performance and require extensive training and calibration [36].

Each participant wore a Zephyr BioHarness 3™ (Zephyr Technology Corporation, Annapolis, MD, US) used to acquire their electrocardiographic (ECG) signal and respiratory frequency, with a sampling rate of 250 Hz and 18 Hz, respectively. The skin conductance (SC) was recorded with a sampling frequency of 16 Hz using a Shimmer3 GSR+ Unit (Shimmer, Dublin, Ireland) with electrodes placed on the index and middle finger of the right hand of each participant.

The vibrotactile system developed in [72] was employed to provide vibrotactile feedback. Although used in [72] with 2 pairs of motors, this system allows to control up to eight pairs of Eccentric Rotating Mass motors (ERM, Model: 307-103 by Precision Microdrives Inc.). In the present study we used three pairs of motors, which were placed on the wrists and the ankle of the dominant foot (Fig. 5.1B). Within each couple of motors, only one could be activated at a time. It is worth noting that ERMs were chosen for their affordability, compactness, and wearability, ensuring reliable feedback without restricting movement. Although they lack independent control of frequency and amplitude, they are more practical than bulkier, expensive voice coils, which are better suited for static studies. Given the focus of this study on movement performance, ERMs provide an effective solution.

The trimanual augmented task was designed as a 2D application, developed in C# using the Unity3D environment, and projected onto a wall in front of the participants. Three virtual cursors (Figure 5.1) were designed as smoothed hand-shaped rectangles of different colours. The participants could control the cursors' position by moving their real limbs on the horizontal plane. A lateral limb movement produced lateral movements of the virtual effectors (i.e., along the horizontal axis), whereas moving limbs away and toward the body produced up and down effectors' movements (i.e., along the vertical axis of the screen), as it normally happens with a mouse cursor. Real limbs up and down movements were not constrained, but they did not produce any movement of the virtual cursors and participants quickly learned to minimize them. The virtual cursors were allowed to move throughout the whole screen and targets were limited to appear in a centred 30 cm × 30 cm square (referred to the virtual coordinate system) in order to have the same range on both axes. Before starting the experiment, the height of each participant was recorded and used to personalize the scaling factors both for hands ($S_h = 0.21\ h/SD$) and foot ($S_f = 0.164\ h/SD$) movements, where h represents the subject's height and SD is a parameter associated with screen size intended to facilitate the subject's ability to reach all points in the space. The remaining constants are obtained from average anthropometric values corresponding to the length of the arm and the lower leg, normalized to the height [97]. At the beginning of each trial, participants could start with their limbs at the most comfortable distance, which was equal to 10 cm in the virtual environment but not constrained in the real world.

5.2.3 Trimanual Tasks

The task was a two-dimensional (i.e., only planar translations without rotations) trimanual reaching task where three virtual cursors had to be properly moved by one (i.e., *solo session*) or two collaborating participants (*dyad session*).

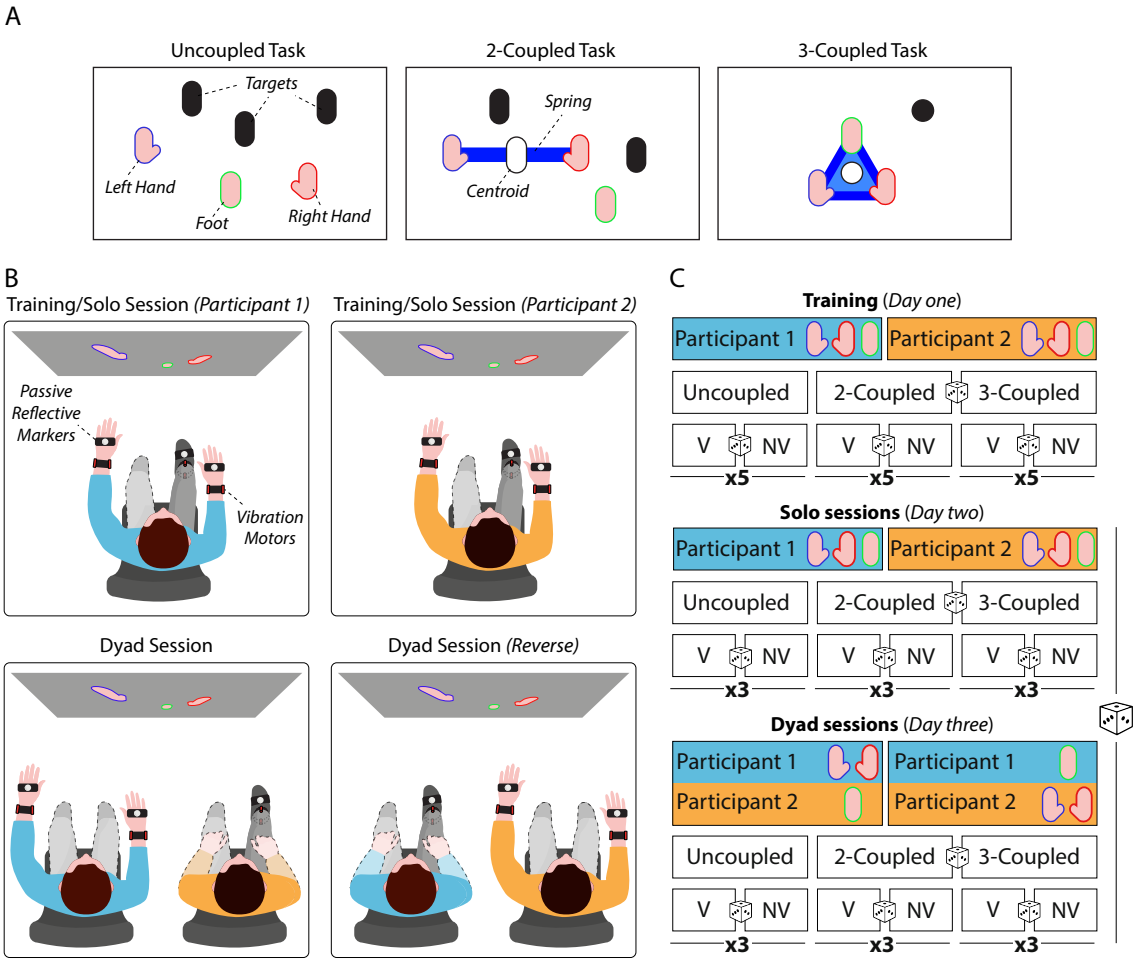

Fig. 5.1 **Experimental setup and protocol. Panel A** shows experimental conditions of the three trimanual tasks (Uncoupled, 2-coupled and 3-coupled). Virtual effectors were controlled with left hand, right hand and foot. The blue band represented the virtual elastic band connecting the effectors, which could be extended or compressed up to the breaking point. Black shapes represent targets that had to be reached with the virtual effectors (in Uncoupled) or with the centroid of the virtual elastic band (in 2-coupled and 3-coupled), represented by the white shape. **Panel B** shows experimental sessions. Each participant completed a training and solo session (with full control of the effectors) and two dyad sessions with the partner (shared control), in which their control roles were reversed. To increase visual clarity of the figure, limbs not involved in the task are outlined with a dotted line. Each couple of vibrator motors was used to encode information on the virtual force exerted by the elastic band connected with the respective effector (one motor for compression force, the other one for extension force). **Panel C** shows the experimental protocol. Effector icons show which effector participants were able to control during each session. Dice icons indicate a random condition order. Uncoupled condition was always performed first. "V" and "NV" letters indicate the presence or absence of vibrotactile feedback, respectively. Numbers below blocks show how many repetitions (i.e., trials) were performed. Solo and Dyad sessions were performed in a pseudo-randomized order among participants. The familiarization carried out during the first day is not shown in the figure for clarity purposes.

In each session, three tasks corresponding to different mechanical constraints (i.e., virtual coupling between cursors) and different numbers of concurrent objectives (i.e., targets to reach) were evaluated:

- *Uncoupled* (U): participants have to reach three different targets independently moving their hands and dominant foot (Fig 5.1A, left); participants were not instructed which limb should reach which target such that they were free to decide this dynamically. The trial is successful if at the same time each target is covered by one cursor. Each set of 3 concurrent targets reached increases the score by one point.

- *2-coupled* (2C): the cursors controlled with the hands are coupled through a virtual spring whose centroid has to be moved on one target while the foot reaches for the second target (Fig 5.1A, center). The two hands have to be simultaneously moved to avoid excessive compression/extension (i.e., more than 30%) of the virtual spring, otherwise the band breaks and a penalty is given (each fail decreases the score by one point).

- *3-coupled* (3C): all three cursors are coupled together via a virtual triangular elastic band (Fig 5.1A, right); participants have to bring the centroid of the elastic band on one single target. Similarly to the 2C, all three virtual springs must avoid excessive changes in length (i.e., in the range of $\pm 30\%$ variations). Overcompression and overextension cause the breaking of the spring and the score decreases by one point.

The choice of these three tasks derives, in general, from the selection of the three most representative different conditions of the diverse coordination types in the case of manipulation with three limbs [34]. Moreover, it allows the comparison with previous studies which employed equal or similar tasks [71, 5, 46].

It is worth noting that the aforementioned coupling was not a physical connection between the real hands or hands and foot, but instead, it was a virtual elastic band presented in the virtual scenario only (Figure 5.1). This band was visualized as a blue segment which changed in thickness and colour depending on the amount of their extension or compression, i.e., the higher the extension, the thinner the band and lighter the colour and vice-versa.

A target was considered reached when the distance between it and the cursor was less than 1 cm (measured in the virtual reference system). However, to succeed participants had to catch simultaneously all the targets presented at once. Each time they succeeded, their score increased by one point and a “coin” sound was played as a reward. Conversely, if they broke the virtual spring the score decreased by one point and a “buzzer” sound effect was played.

Each task repetition (trial) lasted 100 seconds, during which participants had to reach as many target sets as possible. Participants had a maximum of 3 seconds to reach each set of targets. After that time (or as soon as they reach all the targets shown) targets' position randomly changed. The timeout did not affect the score.

5.2.4 Vibrotactile Feedback

The pivotal novelty with respect to the previous work [71] is the presence of vibrotactile feedback encoding information about physical interactions, not perceivable through the virtual environment (see Figure: 5.2). A similar approach showed control performance improvements in HMA context, although with different hardware [50]. In particular, the feedback encoded the following information:

- *Virtual elastic force* (present in 2-coupled and 3-coupled): when the virtual spring is compressed or extended, the resulting elastic force applied to the connected cursors is fed back to the corresponding real limb through a vibration whose intensity is proportional to the magnitude of the force. Depending on the force direction, a different motor within each pair is activated (i.e., the medial motor corresponds to spring compression, whereas the lateral motor to the spring extension). In the 3-coupled task, we considered the resulting force acting on each cursor. For example, in the 2-coupled task, if the hands' cursors maintain their initial distance (spring neither compressed nor extended), no feedback is provided. If their distance increase, causing an extension of the virtual spring, the two ERMs on the lateral side of the wrists start vibrating with an intensity proportional to the amount of the extension, i.e., the elastic force.

- *Collision between cursors* (present in all tasks): when two cursors overlap during their motion, the participant is provided with a 500 ms vibration with high intensity on the correspondent limb. For example, if the right hand cursor collides with the foot cursor, one ERM on the right hand and one ERM on the ankle provide a single burst of vibration. The 500 ms duration was empirically determined to provide a distinctly perceptible vibration while preventing habituation or discomfort.

- *Elastic band breaking* (present in 2-coupled and 3-coupled): when the participant breaks the virtual elastic band the failure is fed back through a 1-second train of ERM's burst vibration with high intensity on the limbs connected to the spring.

Vibration amplitude and frequency are coupled. When conveying the occurrence of discrete interaction events such as a collision or the band breaking, the vibration frequency

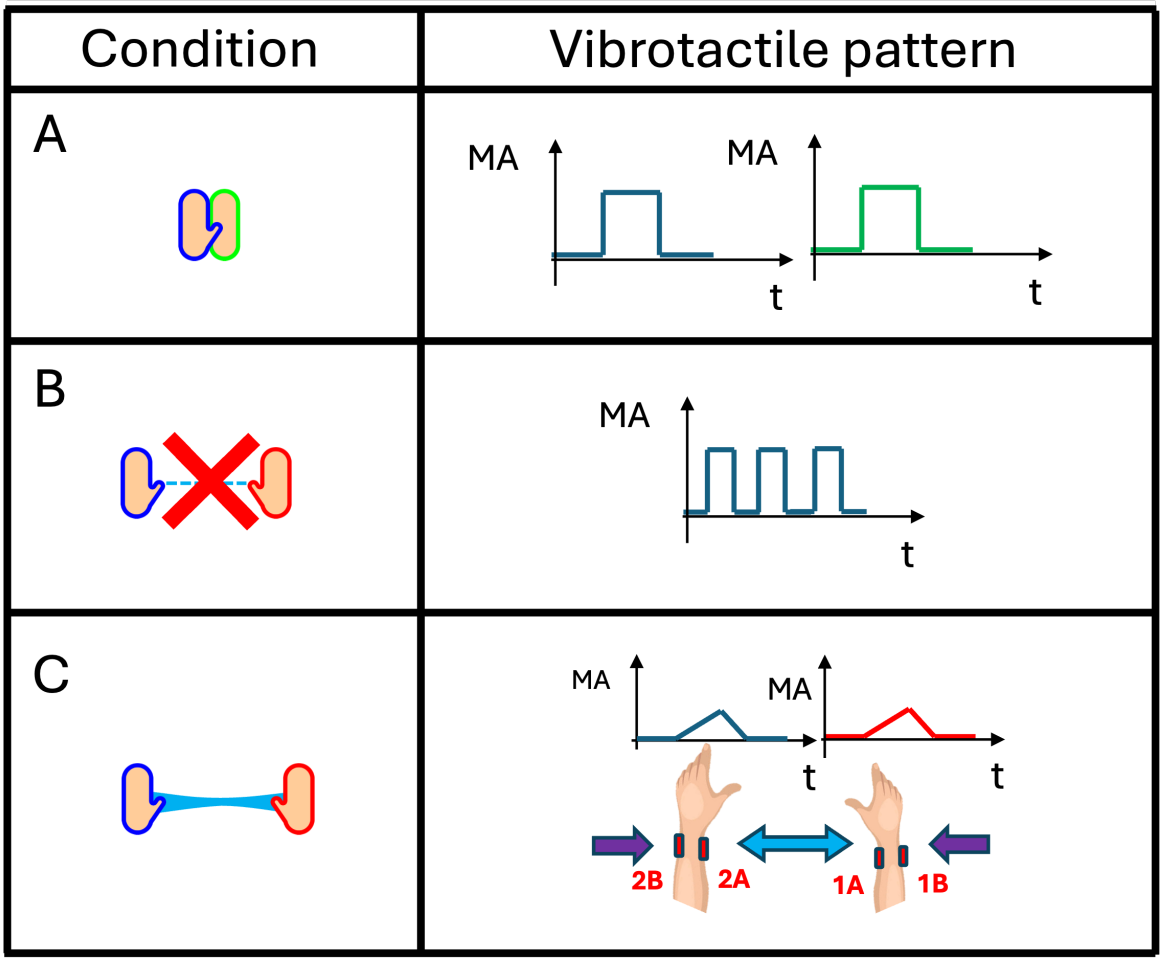

Fig. 5.2 The figure illustrates the vibrotactile patterns employed in the experiment. (A) A collision between the two cursors triggered a 500 ms constant vibration at 250 Hz (the maximum achievable with the motors). (B) The breaking of the virtual spring was signaled to the participant through a 1 s train of bursts delivered to the corresponding limbs. (C) During the 2-coupled and 3-coupled tasks, continuous vibration was provided, with intensity proportional to the force applied to the virtual spring. Compression activated the medial motors, whereas extension activated the lateral motors.

was set to 250 Hz, which corresponded to the highest value the ERMs could reach and to the optimal frequency for human tactile perception [39]. When conveying the elastic force exerted by the virtual springs, the vibration intensity varied proportionally between 0 and 250 Hz, where the minimum value corresponds to a null elastic force and the maximum value to the spring breaking. According to the sign of the force acting on each cursor, we activated either the medial or lateral ERM of the corresponding limb. The frequency range for the vibration covers the one perceivable by the human skin receptors [64].

The same vibration pattern was employed in both the dyad and the solo condition. The only difference was in the allocation of the eccentric rotating mass motors: in the solo condition, all feedback was delivered to a single participant, whereas in the dyad condition the motors were divided between the two. This means that each participant only perceived the feedback related to the cursor under their control (e.g., in the 3-coupled condition, the participant controlling the foot received vibrations on the leg, while the one controlling the arms received vibrations on the arms).

It is worth underlying how, due to the diverse nature of the constraints in the three tasks, the feedback conveys diverse information from one task to the others (i.e., in the uncoupled task there are no mechanical constraints, thus no virtual elastic forces acting on the cursors and thereby no feedback related to such information).

5.2.5 Experimental protocol

The experiment was performed in 3 different days as detailed below:

Familiarization *(Day 1)*. This phase consists of three exercises to make participants confident with the setup and the tasks:

1) Participants are asked to reach a single target with a specific limb. They can independently control the 3 cursors with their hands and foot. One target at a time is presented with the shape and colour of the cursor that should be used to reach it. If it is not reached within 3 seconds it changes color and location. The exercise lasts 100 seconds and it is repeated twice.

2) Participants control the two hands virtually coupled together. They are asked to extend and compress the virtual spring according to displayed instructions while paying attention to the corresponding vibrotactile feedback. All possible spring states are presented (i.e., extension, compression and spring breaking). This phase lasts 100 seconds.

3) Similarly to exercise 2, participants experience the spring deformation and related feedback, but in the case of 3 cursors coupled through the triangular elastic band. All springs configurations are experienced by the participant.

Training *(Day 1).* Each participant performs a training session consisting of the three main tasks (uncoupled, 2-coupled and 3-coupled) described above. The three tasks were repeated ten times each (the single repetition, lasting 100 seconds, is hereafter called *trial*), of which five with the vibrotactile feedback and five without, in a pseudo-random order (permuted block randomization).

Solo *(Day 2 or 3).* Similar to the training, in the solo session each participant performs the tasks alone, controlling the movement of all three cursors. Each task is repeated six times (i.e., three times with vibrotactile feedback and three without, in a pseudo-random order).

Dyad *(Day 2 or 3).* Participants perform the tasks in dyads, sharing the control of the three limbs. The session is repeated twice, first with *participant 1* controlling the hands and*participant 2* controlling the foot, and then vice-versa (see Fig. 5.1 B). Likely to the solo session, for each dyad's session they repeat each task six times, three of which with the vibrotactile feedback.

Familiarization and training sessions were always performed first, while the order of Solo and Dyad sessions on day 2 and day 3 was pseudo-randomized. Half of the dyads started with the Dyad session on day 2, followed by the Solo session on day 3 and vice-versa for the rest of the participants. Within sessions, the uncoupled task was always performed first, to avoid any bias in limbs' control due to the virtual coupling, whereas the 2-coupled and 3-coupled were completed in random order. The order of the tasks, as well as the order of the trials with vibrotactile feedback, was kept constant throughout all the sessions (i.e., solo and dyad) for the members of the same dyad. To rule out the seating position from having an effect, participants kept the same chair during all sessions. Participants were not allowed to verbally communicate throughout the session. It is worth noting there was no difference between the training and the main experimental tasks, except for the number of repetitions completed. The training aimed at participants learning the tasks and the feedback, while potentially improving their augmented motor skills as in [5, 46].

5.3 Analysis

We evaluated different measures to assess the participants' skills (e.g., task performances, motion characteristics, etc.), arousal level (e.g., heart rate, etc.) and subjective experience (e.g., questionnaires).
The performance measures include:

- *Score*: the total number of sets of targets successfully reached in one trial, minus the total number of fails in the same trial.
- *Fails*: the number of times the participant breaks at least one virtual elastic band (this measure only applies to the 2-coupled and 3-coupled tasks) during one trial.
- *Smoothness*: the spectral arc length of each cursor's velocity [7].
- *Spring length variation*: the root mean square (RMS) of the virtual spring's length variation at each time point divided by the initial spring's length. This measure was only considered in the 2-coupled and the 3-coupled (here, as average among the three virtual springs).

The selected metrics allow us to evaluate participants' performance from diverse points of view: score and fails show participants' ability to complete the tasks according to their requirements and constraints; on the other side, spring length variation and smoothness reveal participants' specific motor coordination during the execution of an augmented task.

The participants' physiological state was evaluated through the electrocardiographic (ECG) signal, band-pass filtered between 0.67 Hz and 40 Hz, the breathing signal and the skin conductivity signal, which was band-pass filtered between 0.05 Hz and 2 Hz [24]. From these signals, we computed the following indexes within each trial:

- Heart Rate (HR): the average Interbeat interval (IBI);
- RMSSD: the root mean square of successive differences between normal heartbeats (IBI) expressed in milliseconds [87]. This measure represents an index of heart rate variability, which is typically lower the higher the subject's attention and/or stress;
- Breathing frequency: the average interval between two successive breathing waves;
- Nonspecific skin conductance standard deviation (SCSD): the standard deviation value of the nonspecific skin conductance signal over each 100-second trial [24].

We selected these metrics as indicators of the participants' mental and physical state for their well-known correlation with different states such as relaxation/stress or rest/activity.

We analyzed the subjective experience of the participants through the questionnaires, asking them to rate between 0 and 100 the sessions and tasks in terms of their perceived enjoyment, difficulty, overall workload and usefulness of the vibrotactile feedback.

For the statistical analysis, we treated each dyad as a singular unit by averaging their performance in the two solo and two dyadic sessions. Sphericity and normality of all data

distributions were evaluated respectively with Mauchly's and Shapiro-Wilks tests. In the case of the average Spring length variation, the analysis was conducted after having normalized data with the log10 operation.

Since the vibrotactile feedback conveyed qualitatively different information in the different tasks, we ran separate analyses for each task (i.e., one for uncoupled, 2-coupled and 3-coupled respectively). Indeed, in the uncoupled task the feedback only alerted the participant in case of effectors collision. Conversely, in the 2-coupled task participants were provided with a continuous feedback on the elastic force exerted on the effectors by the virtual spring, plus an alert signal in case of elastic band breaking. In the 3-coupled task the continuous feedback on the elastic force is provided for three virtual springs rather than one. Thus, we analyzed the data through a 2-way repeated measures ANOVA with vibrotactile feedback (vibrotactile, no-vibrotactile) and session (solo, dyad) as factors to analyse the score, fails and spring length variation indexes. The smoothness index was analysed with a 3-way RM ANOVA, with an additional factor accounting for the different cursors (i.e., dominant hand (DH), non-dominant hand (NDH) and dominant foot (DF)). Multiple comparisons were corrected with Bonferroni.

Physiological measures were normalized with respect to the average baseline value b as $(x-b)/b$ considering x the evaluated index and analyzed through Generalized Linear Mixed-Effect Models, in order to take into account all the factors (i.e., tasks, sessions and feedback).

Questionnaires were evaluated separately for each index with the Friedman test considering as factors the tasks (i.e., uncoupled, 2-coupled and 3-coupled) performed within each session (i.e., solo, dyad controlling the hands, dyad controlling the foot) and then the sessions, compared for the same task. Multiple comparisons were corrected with Bonferroni.

5.4 Results

5.4.1 Game performance

Overall, dyads outperformed solo participants in all the tasks and most of the evaluated metrics, even though this effect was much less pronounced in the 3-coupled task. Most importantly, providing vibrotactile feedback improved the performance of participants in all metrics during the 3-coupled task.

Specifically, the feedback significantly improved the **score** (F=10, p=0.012) and reduced the number of **fails** (F=20, p=0.002) compared to no-feedback condition, in the 3-coupled task (see Fig. 5.3). In particular, within the solo session the score increased on average by 5.87

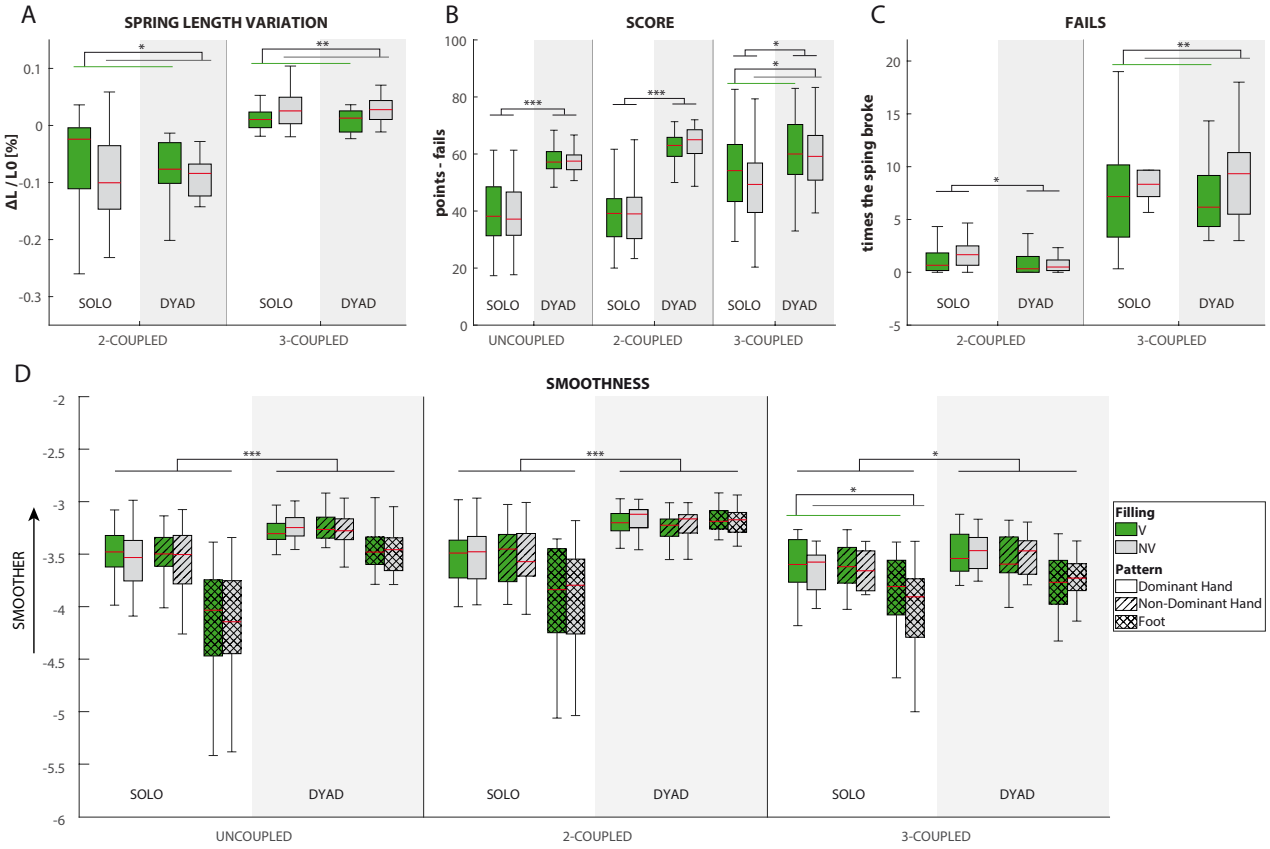

Fig. 5.3 **Performance obtained by participants during tasks.** The figure shows the average length variation of the virtual elastic band (**Panel A**), where negative values indicate a compression and positive values an extension of the virtual band; the score (**Panel B**); fails (**Panel C**), meant as the number of times the virtual elastic band broke due to overcompression or overextension; smoothness (**Panel D**) of participants movements in controlling the effectors. All measures reported are dimensionless and they are averaged across trials. In all panels, green filling indicates trials with vibrotactile feedback (V in the legend), while grey filling without (NV in the legend) and the red lines indicate the median. In panel D, the absence of a filling pattern indicate performance obtained by controlling an effector with the dominant hand, the single-lined filling indicates a non-dominant hand and the crossed filling indicates the foot. Asterisks indicate a p-value <0.05 (*), <0.01 (**) and <0.001 (***)

points, i.e., by the 13% and the fails decreased on average by 2.15 times, which corresponds to a 22% decrement. Moreover, the vibrotactile feedback improved the **smoothness** in the solo session of the 3-coupled task (p=0.035, Bonferroni correction used for multiple comparisons; improved by 3% on average.).

The feedback significantly impacted the **average length variation** of the virtual elastic band (Fig. 5.3 A), in both the tasks with virtual elastic coupling. Indeed, the vibrotactile feedback helped participants maintain the virtual elastic band length and avoid both its compression and extension, compared to the no-feedback condition, in the 2-coupled (F=6, p=0.041) and the 3-coupled task (F=15, p=0.004). On average the length variation decreased by 2%, although this value is likely flattened as it results from successive means among conditions and participants, in turn obtained from the average along both the whole trial duration of 100 seconds and the total number of trials. Except for the average length variation, providing feedback did not affect the performance in the uncoupled and 2-coupled tasks.

Participants, in general, obtained higher **score** (see Fig. 5.3 B) in dyad condition compared to solo, and this gap resulted smaller in the 3-coupled task (F=10, p=0.011) compared to the uncoupled (F=62, $p<0.001$) and 2-coupled (F=75, $p<0.001$) ones.

Considering the number of **fails** (Fig. 5.3 C), i.e., times the virtual elastic band broke for overcompression or overextension, we found no significant difference between solo and dyad sessions in the 3-coupled task, while in the 2-coupled task, participants obtained more fails during solo compared to dyads (F=6.36, p=0.033).

Similarly to the score, participants showed higher **smoothness** (see Fig. 5.3 D), when working in dyads compared to the solo session in the uncoupled (F=49, $p<0.001$), 2-coupled (F=40 and $p<0.001$) and 3-coupled (F=10, p=0.011) tasks.

No significant differences emerged between solo and dyad concerning the average length variation. It is worth noting how participants tended to compress the band in the 2-coupled task (negative values of the variation $\Delta L/L0$, with L and $L0$ the actual and initial length) and to extend it in the 3-coupled task (positive values).

Physiological measures

Physiological measurements were analyzed in terms of heart rate, heart rate variability (evaluated as RMSSD [87]), breathing rate and skin conductance, all normalized with respect to the corresponding average baseline value. We evaluated the results through the Generalized Linear Mixed-Effect model (due to the number of factors to take into account in this analysis) considering the session (solo, dyad controlling hands, dyad controlling foot), the feedback (vibrotactile or without vibrotactile) and the task (uncoupled, 2-coupled and 3-coupled) as fixed effects and the participants as a random effect.

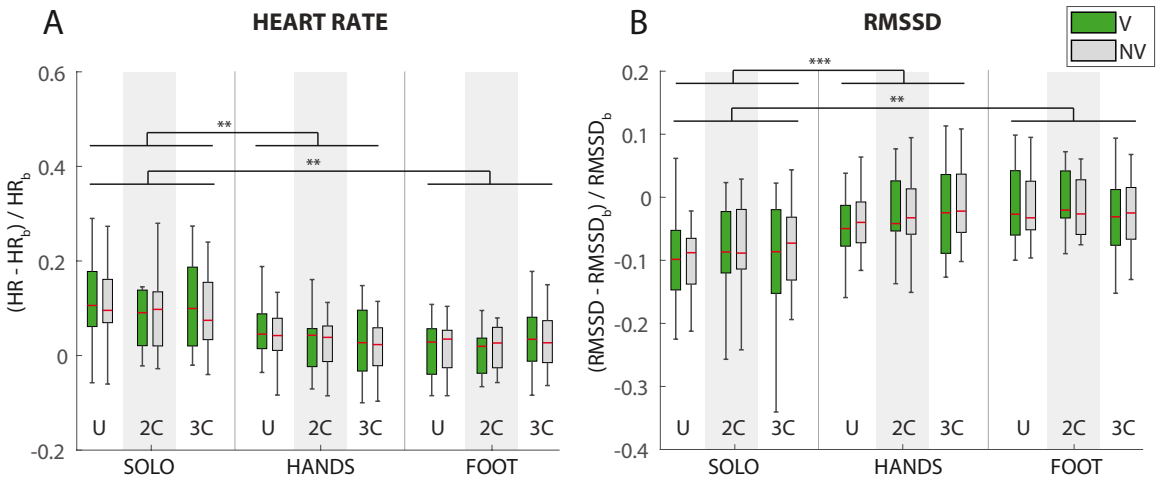

Fig. 5.4 **Physiological measures. Panel A** shows the heart rate of participants during tasks while **Panel B** shows the heart rate variability expressed as the root mean square of the standard deviation (RMSSD). Both measures are normalized with respect to the baseline as value=(measure-baseline)/baseline. Thus, measures represent the percentage variation with respect to the baseline. In both panels, green filling indicates trials with vibrotactile feedback (V in the legend), while grey filling without (NV in the legend)a nd the red lines indicate the median. Asterisks indicate a p-value $<$0,01 (**) and $<$0,001 (***)

No significant differences emerged among fixed factors in terms of **breathing frequency** or **skin conductance**. Conversely, both the **heart rate** (p=0.004) and the RMSSD (p=0.001) show an effect of the session, as depicted in Fig. 5.4 A and B, respectively. In particular, participants increased their heart rate during the solo session, compared to the dyadic sessions, regardless of whether they controlled the hands (p=0.001) or the foot (p$<$0.001). No significant difference emerged between the two dyadic sessions. Accordingly, the RMSSD decreased (thus suggesting a state of high focus/stress/arousal [87]) in the solo session compared to the dyad session controlling the hands (p$<$0.001) and the dyad session controlling the foot (p$<$0.001).

Subjective perception

Participants provided in general high enjoyment scores for all the tasks, with no differences among the sessions or the tasks (see Fig. 5.5 A-B).

The vibration was found useful in all the sessions when performing the 3-coupled task, but only in the solo and dyad-hand session in the 2-coupled task and not useful at all in the uncoupled one (see Fig. 5.5 C-D). Specifically, in the coupled tasks, vibration usefulness was perceived as higher both in the solo session (all p$<$0.007) and in the dyad when controlling

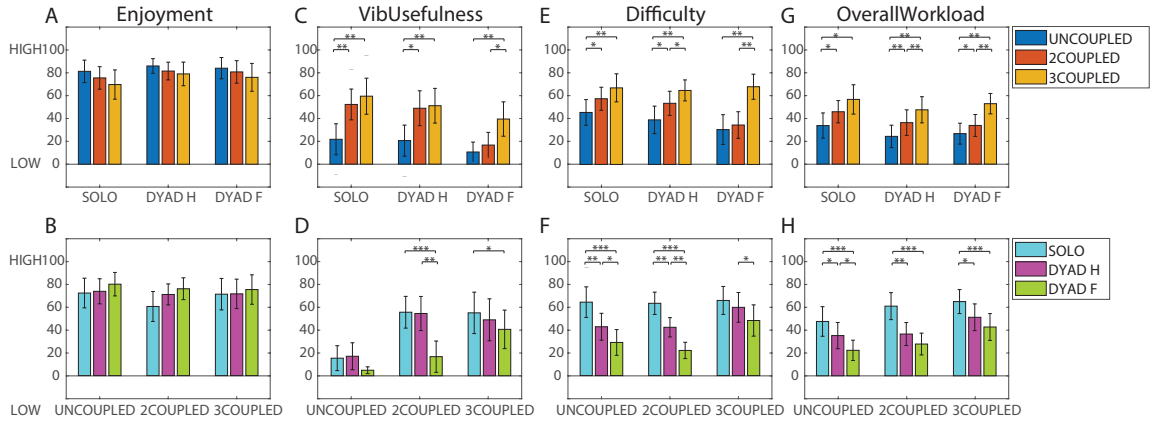

Fig. 5.5 Questionnaires. The top row shows the average evaluation participants provided after each session for the three tasks performed; the bottom row shows their evaluation at the end of the experimental protocol to assess each task across the different sessions. Participants scored the Enjoyment (A and B), the usefulness of the vibrotactile feedback (C and D), the perceived difficulty (E and F) and the overall Workload (G and H), with values ranging from 0 (low) to 100 (high). Colored bars represent average values and error bars show the 95% confidence intervals. Results were analyzed through Friedman test within each session/task and Bonferroni correction was used for multiple comparisons among tasks/sessions, respectively. Asterisks indicate a p-value <0.05 (*), <0.01 (**) and <0.001 (***)

the hands (all $p<0.023$). Conversely, in the dyad when controlling the foot, the feedback was perceived as more useful in the 3-coupled task compared to the others (all $p<0.046$).

Interestingly, participants perceived the difficulty increasing from the uncoupled task, to the coupled ones (Fig. 5.5 E-F). In particular, when performing the task alone they refer to the uncoupled task as the least difficult (all $p<0.048$), with no significant differences between the two coupled ones. When sharing the control they perceived the 3-coupled task as the most difficult one (all $p<0.044$).

In the solo session, participants did not perceive significant differences between the 2-coupled and 3-coupled tasks for any of the considered metrics. On the other hand, they perceived both the coupled tasks as more demanding in terms of difficulty and overall workload compared to the uncoupled one (Fig. 5.5 G-H).

In general, in both the uncoupled and 2-coupled tasks, the solo session resulted to be the most difficult and demanding. The 3-coupled task represented instead the case in which the least difference was perceived among the sessions, except the solo was perceived as more demanding in terms of overall workload.

5.5 Discussion

In this work, we tested the effect of vibrotactile feedback on human performance in trimanual tasks. Overall, we confirmed previous results found in [71] by showing that i) dyads generally outperform participants who control the three limbs on their own and ii) 3-coupled task allows for the highest performance compared to other tasks and the lowest gap in performance between solo and dyads.

We demonstrated a significant improvement in the 3-coupled task performance when the vibrotactile feedback was provided. This outcome represents a solid finding recurring in several indexes such as score, length variation of the virtual elastic band, number of fails and smoothness.

It is worth noting how the feedback benefits emerge particularly in the management of the virtual physical interaction, i.e., when dealing with the virtual spring. This is evident from the reduced number of fails in the 3-coupled task and the reduced variation of the spring length even in the 2-coupled task. Importantly, for some indexes such as the smoothness, the vibrotactile feedback showed a useful impact only in the solo session, suggesting that this feedback could be particularly useful in the augmentation scenario, in which a single user is required to perform augmented (e.g., trimanual) tasks, controlling three effectors, alone.

Differently from what showed in previous literature, as in [46], the initial training did not allow solo participants to reach the performance level of dyads. This can be due to the

different approaches used for the training in the two studies. Indeed, in our case, the training involved three different tasks and part of it was dedicated to becoming confident with the vibrotactile feedback. This means the individual amount of time assigned to the 3-coupled training only was lower than in [46] and, thus, probably not sufficient for reaching a plateau in performance similar to dyads. In total, the net training duration was less than 1 hour, including all three tasks and different conditions. Although such short amount did not induce sufficient learning to level solo and dyad performance as in [46], it was enough to observe the significant improvement achieved with the vibrotactile feedback.

Summing up, when performing trimanual tasks which involve physical constraints like the 3-coupled task, providing vibrotactile feedback significantly improves the performance in several respects. These findings point out the importance of providing supplementary feedback (e.g., vibrotactile) when dealing with physical interactions in augmented tasks. In other words, our results suggest that the design of SRLs, and in general interfaces for HMA, should embed haptic feedback to convey the interaction forces of the supernumerary effector to guarantee good performance in augmented tasks involving physical interactions and constraints.

At first glance, this might seem in contrast with previous attempts in the control of an extra virtual limb where supplementary feedback did not improve the performance [32]. However, despite the intended application in augmentation contexts, Dominijanni and colleagues tested their platform in unimanual and bimanual tasks rather than in actual trimanual tasks. We reckon that this aspect and the limitations of their control approach (e.g., limited number of controlled DoFs, latency and encoded feedback information) might be the main reason haptic feedback did not produce significant improvements in their case. In [16] instead, users regulated the SRL interaction force (along one direction) significantly better when provided with vibrotactile feedback, compared to relying solely on the inherent feedback from physical contact between the worn SRL and the users' body. Our results support these findings, i.e., the relevance of supplementary feedback when the SRL physically interacts with the environment, and extend them to a 2D trimanual task.

A further contribution of the present work is the assessment of the physical and cognitive burden through quantitative physiological measures. As expected, the electrocardiographic signal shows that trimanual tasks are more demanding and challenging when performed alone rather than in partnership with someone else (regardless of the controlled limb/s). However, other physiological indexes collected here, such as skin conductance response and breathing frequency, do not show any statistical significant difference. It is worth noting that both these signals were particularly affected by noise and motion artifacts during the data collection,

requiring the exclusion of several trials in the data analysis. Thus, further analyses with a bigger amount of data are necessary to deepen this aspect.

Contrarily, and contrary to what ECG data suggest, participants perceived the 3-coupled task as the most difficult and demanding and the uncoupled task as the easiest and the most enjoyable. This result is in contrast with our previous study [71] and also opposite to the quantitative measures of performance. This could be due to the slight difference with respect to the previous work concerning the scaling between the real and virtual limbs' movements. Specifically, in the present study, participants had to perform bigger movements with their hands. This choice was made to perform motions more similar to a real task, where the two hands have to cover quite a big workspace, whereas the foot movement, used for the SRA control, can be scaled and reduced to avoid fatigue. This aspect may have somehow made the 3-coupled task more difficult compared to the previous work due to the higher coordination required among the limbs covering different distances. Conversely, the uncoupled task may have been perceived as easier and thus performed with less attention, leading to worse performance.

5.6 Conclusion

In the context of human movement augmentation, especially within the Degrees of Freedom (DoF) paradigm, being able to concurrently controlling three effectors is the foundation necessary to accomplish trimanual tasks. Importantly, trimanual tasks represent a broad category of actions rather than a single standardized task. This raises a practical question: are humans equally capable of managing all forms of trimanual coordination, or are some task types inherently easier or more intuitive to perform?

Accordingly, we selected three virtual tasks, widely used in previous research, which replicate distinct constraint patterns between effectors. These serve as proxies for a diverse set of real-world coordinated actions. In particular:

- *Uncoupled*: all effectors can be moved independently, mimicking a multi-object pick-and-place task.
- *Two-coupled*: two effectors must be moved in coordination, while the third is employed to complete another part of the general task—for example, holding a tray while opening a door.
- *Three-coupled*: all three arms cooperate to achieve a single, shared goal, for example, holding a large and fragile object.

Previous studies have shown that the three-coupled condition minimizes the performance gap between solo and dyad execution, making it a promising candidate for movement augmentation scenarios [71]. Furthermore, other research has shown that with training, this performance gap can be further reduced, even to the point of no statistically significant difference between solo and dyad conditions [46].

However, our results only partially confirmed these findings. While the three-coupled condition resulted in the smallest performance difference, it never matched the dyad performance level. It is worth noting that these differences may stem from substantial variations in the experimental protocols. In [46], participants underwent a longer training phase, and only a single condition (i.e., the three-coupled) was evaluated. In contrast, our study assessed multiple conditions, and training was not the primary experimental question. Moreover, while in our experiment the trial duration was fixed, in their protocol the number of targets per block was fixed, leading to a different task structure.

Moreover, most of these studies overlook one important factor: the supplementary feedback. As discussed throughout this thesis, supplementary feedback can be beneficial in motor tasks. In this context, we designed different feedback strategies tailored to each task constraint. Our results show that supplementary feedback improved all relevant performance metrics in the three-coupled condition, and improved only spring length variation in the two-coupled condition.

The lack of significance in the uncoupled condition was expected: in this scenario, feedback was only provided after an error occurred (e.g., collision between cursors), offering no predictive information, or the actual status of cursors, to help avoid it.

The feedback's success observed in the three-coupled task could be due to the synergy between the richer feedback (i.e., informing about all involved effectors) and the task structure.

Interestingly, in the two-coupled condition, the variable that improved was the ability to maintain the spring unbroken, which reflects improved coordination between the two effectors.

These results, beyond their statistical significance, may also have practical relevance in real-world applications. For instance, a reduction in failures of more than 20% compared to the no-feedback condition could have a substantial impact depending on the task. In a scenario such as handling fragile objects, fewer errors could directly translate into fewer damaged items. Similarly, the observed increase in score suggests greater efficiency, potentially reducing the time required to complete a task. Of course, the meaning of "failures" and "score" may differ substantially depending on the real-world context. Nevertheless, such improvements could still prove highly valuable in the long run.

These preliminary results represent a first step toward evaluating the effectiveness of supplementary feedback in trimanual coordination tasks. Moreover, these results are consistent with the findings of Chapter 4. Supplementary feedback brought benefit both in interaction task force, both in helping improving the coordination ability of participants during high complex and coupled task. All together, these results provide an hint in support of the relevance of supplementary feedback, and consequently in closing the sensorimotor loop in the HMA scenario.

Chapter 6

A Closed-loop Platform for the Embodiment of Supernumerary Robotic Limbs During Augmented Tasks*

6.1 Introduction

Most research in the field of human movement augmentation has focus on enhancing control strategies for supernumerary robotic limbs [1, 48, 41]. At the same time, as shown in previous chapters (i.e., Chapters 4, 5), significant attention has been devoted to how supplementary feedback and training protocols affect users' motor learning and performance [16, 76, 71, 78]. Nevertheless, a critical and often neglected question concerns the depth of the human-robot relationship in HMA. It is essential to examine the reciprocal influence between the user and SRL, considering not only the functional aspects but also the cognitive and perceptual dimensions. In this chapter we explore how such interactions might reshape the brain's representation of the body [33]. In particular, we question whether this relationship can evolve to the point that the robotic limb is no longer perceived as an external device, but as an integrated part of the body itself, can SRLs be "embodied"? This question is of central importance: the embodiment of the device, understood as the experience of ownership and agency over it [62, 15], could meaningfully enhance motor performance [52, 95] and enable more effective human-machine collaboration.

To answer this question, we developed and tested a robotic platform that creates a closed-loop between a human and a robot, enabling the user to control an SRL and receive

*This chapter is based article [51] (Accepted)

As a co-author, my contribution involved the development of the experimental setup, the definition of the experimental protocol, the data analysis, and the subsequent writing and revision of the manuscript.

supplementary feedback from it, during a trimanual task in Augmented Reality (AR). Indeed, the concurrent exchange of afferent and efferent information through a closed-loop strategy has been demonstrated to play a key role in motor control and embodiment [74, 30].

We then assessed whether the platform use led to the embodiment of the SRL by means of a Multisensory Reaction Times Task (MRTT) that can chart the boundaries of the user's peripersonal space (PPS). PPS [84] refers to the space immediately surrounding the body, where critical interactions between the body and the environment occur. It has been demonstrated that tool use can extend the boundaries of PPS to include the tool itself. This suggests that the space surrounding the tool is processed by the nervous system similarly to the space surrounding our body [19]. This mechanism is commonly considered as a proxy of embodiment, since it is demonstrated that the PPS is anchored to our body and can shift and expand to include whatever is considered to be part of it (i.e., whatever is embodied) [73].

A key feature of PPS is the facilitation of multisensory integration: multisensory stimuli (i.e., audio-tactile stimuli) within this space are processed more effectively, resulting in faster reaction times when responding to them. Conversely, interactions with multisensory stimuli outside the PPS are characterized by slower responses. A well-established protocol to determine the extension of PPS involves recording reaction times in response to a low-intensity electrical stimulation delivered while the participant listens to a looming sound source [18]. The distance between the sound source and the participant at which there is a steep decrease in reaction time, is considered as the boundary of the PPS. In this preliminary study, we compared the extent of the PPS before and after the use of an foot-controlled SRL in an AR trimanual task, expecting a PPS extension toward the SRL to testify its embodiment. Furthermore, we engaged participants in the trimanual task twice, changing the distance between the SRL and the user in order to assess the cause of the PPS shift. Indeed, if the extension of the PPS is truly "locked" on the robotic arm, due to it being embodied, rather than on the space it acted upon, then shifting the robot farther away from the user should produce a broader PPS extension.

6.2 Methods

6.2.1 Participants

Five participants took part in the experiment (3 female, 32.6 ± 8.0 years old) after having signed a written informed consent. The experimental protocol has been approved by the Ethics Committee of Università Campus Bio-Medico di Roma (HUROB protocol) and conducted according to the Declaration of Helsinki.

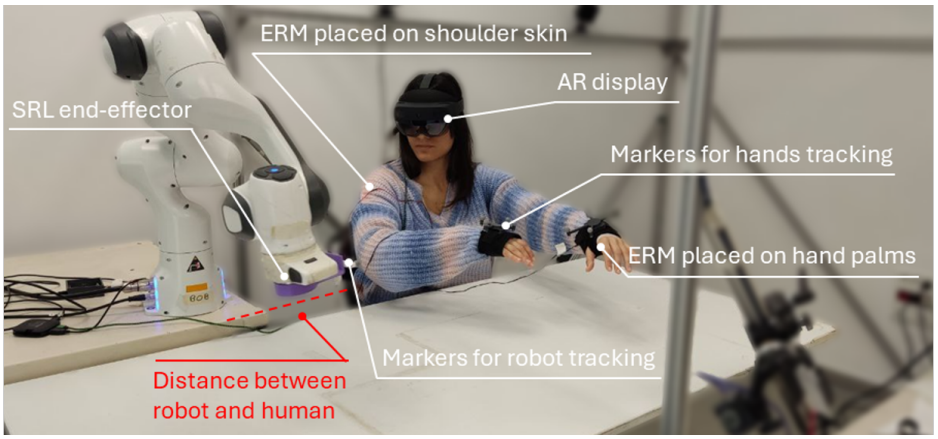

Fig. 6.1 Experimental setup in the experimental Far condition. The participants is using their natural limbs concurrently with the SRL effector to press all three holographic buttons (only visible within the AR environment) simultaneously. The robot was positioned on the participants' right side at 35 cm from the shoulder. In the Close condition the distance was 5 cm.

6.2.2 Experimental platform

Participants were comfortably seated on a chair in front of a table, wearing a head-mounted AR display (Hololens 2 by Microsoft). A robotic manipulator (7-DoF Panda robot by Franka Emika GmbH) was located to their right and was used as an SRL (Fig 6.1). Its distance from the participants was 5 cm (Close condition) or 35 cm (Far condition) depending on the experimental condition (see Fig 6.2). The AR headset was used to present three identical holographic buttons with a 10 cm diameter each, as if they were laid out on the table. Buttons' positions, in terms of x, y and z coordinates, were controlled with a custom software developed in C# language in Unity3D environment.

The space in front of participants was divided into three virtual portions and only one button could appear in each of them. All three workspaces had the same dimensions (45 cm x 35 cm x 10 cm) (Fig 6.3) and a constraint was implemented so that no button could be generated within 11 cm from the center of another button, to prevent them from overlapping. Passive reflective markers were placed on both participants' hands and dominant foot (which was right for all participants as determined through the ball kick dominant leg test [94]), and their movements were tracked using seven infrared cameras (Prime 13W by OptiTrack) operated with Motive software (NaturalPoint, Corvallis, Oregon, USA) on a Windows PC. The limbs' position was used by the Unity application to interact (i.e., press) with the holographic buttons and to move the SRL end-effector. The foot movements were transmitted through the UDP protocol from the Windows PC to a second one running Ubuntu 16.04 operating system. This information was used to control the robot end-effector position. The

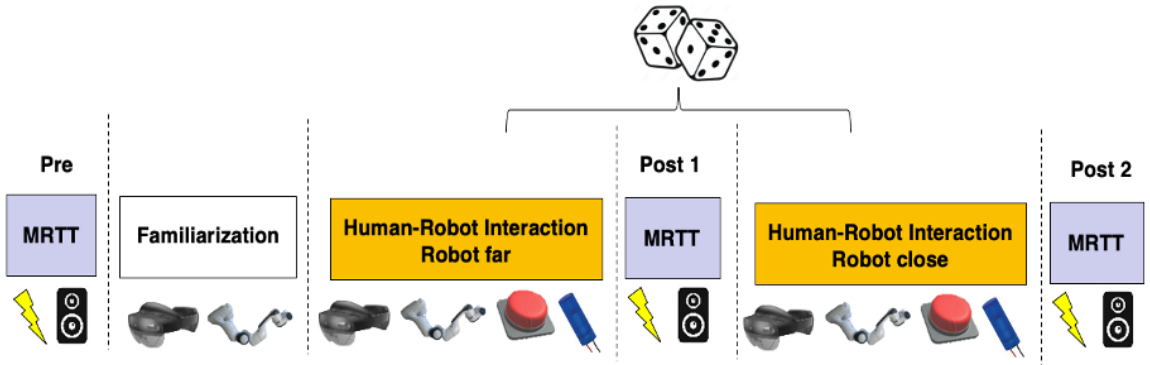

Fig. 6.2 Experimental protocol. 3 Multisensory Reaction Time Tasks were executed before and after the Augmented trimanual tasks. The augmented task was performed two times, changing the human-robot distance. A brief familiarization phase was performed to allow the participant becoming familiar with the setup.

torque-based robot control was implemented in C++ using Qt libraries and involved a scaling factor of 1.5 with respect to the foot movement [69].

Motion tracking data were low-pass filtered at 10 Hz before being used in the robot control. This cut-off frequency was chosen to be consistent with the dynamics of the human musculoskeletal system.

Eccentric rotating mass motors (ERM; model 307–103 Precision Microdrives Inc.), controlled through a custom Printed Circuit Board (PCB), were positioned on the right shoulder and on participants' hand palms to deliver supplementary sensory feedback [72].

To properly close the human-robot loop, whenever Unity detected an interaction between buttons and effectors, the buttons vibrated with a 60 Hz frequency and the ERMs were powered in order to obtain a vibration frequency of approximately 60 Hz too, thus emulating physical contact between effectors and buttons. Since this vibrotactile feedback was designed solely to provide a congruent visuo-tactile stream of information in an on-off fashion, the vibration frequency was not calibrated for different body parts, as slight differences in perceived frequency would not affect the informative content of the feedback.

6.2.3 Augmented trimanual task

Before starting the task, a calibration phase was required to establish the mathematical relationship between the different reference frames (Motive, Unity, and the robot base frame). This step enabled accurate communication of position data across the three distinct Cartesian systems. The calibration was achieved by projecting three holographic references (i.e., hand-shaped virtual objects) via the AR headset in Unity, and instructing participants to align their

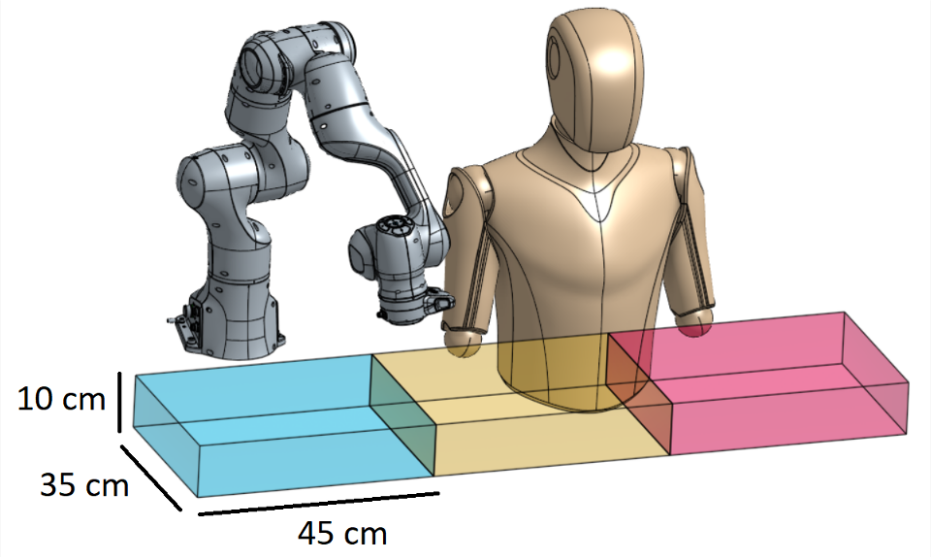

Fig. 6.3 Workspaces. All the 3 workspaces had the same dimensions. The cyan workspace was dedicated to the robot and buttons presented there were not reachable by the participants' natural limbs. Buttons within the yellow and magenta workspaces had to be pressed with natural hands, and participants were instructed to use their left or right hand as they saw fit.

real hands and the robot end-effector with the virtual hands, and the corresponding position in all reference system was recorded. This allowed for the determination of the relative transformations among the three reference frames, ensuring consistent coordinate mapping of object positions across the various software tools in use. This procedure also inherently accounts for the participant's perceptual alignment between the real and AR space, although it does not provide an independent ground-truth validation of the mapping. After the calibration, participants performed a brief familiarization phase to become confident with the setup and the robot control. Then, they completed a trimanual task in augmented reality. During each trial of the task three holographic buttons were presented simultaneously in randomized positions within their respective workspace. Participants had to reach, with their hands and the SRL, the three buttons and keep them pressed for 2 seconds before a new trial started. No time constraint was given to reach the buttons and participants performed in total 250 trials. The configuration of buttons' workspaces (Fig 6.3) was designed so that participants could not reach and press all three buttons simultaneously using only natural limbs, and they were forced to rely on the SRL. The whole task (250 trials) was performed twice by changing the human-robot relative distance (i.e., Far and Close condition). Participants started with the Far or Close condition in a pseudorandom order, to avoid any possible learning effect on the expansion of the peripersonal space.

The buttons' workspace was held constant for both experimental conditions despite the different human-robot distance. This was done to test if the extension of the PPS is triggered by the augmented workspace (i.e., Far and Close condition should produce the same PPS extension) or if it is "locked" on the robot itself (i.e., Far condition should produce a broader PPS extension than Close condition). The trimanual task lasted roughly 40 minutes for each condition.

6.2.4 Multisensory reaction time task

A multisensory reaction time task was performed 3 times: before and after the first trimanual task and after the second one (see Fig 6.2), to estimate the participants' PPS boundaries before and after the interaction with the SRL.

For the reaction time task, participants were seated in the same environment used for the trimanual task with their eyes closed, their left arm relaxed, and the right hand's index finger over a numeric keypad. They were asked to press the keypad as soon as they perceived an electrotactile stimulation (intensity equal to twice the participant's sensory threshold) delivered on the chest through a stimulator model DS7A (Digitimer, USA). Two speakers (Logitech Z313), one positioned 5 cm from participant's right arm (Near speaker), and the other one 175 cm from the arm (Far speaker), reproduced simultaneously two 3-second-long different sounds: the far speaker reproduced white noise with exponential decay from 100% to 25% of maximum intensity, while the close speaker reproduced white noise with exponential growth from 0% to 100% of maximum intensity. The volume measured at the participant position ranged from 50 dB at the sound onset to 75 dB at the end. A series of pilot experiments were performed to optimize these audio settings so that all participants could clearly perceive the sound source as looming toward them. This protocol is commonly employed to simulate a looming sound approaching the participant, which is known to be a particularly effective strategy to highlight the PPS border [18] (Fig 6.4).

Each reaction time task consisted of 90 looming sounds (i.e., 90 trials), 75 of which were accompanied by an electrotactile stimulus that was delivered with a pseudo-random delay from the sound onset, and 15 without any additional stimuli (i.e., catch trial, to make sure that the participants were responding only to electrotactile stimuli). The pseudo-randomization of the delay was performed as follows: we created 5 time windows lasting 600 ms each, and within each window we randomly chose 15 time points in which the electrotactile stimulation was delivered. This approach allowed us to distribute evenly the electrotactile stimulations along the entire duration (3 seconds) of the looming sound. Between trials there was a random pause lasting from 0.5 s to 4.5 s to minimize the ability to predict the occurrence of

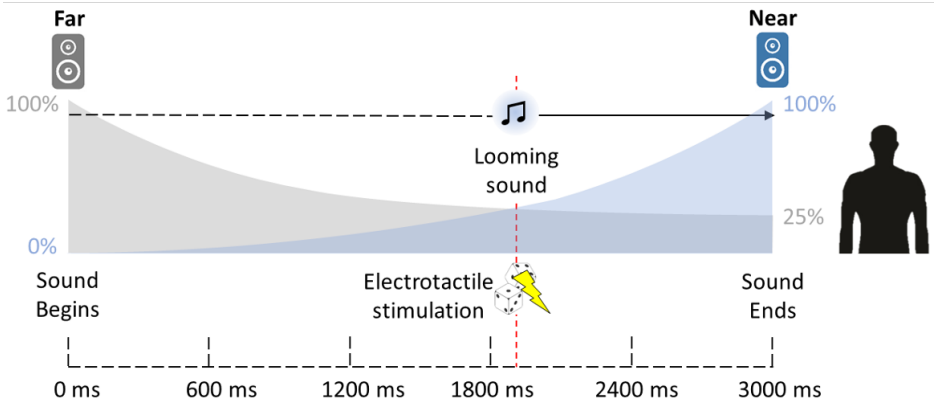

Fig. 6.4 Schematic representation of a single trial of the multisensory reaction time task. The distance between Near and Far speaker was 170 cm. During the illusory movement of the looming sound, an electrotactile stimulation was delivered with a pseudo-random delay. The dotted, portioned bar on the lower side of the image represents the 5 time windows, containing each 15 electrotactile stimulations. The grey and blue shades represent qualitatively the changes over time in volume of Far and Near speaker respectively. The dotted red line represents the instant in which the electrotactile stimulation is delivered

the electrotactile stimulus. OpenSesame (OpenSesame Inc., Portland, USA) was employed to synchronize the audio-tactile stimulation and to record the participants' reaction times.

6.2.5 Robot control

Foot movements were tracked in real-time through the infrared cameras and transmitted to the robot controller to determine the desired position of the robot end-effector at the next time point. The motion of the foot was scaled by a factor of 1.5 to allow participants to cover the whole SRL workspace with feasible foot movements. For the purpose of the task, only the 3 translational DoFs of the end-effector were controlled while keeping constant, for all the experiment, its orientation. The robot joints torque was calculated using the following equation (i.e., torque control):

$$\tau = \mathbf{J}^T \left[\mathbf{K}(\mathbf{p}_d - \mathbf{p}) - \mathbf{D}(\mathbf{J}\dot{\mathbf{q}})\right] - c_j \mathbf{W}\dot{\mathbf{q}} + \mathbf{C} + \mathbf{g} + \left\{(\mathbf{I} - \mathbf{J}^T \mathbf{J}^{\dagger})\left[\mathbf{K}_n(\mathbf{q}_{dn} - \mathbf{q}) - \mathbf{D}_n\dot{\mathbf{q}}\right]\right\}. \quad (6.1)$$

In the first part of Equation 6.1, $\mathbf{J}$ represents the Jacobian matrix (6×7), $\mathbf{K}$ is the diagonal stiffness matrix (6×6, with values equal to 1200 N/m for translational components and 10 Nm/rad for rotational components), and $\mathbf{D}$ is the diagonal damping matrix (6×6, where $D_i = 3\sqrt{K_i}$). $\mathbf{p}_d$ and $\mathbf{p}$ are the desired and actual pose vectors (6×1), respectively. $\mathbf{q}$ is the joint angle vector (7×1), $\mathbf{C}$ is the Coriolis vector (7×1), and $\mathbf{g}$ is the vector (7×1) of the

gravitational forces. $\mathbf{W}$ is a diagonal matrix used to compensate for joint friction, with values derived from a linear regression between the torques and joint velocities obtained during manual operation of the robot in Zero-Torque control. c_j is a scalar equal to 0.8.

In the second part of Equation 6.1, redundancy was exploited to prevent the robot from reaching singular configurations. Here, $\mathbf{J}^{\dagger} = \mathbf{J}^T(\mathbf{J}\mathbf{J}^T)^{-1}$ is the pseudo-inverse Jacobian, while $\mathbf{K}_n = 20$ N/rad and $\mathbf{D}_n = \sqrt{\mathbf{K}_n}$ are the stiffness and damping values projected in the null space. $\mathbf{q}_{dn}$ is the vector of desired joint angles in the null space, which corresponds to the robot's initial configuration.

To ensure the safety of participants, two protective measures were implemented. First, a limit on the maximum values of the joint torques was implemented to prevent unexpected abrupt movements (e.g., in case of motion tracking malfunctioning or unforeseen events), and damage to the robot and/or participant. Second, an "invisible wall" was established 37.5 cm from the participants' sagittal plane, toward the robot, preventing the robot from encroaching on the space near the subject.

6.3 Analysis

Data analysis was conducted using Matlab 2022b. All reaction times (RTs) below 80 ms and above 1000 ms were excluded to avoid the inclusion of erroneous responses. Additionally, outliers were removed from each 600 ms time window for each subject, using a threshold set at twice the standard deviation [18]. Subsequently, RTs within each time window were averaged to produce a single data point per window. This resulted in five data points for each condition, which were used to fit a sigmoid function through regression using a least squares algorithm, based on the following equation:

$$y(x) = \frac{y_{\min} + y_{\max} \cdot e^{\frac{x-x_c}{b}}}{1 + e^{\frac{x-x_c}{b}}} \tag{6.2}$$

In Equation 6.2, $y_{\max}$ was calculated as the mean of the RTs within the first time window (i.e., from 0 to 600 ms from the sound onset), gathering together the data from all the conditions (i.e., Pre, Close, and Far). Analogously, $y_{\min}$ was calculated considering the last time window (i.e., from 2401 to 3000 ms from the sound onset). This approach was necessary because the limited number of subjects led to high variability that impeded the three curves from converging at a plateau value, as would be expected with a larger dataset. Indeed, multisensory RTs were shown to be modulated only across the border of the PPS, as an effect of the abrupt switch in multisensory integration efficacy, while within it (close to the participant) or outside of it (very far from the participants) they tend to plateau [18].

The parameter b is inversely related to the slope of the curve, and x_c corresponds to the time point at which the curve reaches its midpoint value, $(y_{\min} + y_{\max})/2$. This point can be considered the transition between PPS and extrapersonal space.

6.4 Results

Results of the fitting are shown in Fig 6.5

The boundaries of the PPS, represented by x_c, are shifted across the three experimental conditions. The x_c values for each condition are reported in Table 6.1. Lower time delay values (x axis) mean that the electrotactile stimulation was delivered when the looming sound was perceived farther from the participant, hence lower x_c values indicate that the PPS border is shifting farther away from the participant and toward the robot, expanding the PPS. In the third column of the table, and estimation of the PPS extension is provided. This expension was calculated with the assumption that the looming sound is moving with a constant velocity. An increase of 10 cm is obtained for the Close condition, and of 18 for the Far.

Condition	x_c **(ms)**	**PPS extension (cm)**
Pre	1641.10	-
Close	1462.25	$\sim$10
Far	1311.61	$\sim$18

Table 6.1 x_c values for the three conditions (Pre, Close, and Far). The right column shows the estimated extension of PPS in Close and Far condition compared to Pre.

6.5 Discussion

In this study, we designed and tested a platform to assess the feasibility of inducing embodiment over an SRL. Two experimental conditions were evaluated: one with the robot placed close to the participant (i.e., 5 cm) and one with the robot positioned 35 cm away. This was done in order to disentangle whether a potential expansion of the PPS was rooted in the robot itself or in the space in which it was operating (i.e., for attention factor [45]).

Our preliminary results suggest that both Close and Far conditions led to an expansion of the PPS with respect to the Pre condition (i.e., before using the SRL), suggesting that the SRL is embodied. Notably, the Far condition produced a more pronounced expansion of the PPS than the Close condition, indicating that this effect could be linked to the SRL itself rather than its workspace, which remained consistent across both conditions. Assuming that the looming sound is perceived as moving with a constant velocity, the differences in x_c

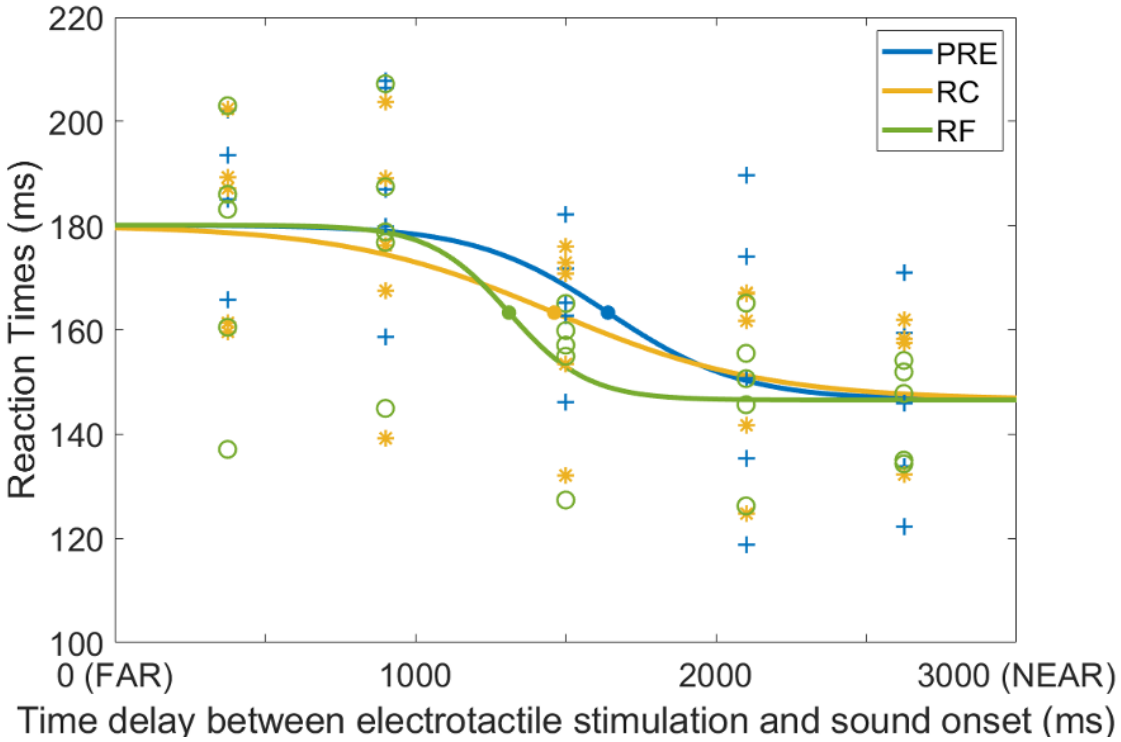

Fig. 6.5 Results of the MRTT. The graph illustrates the three fitted curves (one for each experimental condition) representing RTs in response to electrotactile stimuli (y-axis) as a function of the delay between the electrotactile stimulus and the sound onset (x-axis). It is important to note that when the stimulus was delivered after a short time delay from sound onset (lower x-axis values) the subject perceived the sound source as distant from their body, whereas stimuli delivered after a longer delay (higher x-axis values) were perceived as closer to the participant. The blue curve corresponds to RTs recorded prior to the SRL tri-manual task (PRE), the yellow curve reflects RTs following the task with the SRL in the close position (RC: Robot Close), and the green curve represents RTs after the task with the SRL in the distant position (RF: Robot Far). The dots positioned at the 50% value of each curve represent the x_c, marking the boundary of the PPS.

values between conditions, translate roughly into a PPS extension of 10 cm in Pre vs Close condition, and 18 cm in Pre vs Far condition. One could argue that the reduction in reaction times is due to learning or expectation-related prediction. However, we deem that this is not the case, because if faster reaction times were due to a learning effect, then all reaction times would be lower, including those corresponding to the "far" sound source (i.e., left part of the curves in Fig. 6.5), but this was not observed in our results. As for expectation, it has already been demonstrated that it does not contribute to the decrease in reaction times in this task [18]; rather, the effect is driven by audio-tactile multisensory integration.

6.6 Conclusion

In this chapter, we aimed to address a gap in the HMA literature: the reciprocal influence between humans and robots in augmentation scenarios. This aspect has often been overlooked, with most of the focus placed on control and feedback strategies. However, as discussed in Section 2.3, embodiment is not just a neuroscientific concept, it is also a critical factor for the practical success of HMA, as embodying a tool, or in this case a SRL, could lead to enhanced motor performance. Nevertheless, empirical studies on SRL embodiment are relatively limited and have yielded mixed results.

To explore this, we developed a robotic platform enabling a closed-loop interaction between human and robot during a trimanual task (see Chapter 5 for more details about trimanual tasks) in augmented reality. This setup was designed to both induce and assess the sense of embodiment over the SRL.

Our results show that participants' PPS expanded after a brief augmented trimanual task, suggesting the feasibility of including the SRL into the body representation and thus inducing embodiment over it. Indeed, embodiment seems rooted in the robot itself, given the different extent of PPS expansion in the Far and Close conditions.

These results, although preliminary, provide initial evidence that embodiment may be possible not only for tools (e.g., handheld tools like a stick), but also for SRLs. Multisensory integration of different afferent feedback, combined with closed-loop control, appears to be a crucial step in facilitating embodiment. The findings presented in this chapter highlight that congruent supplementary feedback may play a key role not only in enhancing motor performance, as presented in Chapters 4, 5), but also in making the embodiment process more readily achievable. Nonetheless, despite being promising, these results remain preliminary and require validation in studies with larger sample sizes.

Chapter 7

Conclusion

Overcoming the physical limitations of our body is a fundamental drive that has characterized humanity since its origins. Our history is built upon our ability to understand and interact with the world. Every limit we have overcame has been made possible thanks to our extraordinary ability to use and manipulate complex tools.

These abilities are rooted not only in the morphology of our body, but especially in the remarkable plasticity of the central nervous system (CNS) [29]. Using a tool is not merely an action, it is a deep and complex process that results in modifications of our understanding of both the world and our body, through the formation and adaptation of internal models.

These capabilities have paved the way for Human Movement Augmentation (HMA), a field with the goal of enhancing human motor abilities [34], where the augmentation of Degrees of Freedom (DoF) represents its highest and final objective. However, achieving this goal raises several key challenges. It is necessary to design a control interface capable of extracting high-quality control signals, an effective robotic effector, and a supplementary feedback system to close the sensorimotor loop. At the same time, the cognitive load and the capacity of the CNS to manage additional effectors must be investigated in parallel.

None of these aspects can be overlooked. Movement arises from a rich stream of afferent and efferent information. These streams are essential for learning new tasks [98], adapting [65] to the environment, and refining our understanding of our body and the external world. To enable proficient control of a supernumerary robotic limb (SRL), each stream channel must be optimized to provide enough information to emulate what happens with the natural body.

In this thesis, the focus is placed on the feedback interface primarily within the augmentation by transfer scenario. In this framework, the user's available DoFs are mapped from non-task-relevant to task-relevant. This approach offers an optimal trade-off between control complexity, effectiveness and learning time, as the user already possesses voluntary control

over those DoFs (e.g., foot movements), and only needs to understand the mapping to the SRL's movements [34].

SRLs usually provide users with visual feedback. Vision is a rich sensory modality and, in many applications, it is sufficient to complete the task. However, visual information requires constant attention, can be easily occluded, and does not offer direct access to interaction forces, which must instead be inferred indirectly, for instance, through the visual deformation of objects. An often underestimated aspect in SRL control is proprioception. In the framework of augmentation by transfer, the user can infer the SRL's status from proprioceptive signals once the user-robot transformation has been learned. Nevertheless, we argue that tactile supplementary feedback may be a crucial addition. Indeed, it could offload some of the demand on vision direct visual attention more directly on the task, and is a faster sensory modality [22]. Furthermore, supplementary feedback can be tailored to deliver information that is otherwise hard to extract visually or through proprioception, such as subtle interaction forces or the internal state of the SRL.

The CNS naturally integrates sensory inputs, likely following a Bayesian strategy, combining signals from multiple modalities and with the prior belief (especially in the motor control context) [56] to construct a unified and more likely representation of the the body and the environment. Each sensory input is weighted according to its reliability, which depends on both signal noise and confidence in the information it conveys. While one might argue that vision often serves as the dominant afferent channel, especially in structured environments, it is important to note that, in theory, all available sensory modalities contribute to the final perceptual estimate. Crucially, these weights are not fixed: they dynamically adjust depending on the task and environmental conditions. For example, when the SRL is moving outside the user's field of view or during physical interactions with the environment, vision may become unreliable or irrelevant. In such situations, other sensory modalities, such as proprioception or supplementary feedback, can assume a more central role.

For this reason, in this thesis we explored various aspects of supplementary feedback to enhance HMA. Initially, we presented examples of how feedback can be designed and, subsequently, supplementary feedback is tested in a closed-loop augmented task and in a virtual trimanual tasks to assess its effectiveness in supporting motor performance. Finally, we introduce a platform aimed at inducing and eventually capturing the embodiment of SRL.

7.1 Contributions of the thesis

In this section the main findings of this thesis will be addressed.

Stimulator's placement and feedback strategy influence user ability to discriminate the feedback. Designing supplementary feedback is a complex task, and extracting generalizable rules is particularly challenging. The results presented in this chapter offer practical examples of how feedback can be tailored for a specific application.

In the first part, we evaluated different types of bio-feedback and various body locations for conveying information about the activity of two motor units' (MU) (i.e., their firing rate).

Our findings clearly demonstrate the significant impact of body location. Placing two actuators to close to each other on the body results in lower discrimination performance. This suggests that, in general, may be beneficial to fully exploit the user's body surface to make the feedback more distinguishable. However, this guideline must be adapted to the constraints of the specific task where some applications may limit the available body area.

Additionally, we tested two different feedback strategies within the same application: the spike strategy and the continuous strategy. Our initial hypothesis was that the spike strategy, i.e., a direct translation of the MUs' firing rate into discrete vibratory bursts, would be more effective. However, the results showed a trend in the opposite direction: participants were better at perceiving differences in the two stimulation (i.e., one for each MU) when the feedback was continuous. This could be partly due to hardware limitations. The eccentric rotating mass (ERM) motors used in this experiment have relatively slow dynamics, which may hinder the generation of clearly separate vibratory bursts.

From this experiment, a useful practical recommendation emerges: before closing the feedback loop, it is pivotal to test the effectiveness of the feedback strategy, ideally by using body regions not involved in the primary task or unlikely to interfere with it. Moreover, hardware limitations must be considered, and the chosen strategy should leverage the strengths and account for the weaknesses of the specific actuators used.

When exploiting the funneling illusion to increase the spatial resolution of electrotactile stimulation, it is necessary to calibrate the multi-pad activation to match the single-pad perceived intensity. The second experiment presented in Chapter 3 provides some general guidelines for increasing the spatial resolution of the electrotactile stimulation.

When two or more pads are activated simultaneously, users perceive a phantom sensation located in a portion of skin between them. We focused our investigation on perceived intensity, with the goal of creating a smooth transition between stimulation delivered via a single pad and the resulting phantom sensation when multiple pads are activated. Our results showed that in order to perceive the same stimulation intensity, is necessary that the combined activation of the pads must be higher than that of the single pad alone.

Furthermore, the desired phantom location is a critical parameter to consider. The closer the desired phantom location is to one of the pads, the lower the required sum of activation. Conversely, to elicit a phantom sensation exactly midway between the pads (i.e., maximum distance point), a higher overall activation is needed to maintain the same perceived intensity.

Supplementary vibrotactile feedback increases the user's ability to control the SRL end-effector interaction force with the environment. When wearing a Supernumerary Robotic Limb (SRL), the user receives not only visual feedback, but also inherent feedback. Since the robot is physically attached to the user's body, mechanical forces are naturally exchanged. In the work by Guggenheim et al.[40], it was suggested that inherent feedback alone was sufficient to regulate the interaction force exerted by the SRL's end effector on the environment. However, their evaluation was conducted in a simplified scenario involving a 1-DoF robotic system.

For this reason, we aimed to assess a more realistic and complex scenario, using a 7-DoF SRL mounted on the participant's back. The system was tested under different configurations of the SRL and varying environmental properties (e.g., stiff vs. soft surfaces). Our results indicate that inherent feedback alone was not sufficient to achieve the desired interaction force. In contrast, the addition of supplementary feedback significantly improved participants' performance during the task.

These findings can be generalized even further. If supplementary feedback proves beneficial even when inherent feedback is present, then in the case of non-wearable robots, where no physical connection or force exchange occurs, adding a supplementary feedback to convey information about interaction force becomes a critical aspect and should not be overlooked.

During a trimanual task, vibrotactile feedback positively affects the participant's ability to coordinate all effectors when paired (i.e., three-couple task) to achieve a shared goal. When addressing trimanual tasks, we refer to a broad class of actions in which all effectors can be used and coordinated differently depending on the specific task goal. In the literature (e.g., [71, 46]), different coordination strategies have been identified:

- Uncoupled : where all three effectors are free to move independently of one another. This typically models tasks with three concurrent and distinct objectives.
- Two-coupled: where two effectors must move in a coordinated manner to achieve a shared goal, while the third effector operates independently to contribute to a different aspect of the task.

- Three-coupled: where all three effectors must move in a synchronized and coherent fashion to accomplish a single, unified objective.

These virtual trimanual tasks have been extensively studied, mainly focusing on the performance gap between a pair of individuals collaborating on the same task and a single individual controlling all three effectors. The effects of motor learning have also been explored in previous studies[46].

However, the role of supplementary feedback has been largely overlooked. Supplementary feedback could be particularly beneficial in complex tasks, where high levels of coordination are crucial for successful performance. In this study, we aimed to fill this gap by designing an experimental protocol to investigate the impact of supplementary feedback in a virtual trimanual task. Depending on the condition, the effectors (represented as cursors) were linked by virtual elastic bands. Specifically, in the two-coupled condition, the two hand cursors were virtually connected, while in the three-coupled condition, all three cursors were connected using virtual springs. The supplementary feedback was designed to vibrate proportionally to the force exerted by the spring to maintain the connection. If the movements of the cursors became uncoordinated beyond a threshold, the virtual spring would break.

Our results showed that in the three-coupled condition, all relevant behavioral metrics improved with the addition of supplementary feedback. In the two-coupled condition, only the "spring length variation" (i.e., a index that measure how much the distance between cursors changed during the all task) improved. As expected, the uncoupled condition did not benefit from the feedback, since the feedback was only triggered when two cursors overlapped, essentially after the error was already done. Moreover, in the uncoupled task, the feedback did not convey useful information about the motion itself, unlike in the coupled conditions.

Our results are partially consistent with existing literature. As previously reported, dyads consistently outperformed solo participants, and the performance gap between dyad and solo was smallest in the three-coupled condition. However, contrary to the findings of [46], who reported no difference between solo and dyad performance in the three-coupled condition after a learning phase, we did not observe such convergence. These discrepancies may be due to differences in the experimental protocol.

In conclusion, supplementary feedback proved beneficial in the execution of virtual trimanual tasks, especially in the three-coupled condition. Tasks requiring the concurrent coordination of all three effectors seem to benefit the most from additional feedback. In contrast, tasks requiring coordination between only two effectors showed only modest improvement, limited to the reduction of inter-effector distance.

Preliminary results show the feasibility of embodying a SRL. The concept of embodiment is a complex and multifaceted phenomenon. An external object is considered embodied when it is, at least partially, processed as part of our own body [26]. Tool use, for instance, can lead to the integration of the tool into our body representation [19], resulting in its embodiment. In this sense, embodiment can be viewed as a necessary foundation for achieving successful human motor augmentation.

While some studies in the literature have demonstrated tool embodiment after repeated use, a rigorous demonstration of embodiment in the context of SRLs is still lacking.

To address this gap, in this chapter we designed an augmented trimanual task, where participants were required to reach three buttons simultaneously, two with their natural hands and one with the SRL controlled by the foot. Motor tasks are known to be powerful drivers of embodiment, as they involve both afferent and efferent signals related to limb behavior and environmental interactions.

To enhance multisensory coherence, we applied vibrotactile stimulation to the participants' hands and shoulders to simulate the tactile feedback experienced when pressing a vibrating button. This multisensory congruence aimed to strengthen the sensorimotor integration and potentially foster embodiment.

To assess embodiment, we employed a multisensory reaction time task based to estimate participants' peripersonal space (PPS) extension [18]. In this task, a looming auditory stimulus was presented in combination with an electro-tactile stimulus delivered at a random time. This paradigm has been shown to effectively capture the boundaries of PPS. Furthermore, we tested two experimental conditions: one with the SRL positioned close (i.e., 5 cm, Close condition) to the participants' body, and one with it placed farther away (i.e., 35 cm, Far condition). Crucially, the workspace of the robot remained constant in both conditions. This design allowed us to distinguish whether any observed changes in PPS were due to the the embodiment of the SRL, rather than to mere attention or multisensory stimulation in the workspace.

Our preliminary results support the hypothesis that SRLs can be embodied by users, and that such embodiment is linked to the robot itself. In particular, PPS expansion occurred differently in the Close and Far conditions, suggesting a direct involvement of the SRL in modulating body representation.

Although promising, these findings need to be validated with a larger sample size and additional experimental conditions to rule out potential confounding factors. Nonetheless, our platform appears effective both in inducing measurable changes in participants' PPS and in capturing its boundaries.

7.2 Future Works and Open Questions

The complexity of achieving real degrees-of-freedom (DoF) human movement augmentation (HMA) is a dual challenge. On one hand, technological development must be tailored to the specific application. The input interface and feedback device are crucial elements for closing the sensorimotor loop and enabling seamless use of the supernumerary robotic limb (SRL).

On the other hand, the human user is central to the process. While initial work has begun to explore the human ability to control additional DoFs and manage neural resource allocation, such as the ability to simultaneously control more than two limbs, these issues remain far from be fully resolved.

Furthermore, most existing studies rely on simplified versions of augmented tasks. Virtual reality and overly reduced representations of trimanual tasks can provide useful preliminary insights, but the gap between laboratory experiments and real-world applications remains substantial.

7.2.1 Feedback

As described in Chapter 3, designing rich and informative feedback requires considering which types of information are essential for the motor task and designing the appropriate feedback to maximize information transmission, while also accounting for task constraints and hardware limitations.

In the case of vibrotactile biofeedback for the motor unit, the results were influenced by the location of the actuators. When two motors are placed too close together, the vibration from one can affect the perception of the other due to the propagation of vibrations through the skin [89]. Furthermore, vibrators have their own intrinsic dynamics, so selecting the appropriate motor is critical to achieving the desired vibrotactile patterns. For this reason, we believe it would be worthwhile to explore the spike strategy using linear actuators or mini-shakers. These types of actuators are typically used to deliver complex and highly precise vibrotactile patterns [99]. The spike strategy, in our view, provides a more direct translation of motor unit spiking patterns and may require less training for users to interpret it.

Regarding electrotactile stimulation, in this work we attempted to characterize the perceived intensity when switching from single-pad to double-pad stimulation. The double-pad configuration induces a phantom sensation located midway between the two active pads (i.e., funneling illusion). However, our results show that matching the perceived intensity requires a higher combined activation from the two pads compared to the single one.

Although promising, the work presented in Chapter 3 represents only an initial step toward characterizing the funneling illusion in electrotactile stimulation. In real-world applications, a better understanding of how to combine pad activations with different intensity ratios (i.e., resulting in different perceived positions, see Section 3.3 for details) will be necessary. Additionally, our analysis did not focus on perceived location, an essential component of the funneling illusion and often considered its hallmark feature. Finally, different body locations should be evaluated. Mechanoreceptors are unevenly distributed throughout the body [92], and differences in dermatomal representation in the primary sensory cortex [88] may further shape sensory perception. For this reason other pad placements should be tested and characterized accordingly.

7.2.2 Real augmented task

In Chapters 4 and 5 of this work, we addressed two different problems within the augmentation scenario. In Chapter 5, we evaluated the impact of supplementary feedback in trimanual tasks with varying types of coupling. This impact was analyzed both when the task was performed individually and when a partner collaborated on the same class of tasks. In Chapter 4, by contrast, participants wore a real robotic limb and were required to control the interaction force with the environment. Their performance was compared under two conditions: using only inherent feedback, and using both inherent and supplementary feedback.

The results obtained are relevant for the field, as they highlight the importance of supplementary feedback. Indeed, the users' behavioral responses improved when supplementary feedback was provided.

However, both experiments presented some limitations. The augmented reality setup used in Chapter 5 provides a convenient way to test trimanual tasks: it requires minimal hardware and is highly customizable. Nevertheless, the absence of real haptic feedback, replaced by a supplementary signal, could have led to a qualitatively different sensation, and possibly to different outcomes.

In the interaction force experiment (Chapter 4), the force considered was limited to a single direction (i.e., perpendicular to the surface), with the robot held stationary and controlled via body movement.

These experiments should eventually be combined in a more realistic trimanual task, somewhere between the simplified virtual environment of a laboratory and a real-world application. For example, in Eden's study [35], the authors attempted to reproduce a setup similar to that in Chapter 5 using a foot-controlled robotic limb (as described in Chapter 6) to perform a trimanual task. In their study, the results differed significantly from the virtual task: performance was highest in the uncoupled condition, and the dyadic condition did not

outperform the solo one. The authors suggested that these differences may stem, at least in part, from the physical interaction involved in the real task. The nature of the haptic feedback, especially when constrained by real physical interactions, may lead to different perceptions and behavioral responses.

Furthermore, in physical setups, robot dynamics play a crucial role. Unlike a virtual cursor, a robotic device is subject to mechanical constraints and dynamics, and its behavior depends on control and input strategies. Additional elements, such as target occlusion during movement, may also influence performance in real scenarios.

Altogether, these considerations underscore the need to translate the evaluation of augmented trimanual tasks into real-world applications. This transition could help assess the role of supplementary feedback in more ecologically valid scenarios, where incidental sensory cues, such as the sound of the robot, are also present.

7.2.3 Embodiment of the SRL

In the present work, a platform aimed at promoting the embodiment of a supernumerary robotic limb (SRL) was validated. This was achieved through a trimanual task performed in augmented reality, where the user was asked to press virtual buttons. A supplementary feedback (i.e., vibrotactile stimulation) mimicking the contact with the button was provided. The task was designed to close the sensorimotor loop, as the flow of afferent and efferent signals is essential to support the induction of embodiment [42].

To assess embodiment, a multisensory (audio-tactile) reaction time task was used to map the boundaries of the user's peripersonal space (PPS) before and after using the SRL. This type of test has been shown to capture embodiment of external tools [19]. Indeed, when a tool is integrated into the body representation, the PPS expands to include the tool. The results presented in this study offer early evidence supporting the feasibility of embodying an SRL. However, these preliminary findings should be validated by increasing the participant sample size and by controlling for potential confounding factors. For instance, moving the foot near the PPS boundary might increase the allocation of attentional resources to that space [45]. Future experiments should be designed to test alternative control strategies, such as autonomous SRL control, which do not rely on the user's attention.

Moreover, to strengthen the validity of the findings, neurophysiological measures known to correlate with embodiment (e.g., skin conductance [24]) should also be included.

List of publication

- **Deiana, D.**, Pinardi, M., Noccaro, A., Iandoli, M., Di Pino, G. and Formica, D., "Validation of Vibrotactile Feedback to Improve Selective Motor Units Recruitment", 2023 IEEE International Symposium on Medical Measurements and Applications (MeMeA), Jeju, Korea, Republic of, 2023, pp. 1-5, doi: 10.1109/MeMeA57477.2023.10171925.
- Buratti, S., **Deiana, D.**, Noccaro, A., Pinardi, M., Di Pino, G., Formica, D., and Jarrassé, N. (2023). "Effect of vibrotactile feedback on the control of the interaction force of a supernumerary robotic arm". Machines, 11(12):1085. https://doi.org/10.3390/machines11121085.
- Noccaro, A.[†], **Deiana, D.**[†], Pinardi, M., Di Pino, G., and Formica, D. "Vibro-tactile feedback improves performance in 3-coupled trimanual tasks", Heliyon (Submitted).[1]
- **Deiana, D.**, Pinardi, M., Boljani´c, T., Štrbac, M., Di Pino, G., Formica, D., and Noccaro, A. (2025). "Characterization of electrotactile stimulation intensity to exploit the funneling illusion", 2025 47th Annual International Conference of the IEEE Engineering in Medicine & Biology Society (EMBC), (Accepted).
- Iandoli, M., **Deiana, D.**, Pinardi, M., Noccaro, A., Formica, D., and Di Pino, G. (2025). "A closed-loop platform for the embodiment of supernumerary robotic limbs during augmented tasks", 2025 47th Annual International Conference of the IEEE Engineering in Medicine & Biology Society (EMBC), (Accepted).
- **Deiana, D.**, Ansani, A., Di Pino, G., Formica, D., Spence, C., and Di Stefano, N., "Auditory and Tactile Perception of Musical Intervals: A Pilot Study," 2025 IEEE Medical Measurements & Applications (MeMeA), Chania, Greece, 2025, pp. 1-6, doi: 10.1109/MeMeA65319.2025.11068071.
- **Deiana, D.**, Pinardi, M., Noccaro, A., Iandoli, M., Formica, D. and Di Pino, G., "Comparing different vibrotactile strategies to encode motor units' activation states", Poster session, ICRA23 Augmentation Workshop.

[1] [†]These authors contributed equally to this work.

References

[1] Abdi, E., Burdet, E., Bouri, M., and Bleuler, H. (2015). Control of a supernumerary robotic hand by foot: An experimental study in virtual reality. *PLOS ONE*, 10(7):e0134501.

[2] Abdi, E., Burdet, E., Bouri, M., Himidan, S., and Bleuler, H. (2016). In a demanding task, three-handed manipulation is preferred to two-handed manipulation. *Scientific Reports*, 6(1):21758.

[3] Ajemian, R. and Hogan, N. (2010). Experimenting with theoretical motor neuroscience. *Journal of Motor Behavior*, 42(6):333–342.

[4] Al-Sada, M., Jiang, K., Ranade, S., Piao, X., Höglund, T., and Nakajima, T. (2018). Hapticserpent: A wearable haptic feedback robot for vr. In *Extended Abstracts of the 2018 CHI Conference on Human Factors in Computing Systems*, pages 1–6.

[5] Allemang-Trivalle, A., Eden, J., Ivanova, E., Huang, Y., and Burdet, E. (2022). How long does it take to learn trimanual coordination? *2022 31st IEEE International Conference on Robot and Human Interactive Communication (RO-MAN)*, pages 211–216.

[6] Aymerich-Franch, L., Petit, D., Ganesh, G., and Kheddar, A. (2017). Non-human looking robot arms induce illusion of embodiment. *International Journal of Social Robotics*, 9(4):479–490.

[7] Balasubramanian, S., Melendez-Calderon, A., and Burdet, E. (2012). A robust and sensitive metric for quantifying movement smoothness. *IEEE Transactions on Biomedical Engineering*, 59(8):2126–2136.

[8] Barghout, A., Cha, J., El Saddik, A., Kammerl, J., and Steinbach, E. (2009). Spatial resolution of vibrotactile perception on the human forearm when exploiting funneling illusion. In *2009 IEEE International Workshop on Haptic Audio visual Environments and Games*, pages 19–23. IEEE.

[9] Blanke, O. (2012). Multisensory brain mechanisms of bodily self-consciousness. *Nature Reviews Neuroscience*, 13(8):556–571.

[10] Blanke, O., Slater, M., and Serino, A. (2015). Behavioral, neural, and computational principles of bodily self-consciousness. *Neuron*, 88(1):145–166.

[11] Boljanić, T., Baljić, M., Kostić, M., Barralon, P., Došen, S., and Štrbac, M. (2024). Psychometric evaluation of high-resolution electrotactile interface for conveying 3d spatial information. *Scientific Reports*, 14(1):19969.

[12] Boljanić, T., Isaković, M., Malešević, J., Formica, D., Di Pino, G., Keller, T., and Štrbac, M. (2022). Design of multi-pad electrotactile system envisioned as a feedback channel for supernumerary robotic limbs. *Artificial Organs*, 46(10):2034–2043.

[13] Botvinick, M. and Cohen, J. (1998). Rubber hands 'feel'touch that eyes see. *Nature*, 391(6669):756–756.

[14] Bräcklein, M., Barsakcioglu, D. Y., Ibáñez, J., Eden, J., Burdet, E., Mehring, C., and Farina, D. (2022). The control and training of single motor units in isometric tasks are constrained by a common input signal. *Elife*, 11:e72871.

[15] Braun, N., Debener, S., Spychala, N., Bongartz, E., Sörös, P., Müller, H. H., and Philipsen, A. (2018). The senses of agency and ownership: a review. *Frontiers in Psychology*, 9:535.

[16] Buratti, S., Deiana, D., Noccaro, A., Pinardi, M., Di Pino, G., Formica, D., and Jarrassé, N. (2023). Effect of vibrotactile feedback on the control of the interaction force of a supernumerary robotic arm. *Machines*, 11(12):1085.

[17] Burdet, E., Osu, R., Franklin, D. W., Milner, T. E., and Kawato, M. (2001). The central nervous system stabilizes unstable dynamics by learning optimal impedance. *Nature*, 414(6862):446–449.

[18] Canzoneri, E., Magosso, E., and Serino, A. (2012). Dynamic sounds capture the boundaries of peripersonal space representation in humans. *PLOS ONE*.

[19] Canzoneri, E., Ubaldi, S., Rastelli, V., Finisguerra, A., Bassolino, M., and Serino, A. (2013). Tool-use reshapes the boundaries of body and peripersonal space representations. *Experimental Brain Research*, 228:25–42.

[20] Chandrasekaran, C. (2017). Computational principles and models of multisensory integration. *Current Opinion in Neurobiology*, 43:25–34.

[21] Cole, M. (1996). Pride and a daily marathon. *Neurology*, 47(3):856–857.

[22] Crevecoeur, F., Munoz, D. P., and Scott, S. H. (2016). Dynamic multisensory integration: somatosensory speed trumps visual accuracy during feedback control. *Journal of Neuroscience*, 36(33):8598–8611.

[23] Cuppone, A. V., Squeri, V., Semprini, M., Masia, L., and Konczak, J. (2016). Robot-assisted proprioceptive training with added vibro-tactile feedback enhances somatosensory and motor performance. *PLOS ONE*, 11(10):e0164511.

[24] D'Alonzo, M., Mioli, A., Formica, D., and Di Pino, G. (2020). Modulation of body representation impacts on efferent autonomic activity. *Journal of Cognitive Neuroscience*, 32(6):1104–1116.

[25] De Vignemont, F. (2010). Body schema and body image—pros and cons. *Neuropsychologia*, 48(3):669–680.

[26] De Vignemont, F. (2011). Embodiment, ownership and disownership. *Consciousness and Cognition*, 20(1):82–93.

[27] Deiana, D., Pinardi, M., Boljanić, T., Štrbac, M., Di Pino, G., Formica, D., and Noccaro, A. (2025). Characterization of electrotactile stimulation intensity to exploit the funneling illusion. *2025 47rd Annual International Conference of the IEEE Engineering in Medicine & Biology Society (EMBC), Accepted*.

[28] Deiana, D., Pinardi, M., Noccaro, A., Iandoli, M., Di Pino, G., and Formica, D. (2023). Validation of vibrotactile feedback to improve selective motor units recruitment. pages 1–5.

[29] Di Pino, G., Maravita, A., Zollo, L., Guglielmelli, E., and Di Lazzaro, V. (2014). Augmentation-related brain plasticity. *Frontiers in systems neuroscience*, 8:109.

[30] Di Pino, G., Romano, D., Spaccasassi, C., Mioli, A., D'Alonzo, M., Sacchetti, R., Guglielmelli, E., Zollo, L., Di Lazzaro, V., Denaro, V., et al. (2020). Sensory-and action-oriented embodiment of neurally-interfaced robotic hand prostheses. *Frontiers in neuroscience*, 14:389.

[31] Diedrichsen, J., Shadmehr, R., and Ivry, R. B. (2010). The coordination of movement: optimal feedback control and beyond. *Trends in Cognitive Sciences*, 14(1):31–39.

[32] Dominijanni, G., Pinheiro, D. L., Pollina, L., Orset, B., Gini, M., Anselmino, E., Pierella, C., Olivier, J., Shokur, S., and Micera, S. (2023). Human motor augmentation with an extra robotic arm without functional interference. *Science Robotics*, 8(85):eadh1438.

[33] Dominijanni, G., Shokur, S., Salvietti, G., Buehler, S., Palmerini, E., Rossi, S., De Vignemont, F., d'Avella, A., Makin, T. R., Prattichizzo, D., et al. (2021). The neural resource allocation problem when enhancing human bodies with extra robotic limbs. *Nature Machine Intelligence*, 3(10):850–860.

[34] Eden, J., Bräcklein, M., Ibáñez, J., Barsakcioglu, D. Y., Di Pino, G., Farina, D., Burdet, E., and Mehring, C. (2022). Principles of human movement augmentation and the challenges in making it a reality. *Nature Communications*, 13(1):1345.

[35] Eden, J., Khoramshahi, M., Huang, Y., Poignant, A., Burdet, E., and Jarrassé, N. (2025). Comparison of solo and collaborative trimanual operation of a supernumerary limb in tasks with varying physical coupling. *IEEE Robotics and Automation Letters*, 10(2):860–867.

[36] Farina, D., Burdet, E., Mehring, C., and Ibáñez, J. (2023). Roboticists want to give you a third arm: Unused bandwidth in neurons can be tapped to control extra limbs. *IEEE Spectrum*, 60(3):22–46.

[37] Franklin, D. W., Osu, R., Burdet, E., Kawato, M., and Milner, T. E. (2003). Adaptation to stable and unstable dynamics achieved by combined impedance control and inverse dynamics model. *Journal of Neurophysiology*, 90(5):3270–3282.

[38] Gallivan, J. P., Chapman, C. S., Wolpert, D. M., and Flanagan, J. R. (2018). Decision-making in sensorimotor control. *Nature Reviews Neuroscience*, 19(9):519–534.

[39] Goldstein, E. B. and Brockmole, J. R. (2002). *Sensation and perception*, volume 90. Wadsworth-Thomson Learning Pacific Grove, CA, USA.

[40] Guggenheim, J. W. and Asada, H. H. (2020). Inherent haptic feedback from supernumerary robotic limbs. *IEEE Transactions on Haptics*, 14(1):123–131.

[41] Gurgone, S., Borzelli, D., De Pasquale, P., Berger, D. J., Baldi, T. L., D'Aurizio, N., Prattichizzo, D., and d'Avella, A. (2022). Simultaneous control of natural and extra degrees of freedom by isometric force and electromyographic activity in the muscle-to-force null space. *Journal of Neural Engineering*, 19(1):016004.

[42] Hellman, R. B., Chang, E., Tanner, J., Helms Tillery, S. I., and Santos, V. J. (2015). A robot hand testbed designed for enhancing embodiment and functional neurorehabilitation of body schema in subjects with upper limb impairment or loss. *Frontiers in Human Neuroscience*, 9:26.

[43] Hernandez Sanchez, J., Amanhoud, W., Billard, A., and Bouri, M. (2023). Enabling four-arm laparoscopic surgery by controlling two robotic assistants via haptic foot interfaces. *The International Journal of Robotics Research*, 42(7):475–503.

[44] Hogan, N. and Sternad, D. (2012). Dynamic primitives of motor behavior. *Biological Cybernetics*, 106:727–739.

[45] Holmes, N. P., Sanabria, D., Calvert, G. A., and Spence, C. (2007). Tool-use: capturing multisensory spatial attention or extending multisensory peripersonal space? *Cortex*, 43(3):469–489.

[46] Huang, Y., Eden, J., Ivanova, E., and Burdet, E. (2023). Can training make three arms better than two heads for trimanual coordination? *IEEE Open Journal of Engineering in Medicine and Biology*, 4:148–155.

[47] Huang, Y., Eden, J., Ivanova, E., Phee, S. J., and Burdet, E. (2021a). Trimanipulation: Evaluation of human performance in a 3-handed coordination task. *2021 IEEE International Conference on Systems, Man, and Cybernetics (SMC)*, pages 882–887.

[48] Huang, Y., Lai, W., Cao, L., Burdet, E., and Phee, S. J. (2021b). Design and evaluation of a foot-controlled robotic system for endoscopic surgery. *IEEE Robotics and Automation Letters*, 6(2):2469–2476.

[49] Huang, Y., Lai, W., Cao, L., Liu, J., Li, X., Burdet, E., and Phee, S. J. (2021c). A three-limb teleoperated robotic system with foot control for flexible endoscopic surgery. *Annals of Biomedical Engineering*, 49:2282–2296.

[50] Hussain, I., Meli, L., Pacchierotti, C., Salvietti, G., Prattichizzo, D., et al. (2015). Vibrotactile haptic feedback for intuitive control of robotic extra fingers. In *World Haptics*, pages 394–399.

[51] Iandoli, M., Deiana, D., Pinardi, M., Noccaro, A., Formica, D., and Di Pino, G. (2025). A closed-loop platform for the embodiment of supernumerary robotic limbs during augmented tasks. *2025 47rd Annual International Conference of the IEEE Engineering in Medicine & Biology Society (EMBC), Accepted*.

[52] Juliano, J. M., Spicer, R. P., Vourvopoulos, A., Lefebvre, S., Jann, K., Ard, T., Santarnecchi, E., Krum, D. M., and Liew, S.-L. (2020). Embodiment is related to better performance on a brain–computer interface in immersive virtual reality: A pilot study. *Sensors*, 20(4):1204.

[53] Kandel, E. R., Schwartz, J. H., Jessell, T. M., Siegelbaum, S., Hudspeth, A. J., Mack, S., et al. (2000). *Principles of Neural Science*, volume 4. McGraw-hill New York.

[54] Kawato, M. (1999). Internal models for motor control and trajectory planning. *Current Opinion in Neurobiology*, 9(6):718–727.

[55] Khoramshahi, M., Poignant, A., Morel, G., and Jarrassé, N. (2023). A practical control approach for safe collaborative supernumerary robotic arms. In *2023 IEEE International Conference on Advanced Robotics and Its Social Impacts (ARSO)*, pages 147–152.

[56] Körding, K. P. and Wolpert, D. M. (2006). Bayesian decision theory in sensorimotor control. *Trends in Cognitive Sciences*, 10(7):319–326.

[57] Krakauer, J. W., Hadjiosif, A. M., Xu, J., Wong, A. L., and Haith, A. M. (2019). Motor learning. *Comprehensive Physiology*, 9(2):613–663.

[58] Krueger, A. R., Giannoni, P., Shah, V., Casadio, M., and Scheidt, R. A. (2017). Supplemental vibrotactile feedback control of stabilization and reaching actions of the arm using limb state and position error encodings. *Journal of Neuroengineering and Rehabilitation*, 14:1–23.

[59] Lalazar, H. and Vaadia, E. (2008). Neural basis of sensorimotor learning: modifying internal models. *Current Opinion in Neurobiology*, 18(6):573–581.

[60] Latash, M. L., Scholz, J. P., and Schöner, G. (2002). Motor control strategies revealed in the structure of motor variability. *Exercise and Sport Sciences Reviews*, 30(1):26–31.

[61] Liepelt, R., Dolk, T., and Hommel, B. (2017). Self-perception beyond the body: the role of past agency. *Psychological Research*, 81(3):549–559.

[62] Longo, M. R., Schüür, F., Kammers, M. P., Tsakiris, M., and Haggard, P. (2008). What is embodiment? a psychometric approach. *Cognition*, 107(3):978–998.

[63] Ma, K. and Hommel, B. (2015). Body-ownership for actively operated non-corporeal objects. *Consciousness and Cognition*, 36:75–86.

[64] Mahns, D. A., Perkins, N., Sahai, V., Robinson, L., and Rowe, M. (2006). Vibrotactile frequency discrimination in human hairy skin. *Journal of Neurophysiology*, 95(3):1442–1450.

[65] Malfait, N., Gribble, P. L., and Ostry, D. J. (2005). Generalization of motor learning based on multiple field exposures and local adaptation. *Journal of Neurophysiology*, 93(6):3327–3338.

[66] Medina, J., Khurana, P., and Coslett, H. B. (2015). The influence of embodiment on multisensory integration using the mirror box illusion. *Consciousness and Cognition*, 37:71–82.

[67] Merel, J., Botvinick, M., and Wayne, G. (2019). Hierarchical motor control in mammals and machines. *Nature Communications*, 10(1):5489.

[68] Miall, R. C., Rosenthal, O., Ørstavik, K., Cole, J. D., and Sarlegna, F. R. (2019). Loss of haptic feedback impairs control of hand posture: a study in chronically deafferented individuals when grasping and lifting objects. *Experimental Brain Research*, 237:2167–2184.

[69] Noccaro, A., Boljanić, T., Štrbac, M., Di Pino, G., and Formica, D. (2024). Closed-loop platform for human movement augmentation with electrotactile feedback. *2024 10th IEEE RAS/EMBS International Conference for Biomedical Robotics and Biomechatronics (BioRob)*, pages 795–800.

[Noccaro et al.] Noccaro, A., Deiana, D., Pinardi, M., Di Pino, G., and Formica, D. Vibrotactile feedback improves performance in 3-coupled trimanual tasks. *Available at SSRN 4884432*.

[71] Noccaro, A., Eden, J., Di Pino, G., Formica, D., and Burdet, E. (2021). Human performance in three-hands tasks. *Scientific Reports*, 11(1):9511.

[72] Noccaro, A., Raiano, L., Pinardi, M., Formica, D., and Di Pino, G. (2020). A novel proprioceptive feedback system for supernumerary robotic limb. In *2020 8th IEEE RAS/EMBS International Conference for Biomedical Robotics and Biomechatronics (BioRob)*, pages 1024–1029.

[73] Noel, J.-P., Pfeiffer, C., Blanke, O., and Serino, A. (2015). Peripersonal space as the space of the bodily self. *Cognition*, 144:49–57.

[74] Page, D. M., George, J. A., Kluger, D. T., Duncan, C., Wendelken, S., Davis, T., Hutchinson, D. T., and Clark, G. A. (2018). Motor control and sensory feedback enhance prosthesis embodiment and reduce phantom pain after long-term hand amputation. *Frontiers in Human Neuroscience*, 12:352.

[75] Pinardi, M., Longo, M. R., Formica, D., Strbac, M., Mehring, C., Burdet, E., and Di Pino, G. (2023a). Impact of supplementary sensory feedback on the control and embodiment in human movement augmentation. *Communications Engineering*, 2(1):64.

[76] Pinardi, M., Noccaro, A., Raiano, L., Formica, D., and Di Pino, G. (2023b). Comparing end-effector position and joint angle feedback for online robotic limb tracking. *PLOS ONE*, 18(6):e0286566.

[77] Pinardi, M., Raiano, L., Formica, D., and Di Pino, G. (2020). Altered proprioceptive feedback influences movement kinematics in a lifting task. *2020 42nd Annual International Conference of the IEEE Engineering in Medicine & Biology Society (EMBC)*, pages 3232–3235.

[78] Pinardi, M., Raiano, L., Noccaro, A., Formica, D., and Di Pino, G. (2021). Cartesian space feedback for real time tracking of a supernumerary robotic limb: a pilot study. In *2021 10th International IEEE/EMBS Conference on Neural Engineering (NER)*, pages 889–892.

[79] Proske, U. and Gandevia, S. C. (2012). The proprioceptive senses: their roles in signaling body shape, body position and movement, and muscle force. *Physiological Reviews*.

[80] Risi, N., Shah, V., Mrotek, L. A., Casadio, M., and Scheidt, R. A. (2019). Supplemental vibrotactile feedback of real-time limb position enhances precision of goal-directed reaching. *Journal of Neurophysiology*, 122(1):22–38.

[81] Romano, D., Caffa, E., Hernandez-Arieta, A., Brugger, P., and Maravita, A. (2015). The robot hand illusion: Inducing proprioceptive drift through visuo-motor congruency. *Neuropsychologia*, 70:414–420.

[82] Scott, S. H. (2004). Optimal feedback control and the neural basis of volitional motor control. *Nature Reviews Neuroscience*, 5(7):532–545.

[83] Sensinger, J. W. and Dosen, S. (2020). A review of sensory feedback in upper-limb prostheses from the perspective of human motor control. *Frontiers in neuroscience*, 14:345.

[84] Serino, A. (2019). Peripersonal space (pps) as a multisensory interface between the individual and the environment, defining the space of the self. *Neuroscience & Biobehavioral Reviews*, 99:138–159.

[85] Shadmehr, R. and Krakauer, J. W. (2008). A computational neuroanatomy for motor control. *Experimental Brain Research*, 185:359–381.

[86] Shadmehr, R. and Mussa-Ivaldi, F. A. (1994). Adaptive representation of dynamics during learning of a motor task. *Journal of neuroscience*, 14(5):3208–3224.

[87] Shaffer, F. and Ginsberg, J. P. (2017). An overview of heart rate variability metrics and norms. *Frontiers in Public Health*, page 258.

[88] Shah, V. A., Casadio, M., Scheidt, R. A., and Mrotek, L. A. (2019a). Spatial and temporal influences on discrimination of vibrotactile stimuli on the arm. *Experimental Brain Research*, 237(8):2075–2086.

[89] Shah, V. A., Casadio, M., Scheidt, R. A., and Mrotek, L. A. (2019b). Vibration propagation on the skin of the arm. *Applied Sciences*, 9(20):4329.

[90] Todorov, E. and Jordan, M. I. (2002). Optimal feedback control as a theory of motor coordination. *Nature Neuroscience*, 5(11):1226–1235.

[91] Toet, A., Kuling, I. A., Krom, B. N., and Van Erp, J. B. (2020). Toward enhanced teleoperation through embodiment. *Frontiers in Robotics and AI*, 7:14.

[92] Vallbo, A. B., Johansson, R. S., et al. (1984). Properties of cutaneous mechanoreceptors in the human hand related to touch sensation. *Human neurobiology*, 3(1):3–14.

[93] van Beers, R. J., Wolpert, D. M., and Haggard, P. (2002). When feeling is more important than seeing in sensorimotor adaptation. *Current Biology*, 12(10):834–837.

[94] van Melick, N., Meddeler, B. M., Hoogeboom, T. J., Nijhuis-van der Sanden, M. W., and van Cingel, R. E. (2017). How to determine leg dominance: The agreement between self-reported and observed performance in healthy adults. *PLOS ONE*, 12(12):e0189876.

[95] Weser, V. U. and Proffitt, D. R. (2021). Expertise in tool use promotes tool embodiment. *Topics in Cognitive Science*, 13(4):597–609.

[96] Wichmann, F. A. and Hill, N. J. (2001). The psychometric function: I. fitting, sampling, and goodness of fit. *Perception & Psychophysics*, 63(8):1293–1313.

[97] Winter, D. A. (2009). *Biomechanics and motor control of human movement*. John Wiley & Sons.

[98] Wolpert, D. M. and Flanagan, J. R. (2010). Motor learning. *Current Biology*, 20(11):R467–R472.

[99] Yoo, Y., Hwang, I., and Choi, S. (2013). Consonance of vibrotactile chords. *IEEE Transactions on Haptics*, 7(1):3–13.

[100] Zhou, Z., Yang, Y., Liu, J., Zeng, J., Wang, X., and Liu, H. (2022). Electrotactile perception properties and its applications: A review. *IEEE Transactions on Haptics*, 15(3):464–478.